

HYDROCLIMATIC AND CIRCULATION ANOMALIES ASSOCIATED WITH THE
GULF OF MEXICO HYPOXIC ZONE

A Thesis

Submitted to the Graduate Faculty of the
Louisiana State University and
Agricultural and Mechanical College
in partial fulfillment of the
requirements for the degree of
Master of Science

in

The Department of Geography and Anthropology

by
Natalie A. Vines
B.S., Louisiana State University, 2003
May 2005

ACKNOWLEDGMENTS

There are so many people to thank, for without their help this thesis would not have been possible. First of all, I want to thank my entire family for their support during this process, especially my mother and father. Their unwavering support throughout my education at Louisiana State University made my days in graduate school possible. I cannot imagine where I would be without their constant encouragement. I am forever grateful. Thank you for always believing in me.

Next, I would like to thank my advisor, Dr. Robert Rohli. Enrolling in his *Physical Geography: The Atmosphere* class as an undergraduate forever changed the course of my education. His teaching and advice encouraged my love of geography. He has been an amazingly helpful and influential advisor. I feel blessed to have worked with him. The time and attention he gave to this thesis was remarkable. Thank you to my committee members, Dr. Barry Keim and Dr. Maurice McHugh. Their time and expertise was critical to the success of this thesis.

The support of so many of my friends made graduate school a wonderful experience. First of all, thank you to Jillian Wilkerson. Thank you for listening to me every day throughout this process. You have been there every step of the way. Thank you to my fellow geography graduate students, Brady Couvillion and Kalyn Wrona. Your friendship and GIS assistance have been amazing gifts. Finally, to my friend and sister, Emily Vines. Although you are so very far away, you have been with me every minute of this process, often on the phone, and always in my heart.

Thank you to Dr. Nancy Rabalais at the Louisiana Universities Marine Consortium for supplying the Gulf of Mexico Hypoxia data and for offering her expertise

to this thesis. Thank you to Michael Kearney at the Louisiana State University School of Veterinary Medicine who so selflessly gave his time and SAS expertise to this thesis. Thank you to Mark Richter at the Vicksburg Army Corps of Engineers for supplying much needed streamflow data.

TABLE OF CONTENTS

ACKNOWLEDGMENTS	ii
LIST OF TABLES.....	vi
LIST OF FIGURES	vii
ABSTRACT.....	x
CHAPTER 1. INTRODUCTION.....	1
1.1 The Gulf of Mexico Hypoxic Zone	1
1.2 Atmospheric Circulation Variability and the Gulf of Mexico Hypoxic Zone	6
1.3 Statement of Problem.....	8
1.4 Hypotheses.....	9
1.5 Outline of Thesis.....	10
CHAPTER 2. BACKGROUND AND LITERATURE REVIEW	11
2.1 Moisture Indices.....	11
2.2 Streamflow Variability in the Mississippi-Missouri River Basin.....	13
2.3 Climatology of the Mississippi-Missouri River Basin.....	15
2.4 Historical Variability in the Intensity of the Gulf of Mexico Hypoxic Zone	18
2.5 Atmospheric Teleconnections.....	21
2.6 Summary.....	28
CHAPTER 3. DATA AND METHODS	29
3.1 Data.....	29
3.2 Methods.....	35
CHAPTER 4. RESULTS: SURFACE MOISTURE VARIABILITY AND THE GULF OF MEXICO HYPOXIC ZONE.....	39
4.1 Streamflow in the Mississippi-Missouri River Basin and the Gulf of Mexico Hypoxic Zone	39
4.2 Correlations between Moisture Indices and the Gulf of Mexico Hypoxic Zone	39
4.3 Correlations in the Annual Cycle between Monthly Teleconnection Indices and the Monthly Palmer Drought Severity Index	43
4.4 Correlations in the Annual Cycle between Monthly Teleconnection Indices and the Monthly Palmer Hydrological Drought Index.....	53
4.5 Spring Correlations between Monthly Teleconnection Indices and the Monthly Palmer Drought Severity Index.....	59
4.6 Spring Correlations between Monthly Teleconnection Indices and the Monthly Palmer Hydrological Drought Index.....	70
4.7 Summary.....	78

CHAPTER 5. REGIONALIZATION OF MOISTURE VARIABILITY REGIONS	79
5.1 Regionalization Based on the Palmer Drought Severity Index	79
5.2 Regionalization Based on the Palmer Hydrological Drought Index.....	86
5.3 Summary	89
CHAPTER 6: A PREDICTIVE MODEL FOR FORECASTING AND HINDCASTING GULF OF MEXICO HYPOXIC ZONE EXTENT	93
6.1 Preparation of Data	93
6.2 Models Based on Palmer Drought Severity Index.....	94
6.3 Models Based on Palmer Hydrological Drought Index.....	104
6.4 Teleconnection Indices as Predictors.....	108
6.5 Summary	111
CHAPTER 7: SUMMARY AND CONCLUSIONS	112
7.1 Summary	112
7.2 Suggestions for Further Research.....	113
LITERATURE CITED	115
VITA.....	125

LIST OF TABLES

Table 1: GMHZ Surface Area.....	34
Table 2: Correlations between Mississippi River Streamflow and July GMHZ Area	40
Table 3: Eigenvalues of Unrotated PCA Based on PDSI	80
Table 4: Eigenvalues of Rotated PCA Based on PDSI.....	80
Table 5: Percentage of Each Sub-basin Contained in Each Rotated Component Based on PDSI.....	82
Table 6: Eigenvalues of the Unrotated PCA Based on PHDI.....	86
Table 7: Eigenvalues of the Rotated PCA Based on PHDI	86
Table 8: Percentage of Each Sub-basin Contained in Each Rotated Component Based on PHDI	89
Table 9: Smallest Hindcasted GMHZ Surface Areas based on the May PDSI	102
Table 10: Largest Hindcasted GMHZ Surface Areas based on the May PDSI.....	103
Table 11: Smallest Hindcasted GMHZ Surface Areas Based on the April PHDI.....	109
Table 12: Largest Hindcasted GMHZ Surface Areas Based on the April PHDI.....	110

LIST OF FIGURES

Figure 1: Location of the Gulf of Mexico Hypoxic Zone.....	2
Figure 2: Climate Divisions in the MMRB	4
Figure 3: Areas of Subsidence and Uplift in Association with a Hypothetically- positioned Rossby Wave. Storminess will be Suppressed Beneath Areas of Subsidence and Encouraged Beneath Areas of Uplift.	7
Figure 4: Average Annual Precipitation of the MMRB by Climate Division	16
Figure 5: MMRB Sub-basins	36
Figure 6: MAMJ PDSI and GMHZ Correlations ($\alpha \leq 0.05$).....	41
Figure 7: MAMJ PHDI and GMHZ Correlations ($\alpha \leq 0.05$)	42
Figure 8: Monthly SOI Correlations (January – December) with PDSI ($\alpha \leq 0.05$) in the Annual Cycle	44
Figure 9: Monthly Niño 3.4 Correlations (January – December) with PDSI ($\alpha \leq 0.05$) in the Annual Cycle	46
Figure 10: Monthly PDO Correlations (January – December) with PDSI ($\alpha \leq 0.05$) in the Annual Cycle.....	48
Figure 11: Monthly AO Correlations (January – December) with PDSI ($\alpha \leq 0.05$) in the Annual Cycle.....	49
Figure 12: Monthly NAO Correlations (January – December) with PDSI ($\alpha \leq 0.05$) in the Annual Cycle.....	51
Figure 13: Monthly PNA Correlations (January – December) with PDSI ($\alpha \leq 0.05$) in the Annual Cycle.....	52
Figure 14: Monthly SOI Correlations (January – December) with PHDI ($\alpha \leq 0.05$) in the Annual Cycle.....	54
Figure 15: Monthly Niño 3.4 Correlations (January – December) with PHDI ($\alpha \leq 0.05$) in the Annual Cycle	55
Figure 16: Monthly PDO Correlations (January – December) with PHDI ($\alpha \leq 0.05$) in the Annual Cycle	57

Figure 17: Monthly AO Correlations (January – December) with PHDI ($\alpha \leq 0.05$) in the Annual Cycle.....	58
Figure 18: Monthly NAO Correlations (January – December) with PHDI ($\alpha \leq 0.05$) in the Annual Cycle.....	60
Figure 19: Monthly PNA Correlations (January – December) with PHDI ($\alpha \leq 0.05$) in the Annual Cycle.....	61
Figure 20: MAMJ SOI Correlations with PDSI ($\alpha \leq 0.05$).....	62
Figure 21: MAMJ Niño 3.4 Correlations with PDSI ($\alpha \leq 0.05$)	64
Figure 22: MAMJ PDO Correlations with PDSI ($\alpha \leq 0.05$)	65
Figure 23: MAMJ AO Correlations with PDSI ($\alpha \leq 0.05$).....	66
Figure 24: MAMJ NAO Correlations with PDSI ($\alpha \leq 0.05$).....	68
Figure 25: MAMJ PNA Correlations with PDSI ($\alpha \leq 0.05$)	69
Figure 26: MAMJ SOI Correlations with PHDI ($\alpha \leq 0.05$)	71
Figure 27: MAMJ Niño 3.4 Correlations with PHDI ($\alpha \leq 0.05$).....	72
Figure 28: MAMJ PDO Correlations with PHDI ($\alpha \leq 0.05$).....	74
Figure 29: MAMJ AO Correlations with PHDI ($\alpha \leq 0.05$).....	75
Figure 30: MAMJ NAO Correlations with PHDI ($\alpha \leq 0.05$)	76
Figure 31: MAMJ PNA Correlations with PHDI ($\alpha \leq 0.05$).....	77
Figure 32: Loadings for MAMJ PDSI Rotated Component 1	81
Figure 33: Loadings for MAMJ PDSI Rotated Component 2	83
Figure 34: Loadings for MAMJ PDSI Rotated Component 3	84
Figure 35: Rotated PCA Component upon Which Climate Divisions Load Most Highly for MAMJ PDSI Analysis	85
Figure 36: Loadings for MAMJ PHDI Rotated Component 1	87
Figure 37: Loadings for MAMJ PHDI Rotated Component 2	88

Figure 38: Loadings for MAMJ PHDI Rotated Component 3	90
Figure 39: Rotated PCA Component upon Which Climate Divisions Load Most Highly for MAMJ PHDI Analysis.....	91
Figure 40: Climate Division for Which the June PDSI is Used to Predict the Area of the July GMHZ	95
Figure 41: Climate Divisions for Which the May PDSI is Used to Predict the Area of the July GMHZ	96
Figure 42: Climate Divisions for Which the April PDSI is Used to Predict the Area of the July GMHZ	97
Figure 43: Climate Division for Which the March PDSI is Used to Predict the Area of the July GMHZ	98
Figure 44: Climate Divisions for Which the February PDSI is Used to Predict the Area of the July GMHZ.....	99
Figure 45: Climate Divisions for Which the June PHDI is Used to Predict the Area of the July GMHZ	105
Figure 46: Climate Division for Which the May PHDI is Used to Predict the Area of the July GMHZ	106
Figure 47: Climate Divisions for Which the April PHDI is Used to Predict the Area of the July GMHZ	107

ABSTRACT

The Gulf of Mexico Hypoxic Zone (GMHZ) has been observed along the Louisiana continental shelf west of the mouth of the Mississippi River since 1985. Previous research associated the surface area of the GMHZ with runoff in the Mississippi-Missouri River Basin (MMRB), with “wet” years linked to larger GMHZs than “dry” years. This research uses monthly climate divisional Palmer Drought Severity Index (PDSI) data and Palmer Hydrological Drought Index (PHDI) data and monthly atmospheric teleconnection indices are used to predict the GMHZ extent up to several months in advance, using stepwise multiple regression techniques. The predictive equations are then used to reconstruct the extent of the GMHZ for years prior to 1985. To generate a hydroclimatologic regionalization of the MMRB, a principal components analysis (PCA) is performed to identify regions of homogeneous hydroclimatic variability that may contribute to variability in GMHZ extent. Results may be helpful to environmental planners who might use the predictions in defining upcoming seasons for the commercial seafood industry, and to environmental historians who may use the hindcasted estimates to explain variation in seafood harvests.

CHAPTER 1 INTRODUCTION

1.1 The Gulf of Mexico Hypoxic Zone

Atmospheric circulation is an important control on many environmental features (Rogers *et al.* 2003). More specifically, variability in the broad-scale, upper-level atmospheric circulation can have an important impact on the severity of many surface environmental problems. For example, salinity and oxygen content in coastal waters are often related to runoff, which is in turn related to precipitation, which is driven by upper-level atmospheric circulation.

One example of a marine environment in which atmospheric circulation may relate to problematic dissolved oxygen content is along the coast of Louisiana, where the second-largest hypoxic (oxygen-starved) marine zone in the world, after the Baltic Sea, and the largest in the western Atlantic Ocean (Justić *et al.* 1996) is found. This Gulf of Mexico Hypoxic Zone (GMHZ) parallels the Louisiana coast west of the mouth of the Mississippi River (Figure 1), and occurs at depths of 5-60 m at 50-60 km off the coast, and down to 20 m above the ocean floor (Justić *et al.* 1996).

Although hypoxia has only been formally measured in the northern Gulf of Mexico since 1985, hypoxia has been documented in smaller areas off the coast of Louisiana since at least 1972 (Turner *et al.* 2005). Compared to the most recent measurements, the area of the GMHZ was small in the late 1970s to early 1980s (Turner *et al.* 2005).

Nutrient-laden runoff from non-point source pollution in the agricultural heartland of the United States and runoff-induced fluctuations in Gulf of Mexico salinity can have a tremendous effect on the marine environment around the mouth of the Mississippi-

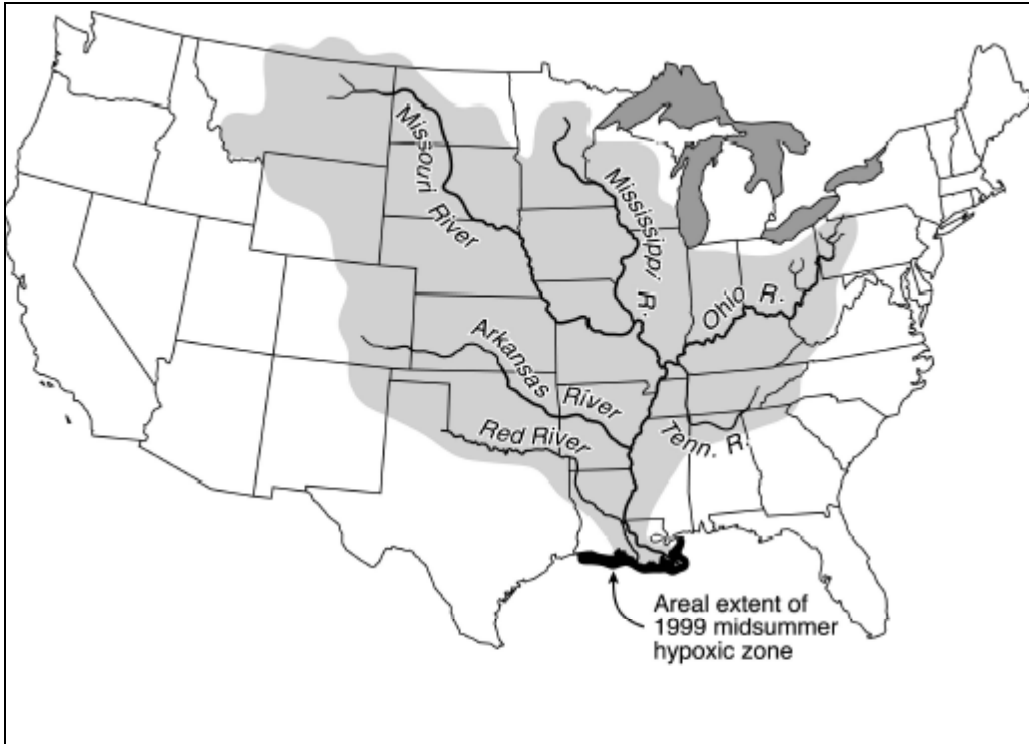


Figure 1: Location of the Gulf of Mexico Hypoxic Zone (Source: Rohli 2001)

Missouri River Basin (MMRB, Figure 2) (Rabalais *et al.* 2002a). The MMRB itself encompasses an approximately triangular area of the U.S. bounded by about 49°N just north of the Canadian border and 29.15°N at the mouth of the Mississippi River and 111.5°W at the headwaters of the Missouri River and 79°W at the Upper Allegheny River in Pennsylvania.

Flooding in the upper MMRB can dramatically increase overland nitrogen runoff, which eventually causes seafood population depletion and species extinction in the GMHZ (Justić *et al.* 1996). A correlation exists between the GMHZ and Mississippi River flow (Justić *et al.* 1993). For example, the Mississippi River flood of 1993 doubled the average size of the GMHZ (Rabalais *et al.* 2002a), and the GMHZ was smaller than average as a result of decreased river discharge in 1988 and 2000 (Rabalais *et al.* 2002a). The relationship between runoff and oxygen content is complicated because high levels of oxygen at the surface of the Gulf of Mexico have a lag time of one month (Justić *et al.* 1993), while low levels of oxygen in the bottom waters have a two-month lag time (Justić *et al.* 1993).

In addition to the ecological implications of the GMHZ, drastic economic consequences for Louisiana will result from hypoxic waters. Oxygen concentrations below 2mg/l, which are characteristic of the GMHZ, are too low to support shrimp and fish (Rabalais *et al.* 2002b). Therefore, the GMHZ can have serious financial implications for the fishing industry in the northern Gulf of Mexico. With 1.4 billion pounds, commercial fish and shellfish harvests in Louisiana were worth \$418.9 million in 2000 (One Gulf 2002). In addition to the commercial seafood harvest, fishing brings important tourist dollars to the local economy. The GMHZ has cost the Louisiana

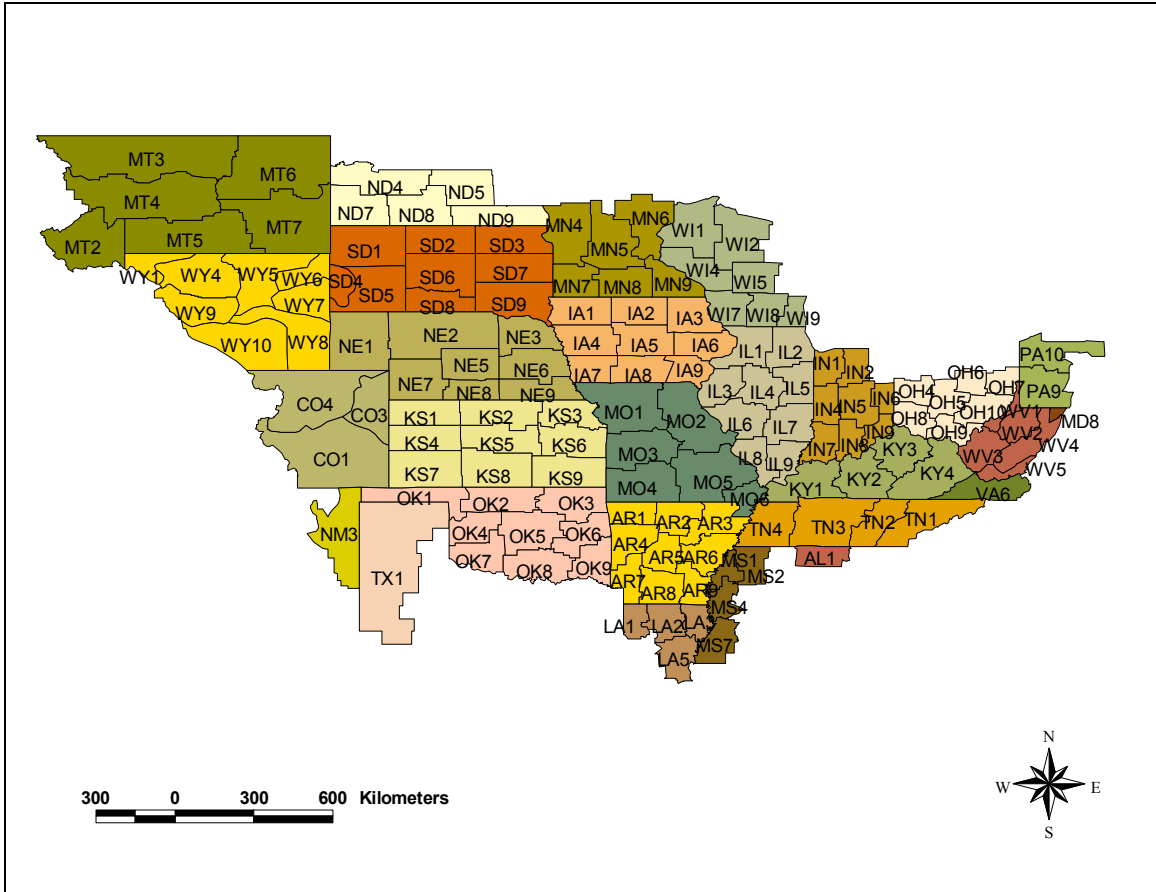


Figure 2: Climate Divisions in the MMRB

economy perhaps almost \$300 million since 1991 by depleting commercial fish harvests, causing health problems, and impacting tourism (One Gulf 2002). Thus, an accurate prediction of the size of the GMHZ could prove beneficial to the seafood and ecotourism industries by providing environmental planners and wildlife and fisheries officials with additional information in setting upcoming seasonal boundaries for commercial fisheries harvests. Furthermore, reconstruction of past GMHZ size could assist in explaining seafood harvests in the past and give an estimate of possible return periods and scenarios for future GMHZ extent. Therefore this study represents an important step in understanding an environmental problem with implications for economic and social systems.

Another complicating factor in the relationship between runoff and the GMHZ involves interannual variations in streamflow and river runoff (McCabe and Wolock 1997). More specifically, an increase in precipitation in the MMRB would likely result in an increase in runoff into the river and affect the concentrations of nitrogen-based fertilizers reaching the northern Gulf of Mexico through the 3.3 million gallons of water that flow into the Gulf of Mexico from the Mississippi River every second (One Gulf 2002). While difficult to quantify, the role of land use and water and agricultural practices may also be important in defining the impact of precipitation variability on river runoff (McCabe and Wolock 1997). Furthermore, interannual and interdecadal variability associated with thermal and circulation properties of the atmosphere and ocean near coastal Louisiana impact the area of the GMHZ. For example, algae are destructive to oxygen levels and bloom vigorously in calmer waters (Schleifstein 2003).

The typical annual cycle of the GMHZ is for decreasing oxygen concentrations in spring and summer, with the lowest levels of oxygen across the largest area between May and September (Rabalais *et al.* 2002a). Oxygen concentrations generally increase in autumn due to winds that mix the stratified water (Rabalais *et al.* 2002a). These winds result from the return of relatively strong cold fronts after the long, hot summer, and tropical cyclones (Rabalais *et al.* 2002a) ranging in strength from weak, disorganized, easterly waves to hurricanes.

1.2 Atmospheric Circulation Variability and the Gulf of Mexico Hypoxic Zone

Although no formal research has investigated the role of atmospheric circulation variability on the GMHZ, one of the most important predictors of the area of the GMHZ may be the behavior of long-wave atmospheric flow. This atmospheric variability can be represented by characteristics of the atmospheric pressure and geopotential height field, because atmospheric motion responds to pressure and geopotential height gradients. The middle- and upper-tropospheric flow pattern gives indications of whether precipitation in the MMRB and the surface frontal activity that would stir up the GMHZ are likely to be supported or suppressed. More specifically, locations under the “trough-to-ridge” side of the upper-tropospheric Rossby waves will be in favorable positions for storminess, while locations under the ridge or on the “ridge-to-trough” side of the wave will generally be experiencing subsidence that would tend to suppress storminess (Figure 3). The pattern of behavior of long-range atmospheric flow can be represented by atmospheric teleconnection indices.

Teleconnections are long distance correlations of atmospheric flow and/or climatic conditions. The state of a teleconnection in one part of the world can affect

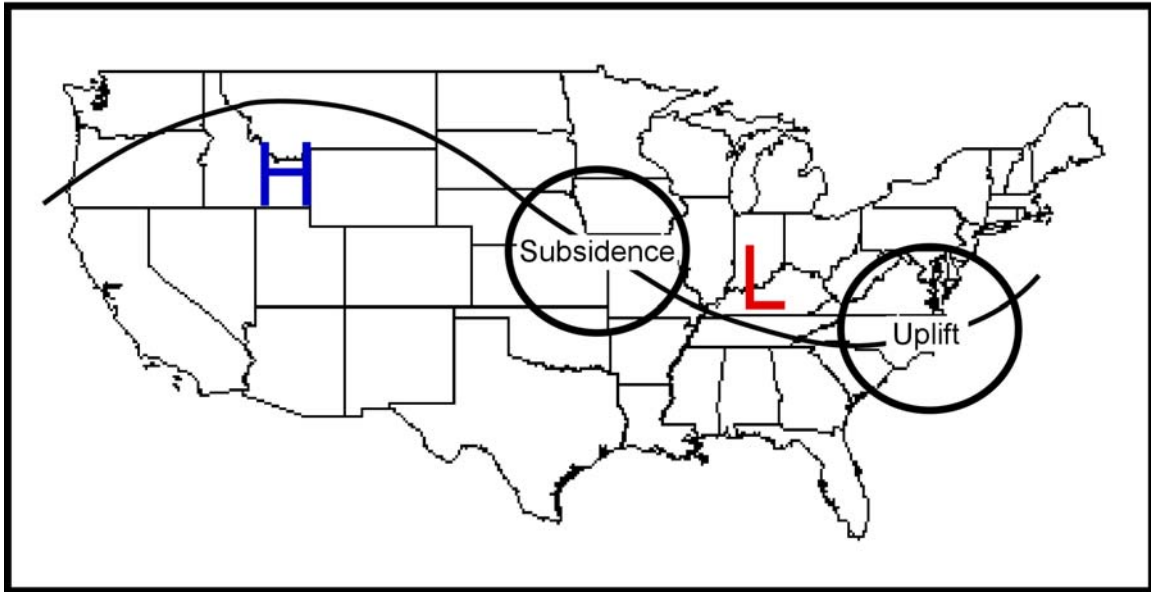


Figure 3: Areas of Subsidence and Uplift in Association with a Hypothetically-positioned Rossby Wave. Storminess will be Suppressed Beneath Areas of Subsidence and Encouraged Beneath Areas of Uplift.

weather globally. For example, the atmospheric component of the El Niño phenomenon, the Southern Oscillation (SO), is known to be related to precipitation variability in parts of the continental U.S (Halpert and Ropelewski 1992). Since precipitation is related to runoff, the variability associated with long-wave atmospheric flow can indirectly impact runoff. As a result, nutrient content and salinity structure at the mouth of a drainage basin may be affected as well (Rabalais *et al.* 2002b).

1.3 Statement of Problem

This research links surface moisture variability identified by the Palmer Drought Severity Index (PDSI) and/or the Palmer Hydrological Drought Index (PHDI) to GMHZ area. It also analyzes the relationships between surface moisture in the MMRB and long-wave atmospheric flow patterns, represented by atmospheric teleconnections. Then, the existing seventeen years of GMHZ data will be compared with various existing indices that have been developed to represent the phase of the teleconnections that explain the greatest amount of variability in the long-wave flow of the atmosphere. Relative contributions of identified sub-regions of the MMRB to the GMHZ extent are then analyzed and a predictive model for estimating the size of the GMHZ will be generated from the PDSI and the PHDI and atmospheric teleconnection indices. Finally, PDSI and PHDI records and teleconnection indices prior to 1985 will be input into the model to hindcast possible historical GMHZ extent since the 1890s (*i.e.*, before GMHZ size was measured) due to natural causes, under the precarious assumption that human impacts (*i.e.*, fertilization, land use, *etc.*) remained constant.

1.4 Hypotheses

The following hypothesis will be tested:

Hypothesis 1. Variability in the area of the GMHZ is related to streamflow in the MMRB.

Hypothesis 2. Moisture indices in the MMRB are related to subsequent GMHZ extents.

Hypothesis 3. Teleconnection indices are related to moisture indices in the GMHZ.

Hypothesis 4. Teleconnection indices are related to subsequent GMHZ extent.

Hypothesis 5. Because of its large contribution to streamflow in the lower Mississippi River basin, atmospheric variability in the Ohio sub-basin is the most important region within the MMRB for explaining variability in the GMHZ.

Hypothesis 6. Teleconnection indices are less effective predictors of the GMHZ extent than the PDSI and/or PHDI because 1) they drive the hydroclimatic variability which drives GMHZ area, thereby reducing the explained variance through multiple correlations; 2) unlike moisture indices such as the PHDI and PDSI, they are unavailable on a near-real-time basis, thereby reducing their short-term predictive value; and 3) unlike moisture indices which are available back to 1895 for the MMRB, most historical teleconnection indices are available only since approximately 1950, thereby reducing their long-term hindcasting value.

Hypothesis 7. The GMHZ can be hindcasted for the 1895-1984 period using “predictive” equations, and years in the past with a large modeled GMHZ will correspond to years when runoff was anomalously high.

1.5 Outline of Thesis

This research will address and test the hypotheses above. Chapter 2 provides background on the MMRB and review literature on atmospheric teleconnections. Chapter 3 describes the data and methods used to address the research hypotheses. Chapter 4 presents results of correlation analysis between the PDSI/PHDI and the various teleconnection indices, both for the spring (*i.e.*, the peak runoff season) and annually. Chapter 5 identifies the results of the predictive model for forecasting the GMHZ area, and Chapter 6 discusses results of the hindcasting. Finally, Chapter 7 summarizes findings and identifies future research questions that must be addressed for a more complete understanding of the relationships between the GMHZ, moisture indices, and atmospheric circulation variability.

CHAPTER 2 BACKGROUND AND LITERATURE REVIEW

In this chapter, the literature that uses moisture indices to assess streamflow variability is reviewed, with particular attention to studies of the United States. Then, specific research on streamflow variability in the MMRB is reviewed. Finally, literature on the most important teleconnections that impact the precipitation variability of the Gulf Coast of the U.S. is reviewed, and research that uses these indices to describe moisture variability is described.

2.1 Moisture Indices

PDSI and PHDI are accepted measures of drought conditions and surface moisture variability. One advantage of using the PDSI and PHDI to evaluate moisture variability is that they are standardized to local climate, for easy comparison in various regions with varying climates (Ntale and Gan 2003, NOAA 2005). The following section first discusses research that used the PDSI to assess historical drought and moisture conditions. Then, research that used the PHDI to assess moisture variability is discussed.

Although the PDSI was established as an indicator of meteorological drought, defined as “a prolonged and abnormal moisture deficiency” (Palmer 1965 p.2), the PDSI has been used to assess agricultural drought, defined as a period when “soil moisture availability to plants has dropped to such a level that it adversely affects the crop yield and hence agricultural production” (Panu and Sharma 2002 p.S21) as well. The specifics of the calculation of the PDSI will be discussed in greater detail in Chapter 3.

The PDSI has been used to evaluate historical drought and moisture conditions throughout the world including southwest Asia (Briffa *et al.* 1994), Europe (Briffa *et al.* 1994), the Pampas region of Argentina (Scian and Donnari 1997), and the southern

prairies of Canada (Nkemdirim and Weber 1999). However, most applications of the PDSI have concentrated on the U.S. Specifically, the PDSI has been used to study many different aspects of U.S. drought, including the forecast of drought severity (Lohani *et al.* 1998) and the reconstruction of historical moisture conditions within the U.S. For example, the PDSI was used to show that the “Dust Bowl” of the 1930s was the most severe drought in the U.S. in the past 300 years (Cook *et al.* 1999). The PDSI has also been used to analyze drought persistence throughout the U.S. (Karl and Koscielny 1982) and to reconstruct the hydrometeorological conditions during the Lewis and Clark expedition (Knapp 2004). Some researchers have coupled the PDSI with the Standardized Precipitation Index (SPI) to evaluate drought, such as in the southwestern U.S. (Velasco *et al.* 2004) and Nebraska (Tadesse *et al.* 2004). Finally, the PDSI has also been used to study relationships between moisture conditions and teleconnection patterns in the U.S. (Yin 1994, Piechota and Dracup 1996, Tadesse *et al.* 2004). The PDSI has also been used in combination with precipitation, streamflow, and teleconnection index data to forecast drought (Panu and Sharma 2002). Changes in PDSI, coupled with changes in precipitation, have been used to forecast streamflow fluctuations (Smith and Richman 1993).

Although extreme measurements of the PDSI correspond well with periods of extreme streamflow departures from normal (Palmer 1965), Guttman (1991) argued that the PDSI cannot be used as a real-time tool for drought monitoring. Because the PDSI was designed as a retrospective index (Guttman 1991), another index based on the PDSI - the PHDI - was created to serve as a real-time tool (Guttman 1991).

The calculations used to create the PDSI are modified to produce the PHDI, which is frequently used to assess hydrologic conditions such as streamflow (Soulé 1992) and to monitor water supply (Panu and Sharma 2002). The PHDI is calculated by comparing climatological means and actual precipitation (Rogers 1993). Values of the PHDI, a measure of hydrological drought defined as a “period during which streamflows are inadequate to supply established uses under a given water-management system” (Linsley *et al.* 1975 p.360), lag behind those of the PDSI both during the beginning and ending stages of meteorological drought (Soulé 1992, Rogers 1993) to provide a low-frequency index of moisture variability. In contrast to the PDSI, the PHDI has been utilized somewhat less frequently, with little work conducted outside the U.S. Most applications use the PHDI to represent long-term (*i.e.*, seasonal) surface moisture conditions. For example, the PHDI has been used to study temporal and spatial variability of historical drought in Ohio (Rogers 1993). Coleman and Rogers (2003) also used the PHDI to evaluate a relationship between the Pacific-North American (PNA) teleconnection pattern (discussed more thoroughly in Section 2.5) and surface moisture variability in the Ohio River basin. The PHDI has been shown to respond to anomalous precipitation and is available for real-time analysis of drought conditions (Guttman 1991). Despite the general paucity of studies that have used the PHDI, this index is explored as a possible variable for predicting the extent of the GMHZ because of the long response time in the vast MMRB.

2.2 Streamflow Variability in the Mississippi-Missouri River Basin

Draining 41 percent of the continental U.S. (LaCoast 2005) and a small part of central Canada, streamflow variability in the MMRB has a significant impact on

discharge into the Gulf of Mexico. Discharge from the Mississippi River averages $470,000 \text{ ft}^3\text{s}^{-1}$ (LaCoast 2005), or $13,300 \text{ m}^3\text{s}^{-1}$, but varies greatly as a result of precipitation variation throughout the MMRB. Increases in streamflow lead to increased stratification, which is needed for the GMHZ to exist (Turner *et al.* 2005).

Several studies have analyzed causal mechanisms for streamflow variability in various sections of the MMRB. For example, Groisman *et al.* (2001) found that variations in the North Atlantic Oscillation (NAO) and SO teleconnections (discussed in more detail below) affect circulation over the U.S. to such an extent that precipitation and therefore streamflow are affected. Throughout the western U.S., including western portions of the MMRB, streamflow variability is highly correlated to both the positive and negative phases of the El Niño/Southern Oscillation (ENSO) (Kahya and Dracup 1994). Specifically, streamflow is above average from December to July in the year following an El Niño event, while from February through July of the year following a La Niña event, streamflow was found to be below average (Kahya and Dracup 1994). In the Ohio basin, winter streamflow variability has been significantly linked to variations in the PNA teleconnection pattern (Coleman and Rogers 2003). Not surprisingly, the identification of these relationships has resulted in the use of teleconnection indices (and also soil moisture) to predict runoff in the MMRB (Maurer and Lettenmaier 2003). In summary, because climate variability has a great impact on hydrology (Neff *et al.* 2000) and annual changes in runoff correspond well to annual changes in precipitation and soil moisture (Groisman *et al.* 2001), these factors are hypothesized to be associated with the GMHZ.

2.3 Climatology of the Mississippi-Missouri River Basin

A significant relationship between climate and water resources has been established in parts of the MMRB (Smith and Richman 1993). Therefore, a review of the climate of the MMRB is necessary. The temperature climatology of the vast MMRB is indeed diverse, and this diversity creates wide-ranging hydroclimatological conditions throughout the year. Of the 146 climate divisions in the 27 states located within the MMRB, North Dakota Division 5 (Figure 2) has the lowest mean monthly temperature of 7.0° F (-13.9°C) in January. The lowest average annual divisional temperature of 40.4°F (4.7°C) occurs in Wisconsin 2. By contrast, the highest average monthly divisional temperature of 83.2° F (28.4°C) occurs in Oklahoma 7 in July, where relatively low latitudes combine with an inland location and frequent presence of moisture to prevent significant nocturnal cooling and create ideal conditions for high average temperatures. The highest mean annual divisional temperature occurs in Louisiana 5 at 66.6°F (19.2°C), where winter temperatures remain relatively high.

Likewise, the range of precipitation across the MMRB contributes to the large differences in the amount of water input into the Gulf of Mexico from the various sub-basins. In general, average annual precipitation increases from the northwest to southeast MMRB (Figure 4) (NCDC 2002). The lowest mean divisional monthly precipitation occurs in Montana 6 with an average February accumulation of only 0.27 inches (0.69 cm). The lowest average annual reading (9.71 inches (24.66 cm) per year) occurs in Wyoming 9. On the other hand, the highest mean monthly divisional precipitation occurs in Mississippi 7 with an average of 6.51 inches (16.54 cm) in March. The maximum

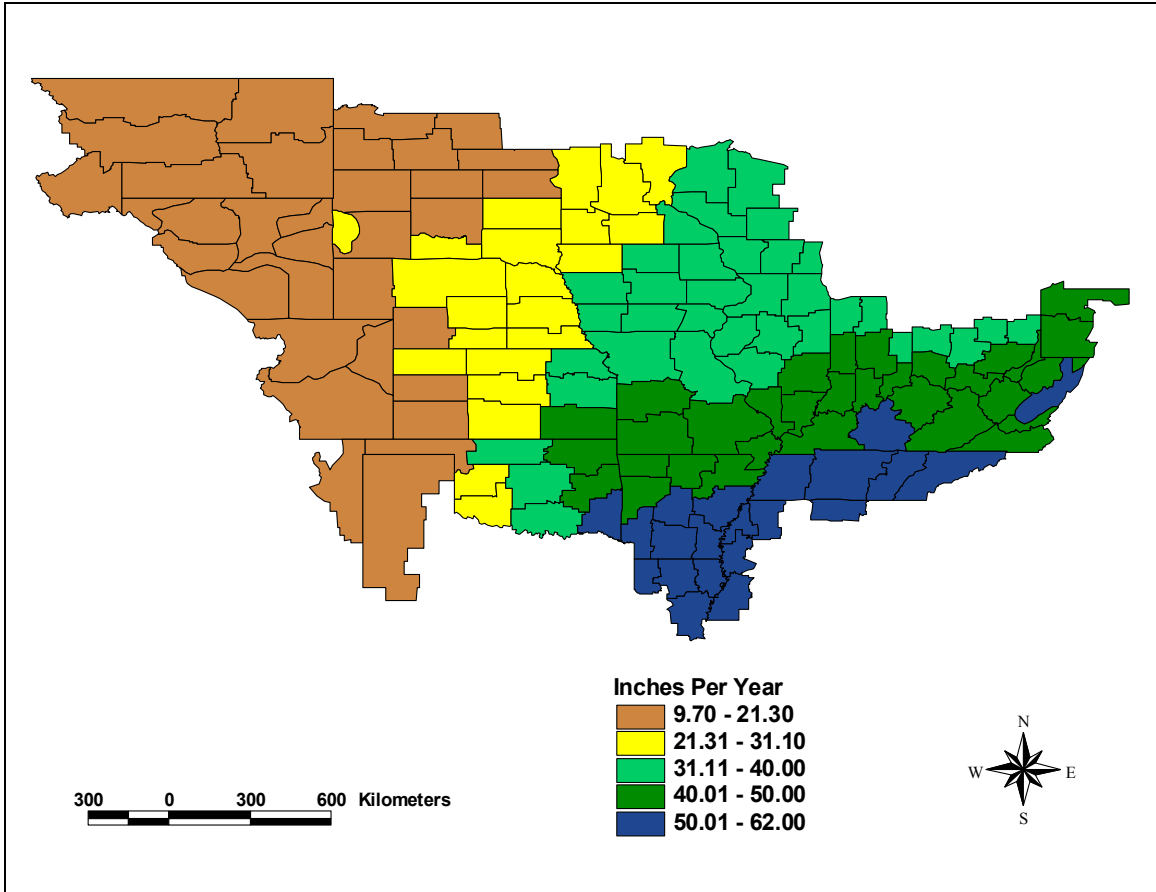


Figure 4: Average Annual Precipitation of the MMRB by Climate Division

mean annual divisional precipitation also occurs in Mississippi 7 at 61.37 inches (155.88 cm) per year.

Record temperatures and precipitation totals in the MMRB are impressive. The highest recorded temperature within the MMRB was 121° F (49°C), which occurred on 6 July 1926 in Steele, North Dakota, within Climate Division 5. The lowest temperature recorded in the region was -70° F (-57°C), which occurred on 20 January 1954 in Rogers Pass, Montana, within Division 4. The record maximum annual precipitation within the MMRB (through 1998) is 114.88 inches (290.02 cm), which occurred in 1957 in Haw Knob, Tennessee, within Division 1 (National Climatic Data Center (NCDC) 2004a). The record minimum annual precipitation is 1.28 inches (3.25 cm), which occurred in 1960 in Lysite, Wyoming, within Division 4 (NCDC 2004b). These extremes can create temperature and precipitation anomalies that can create impressive variability in freshwater input into the north central Gulf of Mexico, and this freshwater input ultimately governs the severity of the GMHZ.

Principal Components Analysis (PCA) has been used along with the PDSI to regionalize the U.S. according to drought and moisture variability (Karl and Koscielny 1982, Yin 1994), as similar analysis has been done for Europe and southwest Asia (Briffa *et al.* 1994). PCA has been used to regionalize streamflow variability in response to ENSO events (Piechota *et al.* 1997), and to evaluate relationships between the various atmospheric teleconnections (discussed more fully in Section 2.5) in the southeastern U.S. (Yin 1994). PCA has also been used to regionalize precipitation and streamflow at the drainage basin scale (Pandzic and Trninic 1991), and to regionalize precipitation

anomalies throughout central and eastern North America and their relationship to anomalies in tropical Pacific sea-surface temperatures (SSTs) (Montroy 1997).

2.4 Historical Variability in the Intensity of the Gulf of Mexico Hypoxic Zone

Hydroclimatic variability can create hypoxia naturally, without any human influence, but often the problem is exacerbated by human influence, particularly in shallow water (Jickells 1997, Vitousek *et al.* 1997). Natural processes, including precipitation and atmospheric circulation, vary the degree of human impact (Carpenter *et al.* 1998, United States Environmental Protection Agency (USEPA) 1999).

A major contributing factor to the problem in the MMRB is that the basin's natural ability to remove nutrients has decreased over time. The loss of freshwater wetlands has been especially problematic in this regard, as states comprising the MMRB have drained and lost 50-80 percent of their wetlands in the past 200 years (USEPA 1999). An additional factor has been large-scale mechanized agriculture resulting from the onset of the Green Revolution. Over the past 200 years, 65 percent of the land in the MMRB has been turned into farmland (Turner and Rabalais 2003). Runoff from this land is a chief source of pollution to rivers throughout the U.S. (Grigg *et al.* 2004).

Nitrogen is believed to exert the greatest influence on algal growth in coastal waters (National Research Council (NRC) 1993), and the concentration determines the type of algal growth (USEPA 1999). The algal growth then tends to cause oxygen reduction. Although many factors exacerbate hypoxia, nitrogen load is the sole factor that can account for its overall magnitude (USEPA 1999). Specifically, nitrates (NO₃) represent the most destructive fertilizer entering the Gulf of Mexico through the MMRB (Grigg *et al.* 2004). Because it is commonly used in the MMRB, is highly soluble in

water, and is easily transported through runoff (Grigg *et al.* 2004), its use has been linked to the GMHZ. Fertilizer use became commonplace in the MMRB beginning in the late 1940s, when the hypoxia problem is believed to have begun in the Gulf of Mexico (Turner *et al.* 2005).

Records indicate that the GMHZ extent has increased as the nitrogen load into the MMRB has increased (Turner *et al.* 2004). Although a reliable, comprehensive inventory on nitrate loadings is unavailable, NO₃ flowing into the Gulf is believed to have increased by 300 percent (Rabalais *et al.* 2002a), increasing to an estimated one million metric tons per year from the 1950s to the late 1990s (USEPA 1999). Agricultural lands in southern Minnesota southward to Iowa and eastward to Ohio contribute the most nitrates to the MMRB (USEPA 1999). Some 90 percent of the NO₃ contributing to the GMHZ is from non-point sources, with an estimated 34 percent coming from the Ohio River basin and 56 percent from above the Ohio River basin (USEPA 1999).

Strong evidence also exists to suggest that freshwater discharge is another important control on GMHZ area (Rabalais *et al.* 2002a). The net effect of climate changes and land use changes has been to increase peak river flows since the 1850s (USEPA 1999). In more recent times, freshwater flow into the Gulf of Mexico has increased 30 percent from the 1950s to the 1990s (Bratkovich *et al.* 1994). Nevertheless, a decrease in MMRB flooding has occurred since the Great Flood of 1927 despite the likely increase in area of the GMHZ since the 1950s as suggested by sediment cores (Rabalais *et al.* 2002a). Human influences on the problem occur in the form of land use changes that affect river flow, including land drainage, flood-control measures, and alteration of navigable streams and canals (USEPA 1999). Three MMRB changes are

most influential in the history of the GMHZ: channels and flood-control mechanisms put in place before the 1950s, deforestation and agricultural drainage peaking in the beginning and the middle of the twentieth century, and an increase in nitrogen-based fertilizers introduced to the MMRB (USEPA 1999). These three activities are believed to have led to the rapid expansion of the GMHZ (USEPA 1999).

Nevertheless, natural climatic variations are also influential to the area of the GMHZ (Justić *et al.* 1997, USEPA 1999). The overriding natural environmental influence on both nutrient loading and freshwater discharge is precipitation. For example, during the drought of 1988, when Mississippi River discharge reached a 52-year low (Justić *et al.* 1997), the area of the GMHZ contracted to 40 km² (Rabalais *et al.* 2004). During the 100-year flood of 1993, when Mississippi River discharge reached a 62-year maximum (Justić *et al.* 1997), the area of the GMHZ doubled from its average size (Rabalais *et al.* 2004).

Sediment core samples taken off the coast of Louisiana identify the major seasonal features of hypoxia in the region. First, the cores show that oxygen levels decrease during the spring with partial recoveries due to wind events (USEPA 1999). The mixing of water prevents stratification, which is necessary for hypoxic conditions to persist (Rabalais *et al.* 2002b). Second, throughout much of the record, hypoxia is persistent from late spring through early fall (USEPA 1999). Third, upwelling occasionally replenishes oxygen supply during the summer (USEPA 1999). Finally, cold fronts and tropical cyclones disrupt the stratification, which leads to hypoxia (USEPA 1999). Sediment cores also identify longer-term features of GMHZ variability, such as

an increase in algae in the area of the GMHZ since the 1950s that coincides with a sharp increase in hypoxia in the area (USEPA 1999).

2.5 Atmospheric Teleconnections

A teleconnection is a long-range correlation in some atmospheric variable (usually pressure or geopotential height because atmospheric motion occurs in response to gradients of these variables). Therefore, teleconnections provide a means for analyzing atmospheric circulation variability. This section will describe the teleconnections that have been shown to represent the greatest variability in surface moisture over the MMRB.

The Southern Oscillation (SO) affects climate globally and operates on a 2-7 year cycle (Halpert and Ropelewski 1992, Hanley *et al.* 2003) and lasts between 6 and 18 months (Mantua 2003). The low- (high-) index phase of the SO is associated with anomalously high (low) SSTs in the central equatorial Pacific and is referred to as a warm (cold) event (Halpert and Ropelewski 1992). During low phases of the SO, referred to as El Niño events in the ocean, the normally-cold waters off the western coast of South America are replaced by relatively warm water from the western Pacific due to the weakening of the easterly trade winds, which allows warm tropical surface water to slosh eastward across the tropical Pacific. In other words, the normally-lower pressure in the western tropical Pacific and higher pressure in the eastern tropical Pacific are reversed during warm ENSO events.

The high-index phase of the SO, known as La Niña, is an intensification of the normal conditions of relatively lower pressure in the western tropical Pacific than in the eastern tropical Pacific. In La Niña events, waters off the coast of South America are

even colder than normal, and the normally-high pressure off the coast of Peru is intensified, as is the normally-low pressure near Indonesia.

The SO Index (SOI) is often used to represent the phase of the oscillation. It measures the standardized sea level pressure (SLP) difference between Tahiti and Darwin, Australia (McGregor and Nieuwolt 1977). Thus, high (low) values of the SOI are associated with cold (warm) events and La Niña (El Niño) oceanic conditions.

In addition to the SOI, the Niño 3.4 Index has been used in recent years to measure anomalies in the state of the SO using SST data (in contrast to pressure, as in the SOI) between 5°N and 5°S latitude and 170°-120°W longitude (Hanley *et al.* 2003, Kousky 2003). This index detects warm phase (or positive anomaly) oceanic events (*i.e.*, El Niño events) at their beginning in late summer (Hanley *et al.* 2003). Both the SOI and Niño 3.4 Indices are available monthly from 1950 through 2003 (Climate Prediction Center (CPC) 2003a, 2003b). The Niño 3.4 Index is also available weekly since 1990 (CPC 2003c).

Although variations in the SOI and Niño 3.4 Index are most noticeable in the tropics, they also impact precipitation in the midlatitudes including the central U.S. (Halpert and Ropelewski 1992, Ropelewski and Halpert 1996, Mauget and Upchurch 1999). Warm events in the eastern Pacific result in unusually strong circulation across the Gulf of Mexico and the Pacific and Atlantic Ocean basins off the U.S. coast (Douglas and Englehart 1981), which affects hydroclimatic surface variables in the U.S. (Kahya and Dracup 1993). Specifically, during El Niño (La Niña) events, winter precipitation is generally above (below) average in most of the southeastern U.S. (Halpert and Ropelewski 1992), particularly in south-central Florida (Douglas and Englehart 1981),

and also in the Gulf of Mexico region between October and March (Ropelewski and Halpert 1986, 1996). A splitting of the polar front jet stream over North America is characteristic of warm events in the central/eastern Pacific, and this bifurcation results in a southern branch that advects moisture from the Gulf of Mexico across the southeastern U.S. on the trough-to-ridge side of the upper-tropospheric Rossby wave. Such a configuration encourages moist air to rise to replace the upper-level air that accelerates on the trough-to-ridge side of the wave in response to the balance of forces created by the upper-level geopotential height gradients.

Further research focused on the mouth of the Mississippi River corroborates this evidence during El Niño (McCabe and Muller 2002) and La Niña (Mauget and Upchurch 1999). During July, August, and September in warm phase events, areas within the Missouri River drainage basin also tend to display anomalously high precipitation, as do areas of Texas, Oklahoma, and Kansas (Mauget and Upchurch 1999). Ropelewski and Halpert (1996) suggested that the SO may also affect precipitation in the Mid-Atlantic states and New England, where winter precipitation tends to be above (below) normal during El Niño (La Niña) (Bradbury *et al.* 2003). Similarly, other research has shown that in the High Plains region, El Niño is associated with above-average precipitation between spring and early fall while below-average precipitation occurs during La Niña summers (Bunkers *et al.* 1996).

By contrast, in the Pacific Northwest region of the U.S., El Niño (La Niña) events are associated with below- (above-) average precipitation (Miles *et al.* 2000). These precipitation anomalies affect the average annual streamflow and timing of streamflow in the Columbia River basin (Leung *et al.* 1999). In addition, a few states in the MMRB

experience drier-than-normal winters during El Niño events, including Montana, Wyoming, Ohio, and Indiana (CPC 2003d).

Some research has used PDSI and climate divisional data to link El Niño events to streamflow anomalies, such as in Washington and Texas (Piechota and Dracup 1996) and in the Gulf of Mexico region, the Northeast U.S., the North Central U.S., and the Pacific Northwest (Kahya and Dracup 1993). The strongest relationships are found in the North Central U.S., which is drier-than-normal during La Niña events as a large upper-level ridge and synoptic-scale subsidence are encouraged during La Niña, and the Pacific Northwest, which is wetter-than-normal during La Niña events in response to increased moisture advection from the Pacific Ocean (Dracup and Kahya 1994). PDSI values tend to have a positive correlation with El Niño events in the central U.S. (Englehart and Douglas 2003).

The Pacific Decadal Oscillation (PDO) is a pattern similar to the SO but varies at time scales ranging from 20-30 years (Mantua 2003). The PDO Index is based on Pacific SST and SLP patterns (Mantua 2003) and is available from 1854 through 2003 (NCDC 2003a). Positive values of the PDO Index, known as warm events, indicate relatively low SSTs in the western and central north Pacific, anomalously high SSTs along the Pacific coast of North America, and below-average SLP over the north Pacific (Mantua 2003).

The climatological impacts of the PDO in North America are similar to those of the SO but less acute (Mantua 2003). The effects of the PDO are most strongly felt in the north Pacific and North America and to a lesser degree in the Tropics (Mantua 2003). The PDO is strongly linked to variability in large-scale precipitation (Nigam *et al.* 1999, Mantua 2003), snowpack (Mantua 2003), and streamflow (Nigam *et al.* 1999, Mantua

2003) in the U.S. PDO variability may also explain negative anomalies in summer precipitation in the U.S. (Mantua 2003).

The PDSI has been used to assess the relationship between drought and the PDO (Englehart and Douglas 2003). The PDO has been linked to summer droughts and streamflow anomalies in the U.S. (Nigam *et al.* 1999). In northwestern North America, warm (cold) phases result in below- (above-) average snowpack and streamflow (Mantua 2003), while in the southwestern U.S., warm (cold) phases are associated with above- (below-) average snowpack (McCabe and Dettinger 2002). These patterns generally correspond well with expected and observed patterns during El Niño events.

In addition to the SO and the PDO, the Pacific-North America (PNA) teleconnection is known as a major influence on atmospheric variability in the U.S. (Rodionov 1994). The PNA pattern is represented by a standardized index that identifies zonal versus meridional anomalies in the typical 700 hPa western ridge and eastern trough over the North American midlatitudes by using a combination of normalized height anomalies at four centers: near Hawaii, the north Pacific, Alberta, and the Gulf Coast (Wallace and Gutzler 1981). Positive (negative) PNA Index values are associated with an intensified (weakened) Aleutian Low (Wallace and Gutzler 1981), anomalously intense (weak) ridging over northwestern North America, and anomalously intense (weak) troughing over the Gulf Coast.

Average monthly climatic conditions in particular regions are heavily influenced by changes in the PNA pattern (Wallace and Gutzler 1981). For example, in the upper MMRB, positive (negative) PNA values are associated with a decrease (increase) in precipitation (Leathers *et al.* 1991). When the PNA Index is positive, decreased

precipitation totals tend to occur in the Upper Mississippi River and Ohio River valleys (Leathers *et al.* 1991). Negative PNA Index values are associated with increased precipitation in the same areas due to an increase in Gulf of Mexico moisture in the region (Leathers *et al.* 1991). Moreover, the interannual variability of the western ridge and eastern trough is reflected in precipitation and stream discharge (Keables 1988), particularly in combination with the SOI (Kahya and Dracup 1993), such as in the Ohio River valley, where stream discharge in the area can double during negative PNA winters as opposed to positive PNA winters (Coleman and Rogers 2003). In the Upper Mississippi River valley, positive (negative) PNA values are associated with below-(above-) average precipitation (Keables 1988). Peak correlation between the PNA and precipitation is found in southern Indiana, making it one of the strongest correlations in the northern hemisphere (Coleman and Rogers 2003).

The PNA pattern is most influential to MMRB hydroclimatology in the cold half of the year, when frontal precipitation dominates (Rodionov 1994). Frontal precipitation is largely governed by the trough-to ridge side of the longwave Rossby waves (Figure 3), where the upper-level divergence that supports surface lifting is encouraged. By contrast, summer convective precipitation can occur in the absence of appropriate upper-level support. PNA Index values are available from 1950 through 2003 (CPC 2003e).

The North Atlantic Oscillation (NAO) is another teleconnection that influences North American climate (Thompson and Wallace 2001, Gershunov and Cayan 2003). The NAO is measured by a standardized index with values available monthly from 1950 through 2003 (CPC 2003e). The index is based on surface temperatures and SLP (Wallace and Gutzler 1981) between Ponta Delgadas, Azores, and Akureyri, Iceland

(Rogers 1984, Lamb and Pepler 1987). Positive NAO values represent a strong Icelandic Low and anomalously high pressure at 40°N over the Atlantic Ocean (Wallace and Gutzler 1981). This combination produces strong westerly winds in the North Atlantic (Wallace and Gutzler 1981). Positive values are related to above-normal temperatures in the eastern U.S. (Wallace and Gutzler 1981). The oscillation varies at several temporal scales from intraseasonal to interdecadal (Gershunov and Cayan 2003). The westerly winds associated with the NAO retreat northward in summer and extend southward in winter (Barnston and Livezey 1987) and the NAO itself is prevalent in winter, spring, and summer (Rogers 1984, Rogers 1990).

The Arctic Oscillation (AO) is closely related to the NAO (Ambaum *et al.* 2001) and also measures SLP anomalies north of 20°N latitude (Wallace *et al.* 2000). Similar to the NAO, the AO is a fluctuation of SLP between the Arctic and midlatitudes (Thompson and Wallace 1998, Rogers and McHugh 2002). Positive (negative) AO Index values are indicative of anomalously low (high) SLP over the polar region and anomalously high (low) SLP near 45°N latitude (Buermann *et al.* 2003). In the positive (negative) phase, the AO brings warm and wet (cold and dry) conditions to the interiors of North America and Europe (Buermann *et al.* 2003). The AO exerts a significant influence over the climate of the northern hemisphere (Buermann *et al.* 2003). Outside the tropics, the AO explains 35-48 percent of precipitation variability over land (New *et al.* 2001). Similar to other teleconnections, the AO has its greatest impact on climate in winter months (Buermann *et al.* 2003). The AO Index is available monthly from 1950 through 2003 (CPC 2003f).

Teleconnections often work together to have synergistic impacts. For example, a consistent negative PNA Index coupled with a cold phase of the SOI is strongly related to high streamflow in the Tennessee and Ohio River valleys, which in turn affects streamflow in the Lower Mississippi valley (Rogers and Coleman 2003). In addition, the phase of the PDO can enhance conditions characteristic of the phases of the SO (Bradbury *et al.* 2003). The combination of a warm phase in the SOI and a positive PDO are suspected to have broken patterns of drought in the 1930s and 1950s (Mauget 2003). By contrast, the synergistic effects of a cold-phase SO and negative PDO in the late 1940s to 1950s suggest a relationship with severe drought (Mauget 2003). In the Pacific Northwest, El Niño (La Niña) events coupled with a positive (negative) PDO phase have been linked to dry (wet) winters (springs) (Miles *et al.* 2000).

2.6 Summary

This chapter explored literature that used the PDSI and PHDI to research moisture variability both within the MMRB and elsewhere. The research on streamflow variability and its relationship to surface moisture and climate variability throughout the study region was also explored. Next, the climatology of the MMRB was presented. Then the use of PCA in moisture variability research was reviewed and the historical variability in the intensity of the GMHZ was discussed. Finally, teleconnections that impact the MMRB were reviewed.

Chapter 3 will describe the data, including precipitation, PDSI, PHDI, and teleconnection indices, and methods used to test the research hypotheses presented in Chapter 1.

CHAPTER 3 DATA AND METHODS

The quality of any empirical research project rests squarely upon the data and methods upon which it is based. This chapter will describe the data and methods used to test the research hypotheses listed in Chapter 1, while relying on the theoretical basis for those hypotheses detailed in Chapter 2.

3.1 Data

The study area (Figure 2) consists of the 146 climate divisions in the 27 states located within the MMRB. Although the MMRB does include a small part of Canada's Prairie Provinces, the analysis only includes the part of the basin within the U.S. The climate divisions are included in this analysis if at least half of the geographical area of the division is located within the MMRB. Thus, several climate divisions along the outer rim of the MMRB are excluded from this study because the majority of the divisional moisture does not affect the MMRB. These climate divisions have been used in previous studies to represent the MMRB (Hoff 1994). The climate division is chosen as the unit of analysis because of the utility that it affords for studying long-term hydroclimatic trends and anomalies in the U.S. Specifically, climate divisional data have temporal and spatial continuity since 1895, and the spatial and temporal scale seem appropriate when creating customized regions, including drainage basins (Guttman and Quayle 1996). The drawbacks of using divisional data include potential inaccuracies due to human error and movement of stations (Guttman and Quayle 1996, Keim *et al.* 2005), but such errors are more likely to be ameliorated through the use of a divisional approach rather than a point-based approach. In addition, divisional data provide a spatial extent that would not exist with a gridded data set. Indeed, the divisional precipitation dataset represents the

highest-quality data available that would be suitable for the scale of analysis attempted here.

Prior to 1931, monthly precipitation was calculated by averaging statewide or regional figures (Mauget 2003). Figures are currently calculated using the arithmetic mean of precipitation totals from each available station within a given climate division (Mauget 2003). The precipitation input is used in conjunction with algorithms for computing evapotranspiration to create a water balance approach, based on Thornthwaite's (1948) water balance, for estimating surface moisture. Indeed, water balance-calculated runoff may be a more important predictor of GMHZ extent than the more easily-measured precipitation. The use of a drought index based on the water balance is advantageous because it utilizes the effects of both temperature and precipitation on evapotranspiration, soil moisture, and runoff (Alley 1984). The PDSI is one such index that is often used to study intensity, variability, and the spatial extent of drought (Englehart and Douglas 2003) and other environmental moisture analyses (Karl 1986). The PDSI will be used as a proxy for runoff, and like precipitation, monthly divisional PDSI data are available for the study area from 1895 to 2003 (NCDC 2003b).

The PDSI is calculated using divisional monthly averages for the water balance parameters (Palmer 1965, Guttman 1991, Guttman and Quayle 1996). Guttman (1991) described Palmer's (1965) equation as:

$$Z_i = k(P - \alpha PE - \beta PR - \gamma PRO + \delta PL)$$

where k is a weighting factor to allow spatial comparison, P represents actual precipitation, PE is potential evapotranspiration, PR represents potential recharge, PRO is

potential runoff, and PL is potential loss of soil moisture. The coefficient of α is for evapotranspiration, β is for recharge, γ is for runoff, and δ is for loss.

The index is then scaled so that values between 0.5 to -0.5 indicate normal conditions, -0.5 to -1.0 represent a slight drought, -1.0 to -2.0 indicate mild drought, -2.0 to -3.0 suggest moderate drought, -3.0 to -4.0 represent severe drought, and less than -4.0 indicate extreme drought (Barlow *et al.* 2001). Opposite conditions (*i.e.*, positive departures from zero) correlate to the same severity of wet conditions (Barlow *et al.* 2001). The PDSI standardizes values due to variations in local climates and seasonal changes so that values may be easily compared across space and within a certain space across time (Barlow *et al.* 2001). For example, a value of zero in a particular division represents “average” moisture conditions for that place at that time of year. Thus, a value of zero in Arizona would represent a different degree of soil moisture than a value of zero in Louisiana.

As a meteorological drought index, the PDSI responds relatively quickly to changes in weather trends (NCDC 2003c) independent of soil moisture levels (Guttman and Quayle 1996). In addition, wet winters affect the PDSI more so than dry ones (Coleman and Rogers 2003). The divisional PDSI provides a set of 146 potential independent variables that can be used in a lag correlation to derive a predictive model of GMHZ extent.

In addition to the PDSI, the PHDI is also used to assess moisture conditions. In contrast to the PDSI, the PHDI is a hydrological drought index rather than a meteorological drought index (NCDC 1994). The key difference between the PHDI and the PSDI is that the PHDI does not change from a negative to a positive value until 100

percent of the moisture needed to end a dry spell is received and the normal moisture demand is met (Karl 1986). PDSI values will change from a negative to a positive value in the first month that any amount (*i.e.*, one percent to 99 percent) of the moisture needed to end a drought returns (Karl 1986). Therefore, the PDSI may signal the end of a drought when returning precipitation may only be temporary (Karl 1986). By contrast, the PHDI requires more time to return to normal range than does the PDSI.

The scale used to measure drought with the PHDI is similar to that of the PDSI with PHDI values between 0.5 to -0.5 indicating normal conditions, -0.5 to -1.0 representing a slight drought, -1.0 to -2.0 suggesting mild drought, -2.0 to -3.0 representing moderate drought, -3.0 to -4.0 indicating severe drought, and less than -4.0 suggesting extreme drought (NCDC 1994). Opposite conditions (*i.e.*, positive departures from zero) correlate to the same severity of wet conditions (Barlow *et al.* 2001). Both scales range in values from -7.0 to 7.0 with most values ranging between -6.0 to 6.0 (NCDC 1994). The PDSI and PHDI are both well-accepted as measures of surface moisture conditions by climatologists (Karl and Koscielny 1982, Alley 1984, Soulé 1992, Rogers 1993, Briffa *et al.* 1994, Yin 1994, Piechota and Dracup 1996, Lohani *et al.* 1998, Cook *et al.* 1999, Panu and Sharma 2002, Knapp 2004, Tadesse *et al.* 2004, Velasco *et al.* 2004).

In addition to the PDSI and PHDI data, a possible correlation between GMHZ area and longwave atmospheric flow patterns will be examined using six monthly teleconnection indices: the SOI (CPC 2003c), the Niño 3.4 Index (CPC 2003b,d), PDO Index (NCDC 2003a), PNA Index (CPC 2003e), the NAO Index (CPC 2003e), and the AO Index (CPC 2003f). These indices were selected because they are known to

represent the major modes of variability in atmospheric pressure and/or geopotential height, and therefore they are associated with significant variability in regional to hemispheric flow. Thus, the two moisture indices at 146 climate divisions plus the six teleconnection indices provide a pool of 298 potential independent variables for predicting GMHZ extent.

Although divisional PDSI and PHDI data are available since the early 1900s, the upper-level data from which many of the teleconnections are derived are only available since 1950 when upper-level observations commenced, except that the PNA pattern is undefined for June and July. Therefore, if the derived model requires such teleconnection indices, the estimated area of the GMHZ can be reconstructed only back to 1950. However, if the teleconnection indices fail to appear as independent variables in stepwise multiple regression models, then GMHZ extent may be reconstructed back to the late 1800s.

Data for the predictand variable, GMHZ area, are available from 1985-2003, with the exception of 1989 (Table 1, Rabalais *et al.* 2004). These data were collected by scientists from the Louisiana Universities Marine Consortium and the School of the Coast and Environment at Louisiana State University during five-day mapping cruises in July (Rabalais *et al.* 2004), near the time of peak GMHZ extent (Justić *et al.* 1996, Rabalais *et al.* 2002b). One drawback of using these data is that mapping of the GMHZ is sometimes incomplete due to time constraints or shallow waters near the coastline (Rabalais *et al.* 2002b). Measurements may also be incomplete either offshore or on the western side of the GMHZ (Rabalais *et al.* 2002b). Another drawback is the limited amount of data available. Because of the limited spatial and temporal coverage of the data, caution

should be exercised in the interpretation of results. Despite these limitations, the GMHZ data collected by Rabalais *et al.* (2004) represent the only source of information of its kind and therefore is an indispensable source for analysis.

Table 1: GMHZ Surface Area

Year	GMHZ surface area (km ²)
1985	9774
1986	9432
1987	6688
1988	40
1989	No data
1990	9260
1991	11920
1992	10804
1993	17600
1994	16600
1995	18200
1996	17920
1997	15840
1998	12480
1999	20000
2000	4400
2001	20720
2002	22000
2003	8560
2004	15040

(Source: Rabalais *et al.* 2004)

Even though previous research suggests a relationship between Mississippi River streamflow and GMHZ surface area, correlation analysis between these variables is also performed here, using discharge data from records collected by the U.S. Army Corps of Engineers at Vicksburg and the most updated GMHZ data. The Vicksburg site has the most consistent data set in the southern portion of the study area and is located north of the Mississippi River – Atchafalaya basin diversion (Turner and Rabalais 2003). Also, a minimal number of climate divisions in the study area are located downstream of

Vicksburg. Using streamflow records farther south in Louisiana would represent precipitation from areas outside of the MMRB, as defined in this analysis.

3.2 Methods

Correlations between monthly discharge from the Lower Mississippi River at Vicksburg and the July surface area of the GMHZ are calculated based on monthly streamflow totals from each of the months leading up to the July GMHZ (January through July) for the available period of record (1985 to 2003). Next, possible relationships between moisture indices, teleconnection indices, and GMHZ surface area are investigated using Pearson correlation analysis. Specifically, climate divisional monthly PDSI values throughout the year are correlated with monthly teleconnection index values for the 1950 – 2003 period of record to identify possible relationships between surface moisture variability in the MMRB and low-frequency, long-wave atmospheric flow. A special focus on the spring months is important because spring is the high-flow season which would presumably contribute most to the discharge in the July-measured GMHZ. Climate divisions found to be significantly correlated to individual teleconnection indices at the $\alpha \leq 0.05$ level are mapped using ArcView GIS 3.3. These steps are then repeated using only spring values, and then by substituting climate divisional monthly PHDI values for PDSI values. The resulting maps are overlaid with maps of the MMRB sub-basins, including the Arkansas–White–Red River (hereafter referred to as the Arkansas River for simplicity), Lower Mississippi, Missouri, Ohio, Tennessee, and Upper Mississippi River basins (Figure 5), to evaluate a relationship between atmospheric variability and surface moisture in each of the MMRB sub-basins. Pearson correlations between the monthly PDSI and PDHI vs.

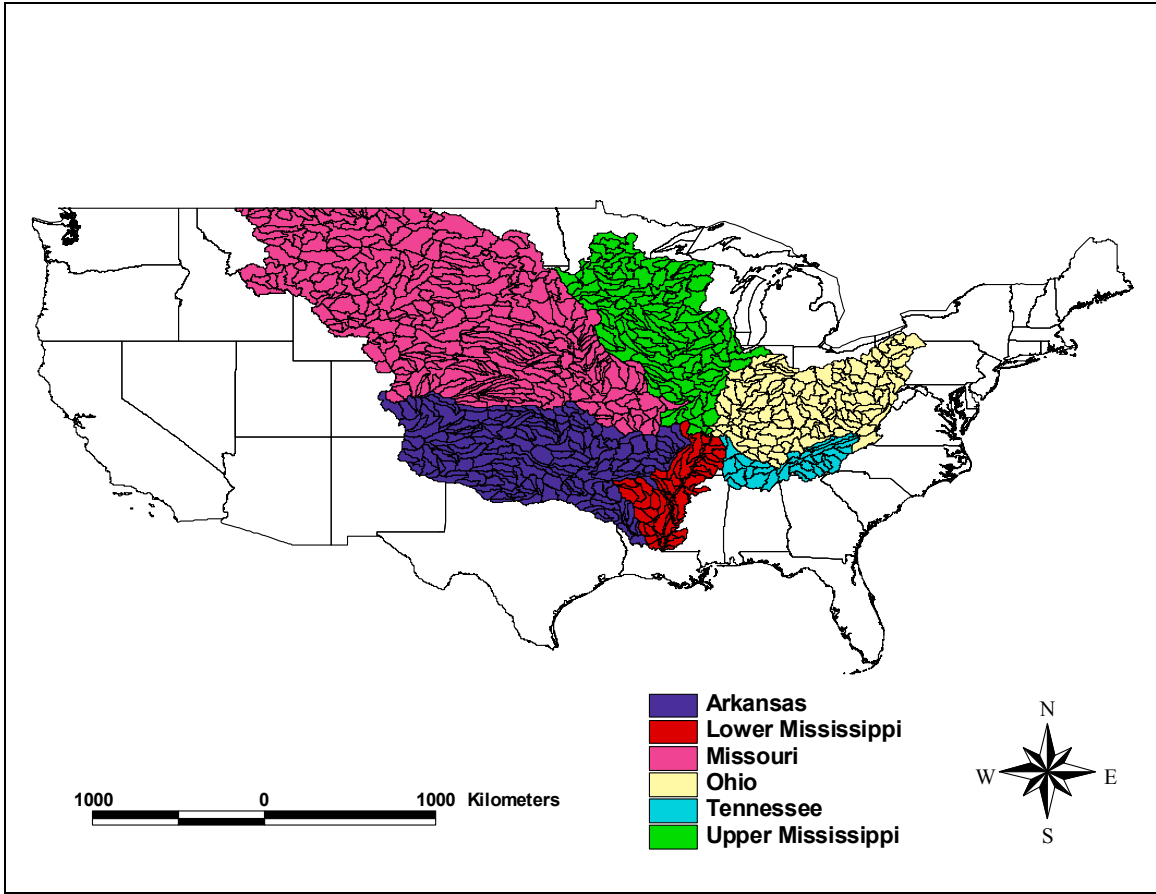


Figure 5: MMRB Sub-basins

GMHZ are calculated based on the 1985 – 2003 period of record and mapped in the same manner as the correlations found between the moisture and teleconnection indices.

Correlations between GMHZ and monthly stream discharge are calculated for 1985 – 2003 through July since discharge in July at Vicksburg and GMHZ are closely related. However, analysis of correlations between PDSI/PHDI and GMHZ end in June to account for the lag time between soil moisture and runoff. To measure the average monthly stream discharge at Vicksburg, daily measurements were averaged for each month from 1985 to 2004. July results should be used with caution since some of the July data will have been collected after GMHZ measurements are made.

Rotated principal components analysis (RPCA) is performed on spring and early summer (March, April, May, and June) PDSI values for the 1895 to 2003 period to identify the most homogeneous surface moisture variability regions. Although Yarnal (1993) recognizes that regionalizations may utilize oblique rotation algorithms, the orthogonal varimax rotation procedure is selected to ensure that no shared variance exists among the components. Then, the MMRB is regionalized in the same manner using spring PHDI values. Using ArcView GIS 3.3, climate divisions loading most highly on each component are mapped, and the resulting maps are also overlaid with maps of the MMRB sub-basins.

Predictive models for the July GMHZ zone are then created using monthly PDSI and PHDI values for the 1985 – 2003 period. To find the longest possible lead time, stepwise multiple regression analyses are conducted to identify the climate divisions that represent the strongest predictors of the surface area of the July GMHZ during each of the four months leading up to the annual measurement. Indices of the SO, Niño 3.4,

PDO, NAO, AO, and PNA patterns are then entered into another stepwise multiple regression equation to predict GMHZ size based only on the teleconnections.

This chapter has described the data sources and methods undertaken to test the hypotheses presented in Chapter 1. In Chapters 4, 5, and 6, results of the tests of these hypotheses, using the data and techniques presented in this chapter, will be described.

CHAPTER 4

RESULTS: SURFACE MOISTURE VARIABILITY AND THE GULF OF MEXICO HYPOXIC ZONE

The PDSI and PHDI are important in this research because they are used as surrogates for surface moisture. Variability in this surface moisture is hypothesized to be related to the surface area of the GMHZ. Therefore, this chapter describes the results of testing of hypotheses presented in Chapter 1 that relate to the role of soil moisture in the GMHZ.

4.1 Streamflow in the Mississippi-Missouri River Basin and the Gulf of Mexico Hypoxic Zone

According to Hypothesis 1, streamflow from the mouth of the Mississippi River is correlated with GMHZ area. A simple Pearson correlation analysis suggests that streamflow in May and June is significantly correlated to the area of the July GMHZ at $\alpha \leq 0.05$ (Table 2). Although the GMHZ is measured in July, Mississippi River streamflow in July does not show a significant correlation to the GMHZ at $\alpha \leq 0.05$. This may be because the time of measurement is typically mid- to late July and some of the streamflow readings are taken after the GMHZ measurements. Of course, the rather small number of years invites caution in the interpretation of the results. Nevertheless, because these results corroborate those found by Rabalais *et al.* (1996) and Justić *et al.* (1993), it seems safe to conclude that Mississippi streamflow is significantly positively correlated with the GMHZ, perhaps with a lag of up to one or two months in spring.

4.2 Correlations between Moisture Indices and the GMHZ

Since it is established that the streamflow is significantly related to the GMHZ, the hypothesis that moisture variability in the MMRB exerts a significant influence on the area of the GMHZ can be tested. To test the hypotheses, simple Pearson correlations

between the monthly PDSI and PDHI by climate division *vs.* GMHZ are implemented. Spring and early summer (MAMJ) drought indices are used in the correlation since soil moisture levels during July will not have a great impact on July measurements of the GMHZ. Of the 146 climate divisions in the analysis, 106 show a significant positive relationship ($\alpha \leq 0.05$) between monthly MAMJ PDSI and the area of the GMHZ (Figure 6). Two climate divisions, OK1 and TX1, show a significant negative relationship ($\alpha \leq 0.05$) between MAMJ PDSI and GMHZ.

Table 2: Correlations between Mississippi River Streamflow and July GMHZ Area

Streamflow Months	Correlation to July GMHZ
January - June	0.29807 $p = 0.0014$
January	-0.07699 $p = 0.7541$
February	0.37549 $p = 0.1131$
March	0.13954 $p = 0.5688$
April	0.21951 $p = 0.3666$
May	0.63576 $p = 0.0061$
June	0.61435 $p = 0.0051$
July	0.30807 $p = 0.1994$

A significant positive relationship (at $\alpha \leq 0.05$) between MAMJ PHDI and the area of the GMHZ exists for 94 of the 146 climate divisions within the MMRB (Figure 7). Four climate divisions, CO4, OK1, OK2, and TX1 show a significant negative relationship at $\alpha \leq 0.05$ between MAMJ PHDI and GMHZ. These four divisions are located in the Arkansas basin (Figure 7), as are those showing a negative relationship between PDSI and GMHZ.

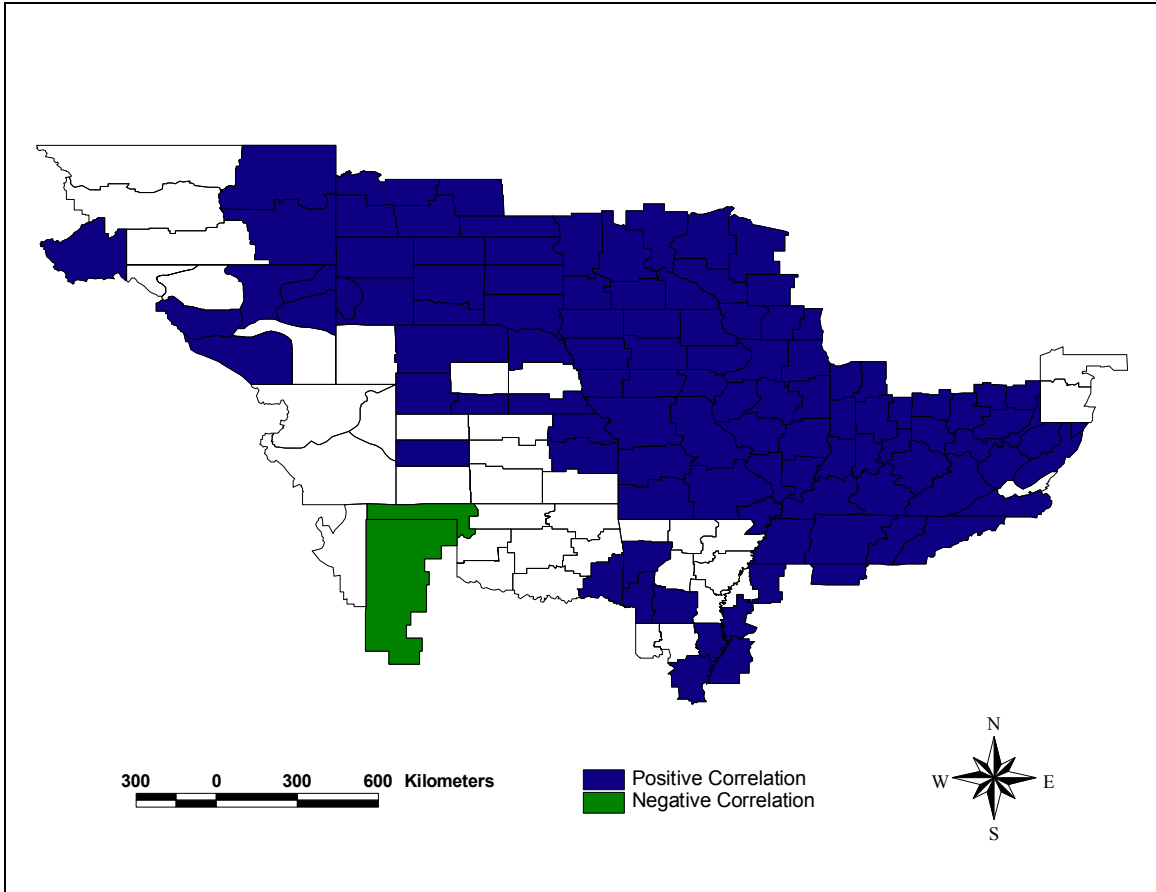


Figure 6: MAMJ PDSI and GMHZ Correlations ($\alpha \leq 0.05$)

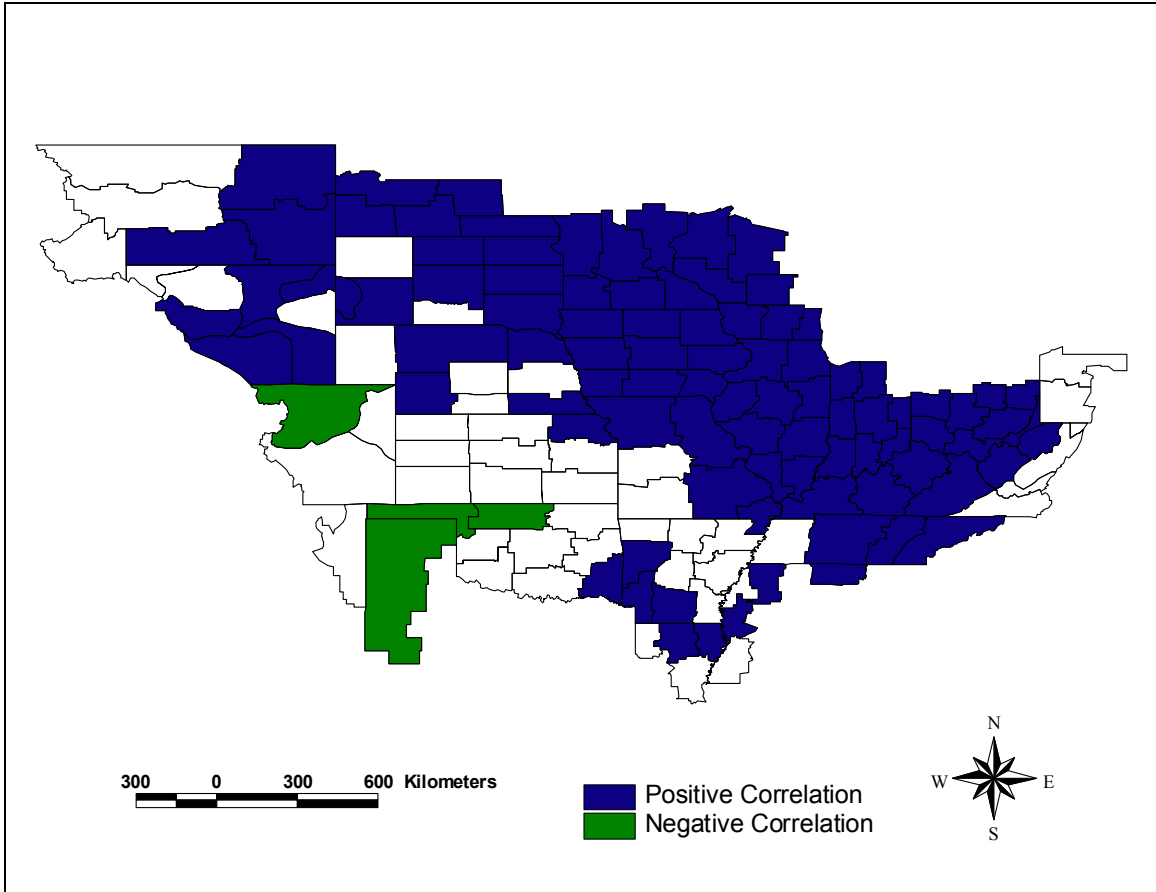


Figure 7: MAMJ PHDI and GMHZ Correlations ($\alpha \leq 0.05$)

The most fundamental result is that the spatial pattern of correlations is nearly identical when the two moisture indices are correlated with GMHZ extent. Collectively, these results suggest that soil moisture in the majority of the MMRB has a significantly positive relationship with the GMHZ area, particularly in the entire Upper Mississippi, Tennessee, and most of the Ohio basin. Much of the Missouri basin also shows a significantly positive relationship with the GMHZ area, though clearly not the entire basin is significantly correlated. Only some climate divisions in the Lower Mississippi basin show a significant positive correlation with the GMHZ area. Although a few climate divisions in the Arkansas basin show a significantly positive relationship with the GMHZ area, this is the only basin showing significantly negative relationships with the GMHZ.

4.3. Correlations in the Annual Cycle between Monthly Teleconnection Indices and the Monthly Palmer Drought Severity Index

In Chapter 1, Hypothesis 3 suggests a possible relationship between monthly teleconnection indices and surface moisture in the MMRB. To test this hypothesis, the six monthly teleconnection indices were correlated with the monthly PDSI values for each of the 146 climate divisions within the MMRB for each month of the year from 1950 to 2003. The purpose is to examine the geography of any significant relationships because these regions may identify the locations where surface moisture is most sensitive to atmospheric variability. Figure 8 shows that throughout the year, SOI is positively correlated with surface moisture at $\alpha \leq 0.05$ in 13 climate divisions, mostly within the Ohio River basin from Kentucky to Pennsylvania and also within a small portion of the Tennessee River basin. Thus, the El Niño phase is associated with dry surface conditions

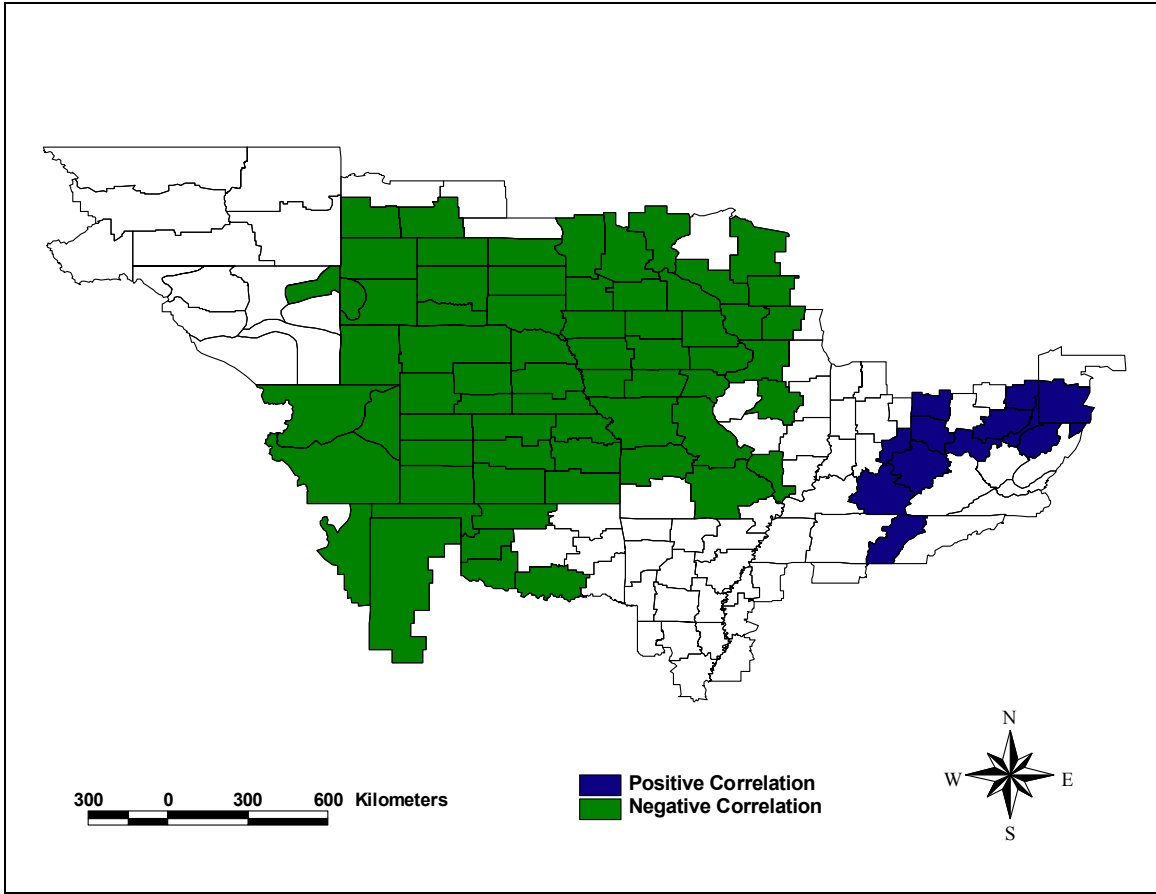


Figure 8: Monthly SOI Correlations (January – December) with PDSI ($\alpha \leq 0.05$) in the Annual Cycle

and the La Niña phase is linked to wet conditions in this extreme eastern part of the study region. On the other hand, the SOI shows a significant negative relationship in the annual cycle with the PDSI over a much larger region, including 66 climate divisions within the Upper Mississippi, southeast Missouri, and northwest Arkansas River basins (Figure 8). This result confirms to that of Mauget and Upchurch (1999) for July, August, and September. Thus, for the annual cycle, El Niño conditions (as evidenced by the SOI) seem to be associated with more runoff over most of the study area, but in regions that contribute relatively less to the runoff into the Mississippi River. By contrast, La Niña conditions tend to be linked to anomalously high runoff in a smaller portion of the MMRB, but in areas that contribute relatively high amounts of runoff to Mississippi flow past the mouth. Therefore, the hypothesis that teleconnection indices are related to drought indices in the MMRB is partially supported by the SOI results.

Expectedly, the annual Niño 3.4 Index shows a positive relationship to the PDSI in very similar locations where the annual SOI relationships to PDSI are negative (Figure 9). PDSIs in 89 climate divisions show a positive association ($\alpha \leq 0.05$) with this teleconnection index, and these divisions are located across the entire MMRB, particularly in the same areas where SOI are strongest, in addition to the Lower Mississippi basin and southwestern Virginia (Figure 9). Figure 9 also suggests that the annual Niño 3.4 Index shows a significant ($\alpha \leq 0.05$) negative relationship with ten climate divisions largely within the Ohio basin, but also small portions of the Missouri and Tennessee River basins. Of course, the calculation of each correlation involves a five percent chance of making a Type I error, so it is possible that some or all of the isolated

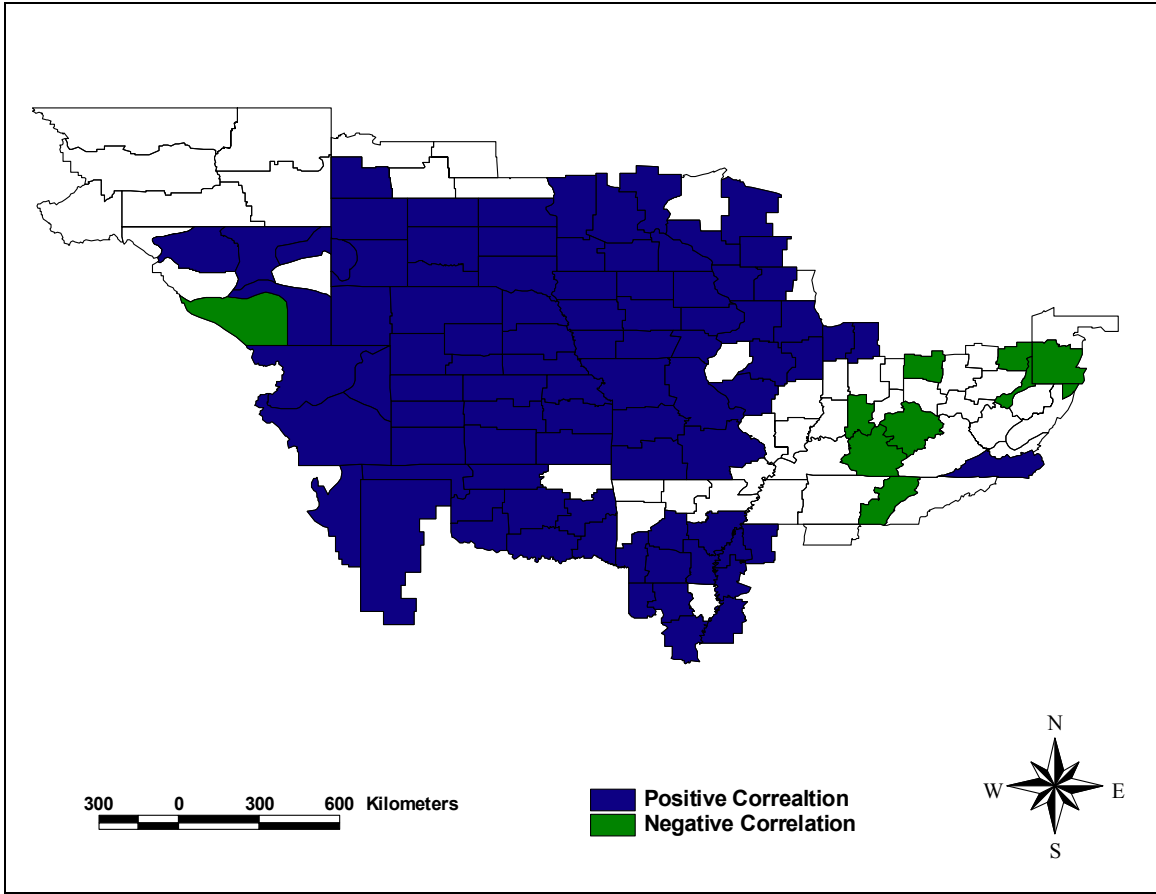


Figure 9: Monthly Niño 3.4 Correlations (January – December) with PDSI ($\alpha \leq 0.05$) in the Annual Cycle

pockets of significant correlations, such as southwestern Virginia, are spurious.

However in general, these results support the hypothesis that teleconnection indices are related to drought indices in the MMRB.

Because the PDO represents similar SST anomalies as ENSO, it is not surprising that the annual PDO index shows a significant ($\alpha \leq 0.05$) positive relationship with 75 climate divisions scattered throughout the MMRB. These divisions are largely located within the Arkansas, Missouri, and Upper Mississippi basins, but also in the Lower Mississippi and Ohio basins (Figure 10). The annual PDO index displays a significant ($\alpha \leq 0.05$) negative correlation with nine climate divisions scattered throughout the northwest Missouri, Lower Mississippi, Tennessee, and Ohio River basins (Figure 10). Again, this spatial pattern is a very similar to that for the Niño 3.4. Likewise, in cases where the Niño 3.4 and the PDO are both in synchrony (*i.e.*, both positive or both negative), the intensity of the moisture anomaly may be magnified in the locations affected, but the insufficient number of observations makes this hypothesis difficult to test.

The annual AO Index displays a significant ($\alpha \leq 0.05$) positive relationship with PDSI in 17 climate divisions within the Upper and Lower Mississippi, Ohio, and (especially) Tennessee basins (Figure 11). Thus, when the northern hemispheric circumpolar vortex is constricted poleward (expanded equatorward), conditions are anomalously wet (dry) in these locations. This result is logical because the positive phase of the AO is associated with moist air advecting into the interior of continents (Buermann *et al.* 2003). By contrast, the annual AO Index shows a significant ($\alpha \leq 0.05$) negative relationship with PDSI in 17 climate divisions within the western Upper

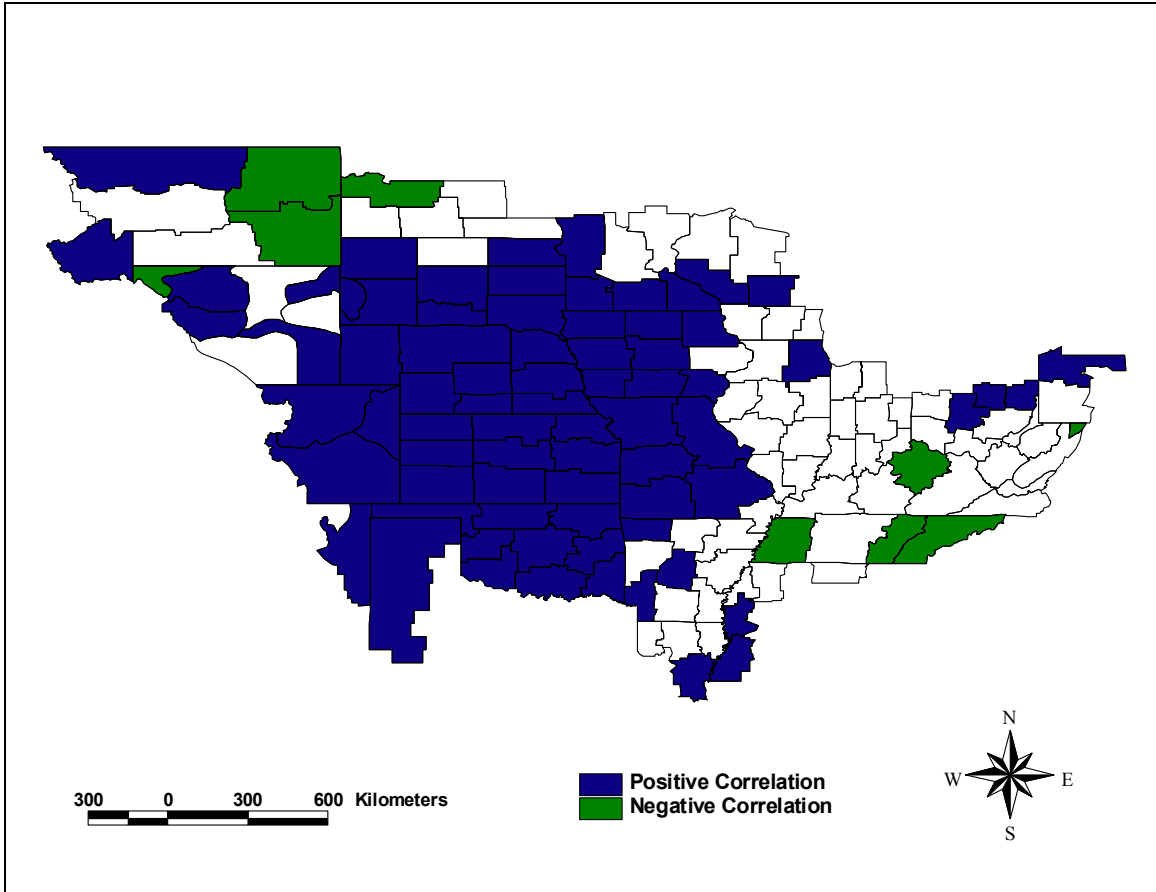


Figure 10: Monthly PDO Correlations (January – December) with PDSI ($\alpha \leq 0.05$) in the Annual Cycle

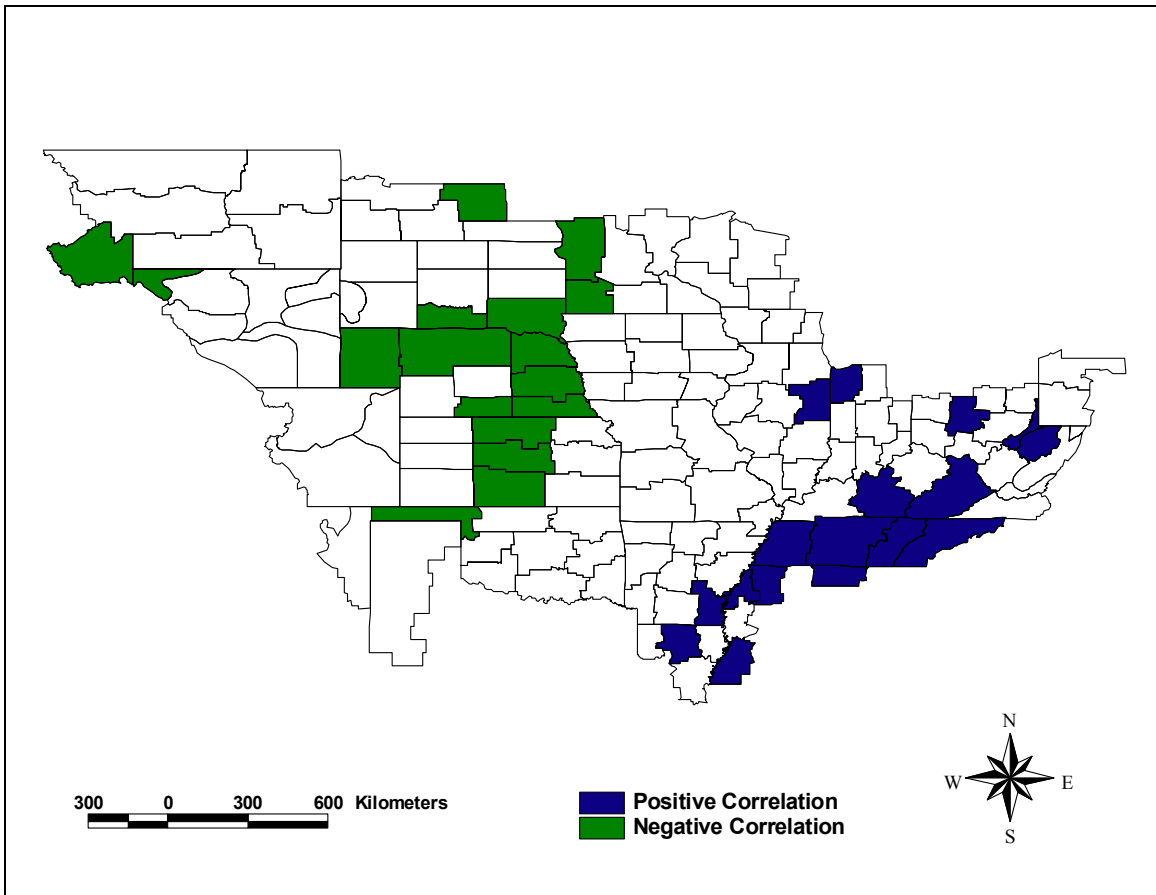


Figure 11: Monthly AO Correlations (January – December) with PDSI ($\alpha \leq 0.05$) in the Annual Cycle

Mississippi, Missouri, and north-central Arkansas River basins (Figure 11) perhaps because these locations are too continental to experience moisture advection during positive AO phases.

Interestingly, despite the fact that the NAO and the AO are intricately associated, the NAO Index does not show a significant positive correlation with any climate division within the MMRB in the January – December cycle. Perhaps the lack of explanation of variance of the NAO during late summer and early autumn, notably September (Rogers 1990), may obscure some of the relationships to the PDSI when all months of the year are included. Nevertheless, the annual NAO Index does show a significant ($\alpha \leq 0.05$) negative correlation with five climate divisions within Kansas, Oklahoma, and Wyoming (Figure 12). These climate divisions lie within the Missouri and Arkansas basins.

However, once again with $\alpha \leq 0.05$ an average of one correlation in twenty will be spurious, so after 146 correlation tests, the appearance of five strong correlations falls within the realm of what can be expected in creating a Type I error. Even so, the spatial cohesiveness of four of these five divisions does suggest that a physical mechanism could explain the pattern. But on the whole, NAO appears to show little connection to the moisture in the MMRB in the annual cycle. This is not very surprising, as Marshall *et al.* (2001) found that the effect of the NAO on North American precipitation is not strong.

The PNA Index shows a significant ($\alpha \leq 0.05$) positive relationship with 10 climate divisions across the southern Great Plains and one in Mississippi. These climate divisions lie mostly within the southern Missouri River and western Arkansas River basins (Figure 13). A more robust negative relationship exists between the PNA pattern

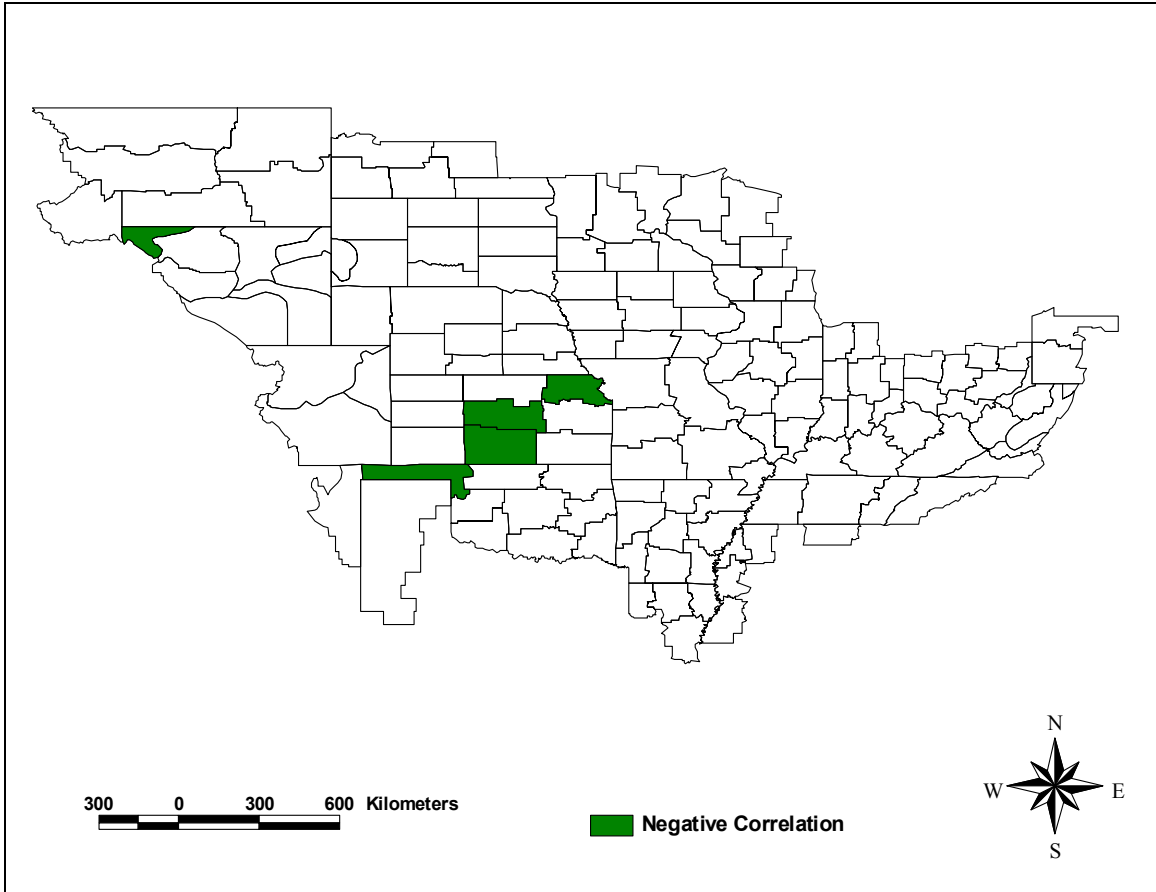


Figure 12: Monthly NAO Correlations (January – December) with PDSI ($\alpha \leq 0.05$) in the Annual Cycle

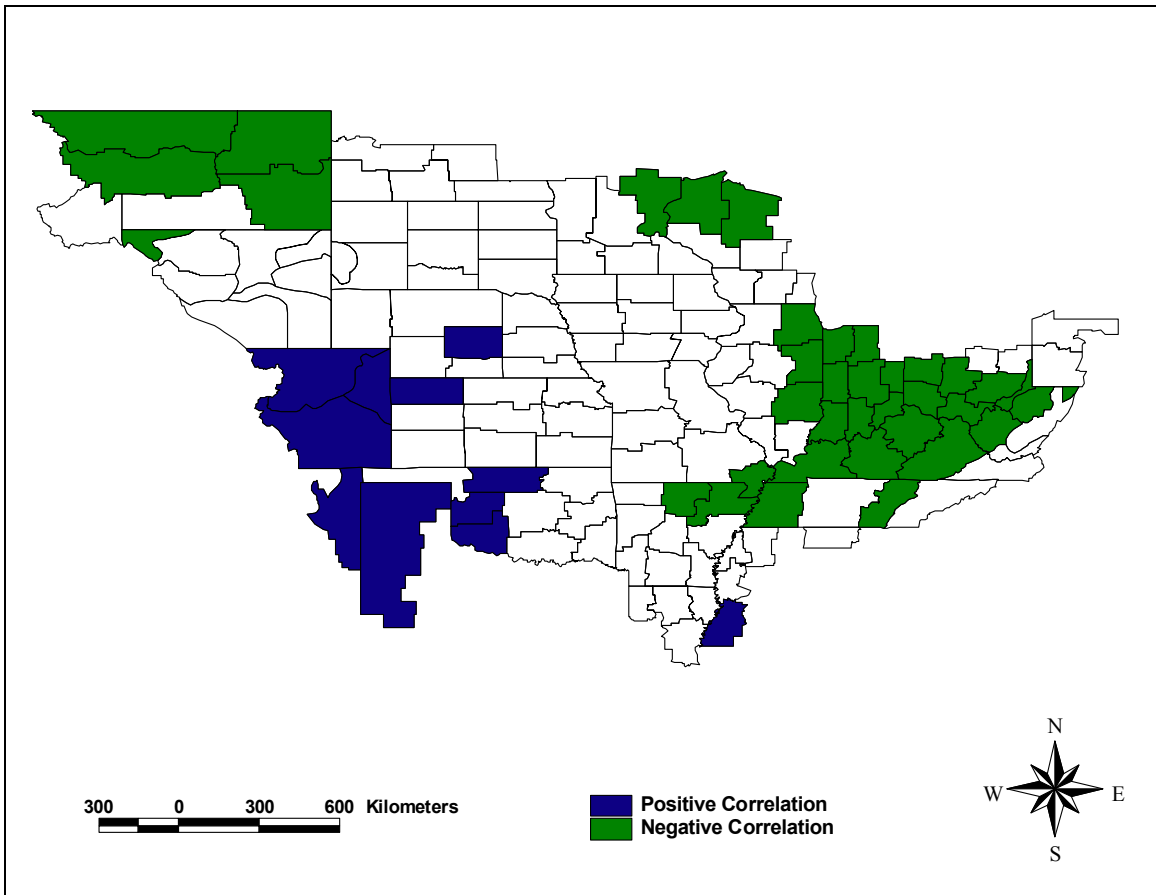


Figure 13: Monthly PNA Correlations (January – December) with PDSI ($\alpha \leq 0.05$) in the Annual Cycle

and the PDSI in the study region, however, as significant ($\alpha \leq 0.05$) negative relationships are found in 37 climate divisions throughout all MMRB sub-basins, including a large portion of the Ohio River basin (Figure 13). Apparently, the characteristic ridge over the western North American Cordillera that is characteristic of the positive PNA pattern produces sufficient subsidence to suppress surface moisture in the annual cycle (and presumably also runoff) in much of the MMRB. This result is interesting because several studies have noted that the PNA pattern is relatively unimportant during months from April to September (Rodionov 1994). Presumably, the strength of the relationship between the PNA pattern and moisture through the rest of the year is sufficient to generate some significant correlations across the MMRB.

4.4. Correlations in the Annual Cycle between Monthly Teleconnection Indices and the Monthly Palmer Hydrological Drought Index

As with the PDSI, the six monthly teleconnection indices were correlated with the monthly PHDI values for each of the 146 climate divisions within the MMRB for each month of the year from 1950 to 2003. Figure 14 shows that throughout the year, monthly SOI is significantly positively correlated with surface moisture at $\alpha \leq 0.05$ in seven climate divisions within the Ohio and Tennessee basins. The SOI shows a nearly identical significant negative relationship in the annual cycle with the PHDI as with the PDSI, including 68 climate divisions within the Upper Mississippi, Missouri, and Arkansas River basins (compare Figure 14 to Figure 8).

Figure 15 shows that the annual Niño 3.4 Index is significantly positively correlated with the PHDI in 99 climate divisions, including all except two of the climate divisions where the annual SOI relationships to PHDI are negative (compare Figure 15

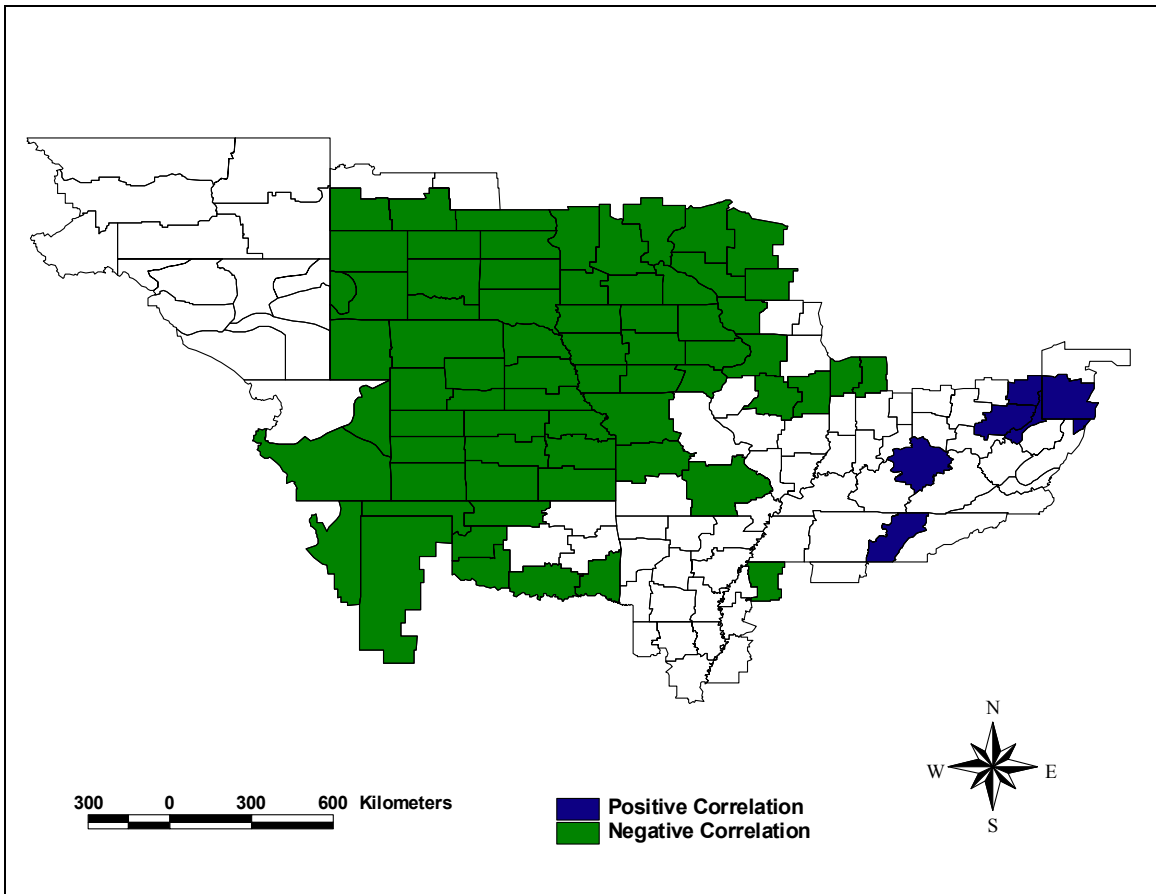


Figure 14: Monthly SOI Correlations (January – December) with PHDI ($\alpha \leq 0.05$) in the Annual Cycle

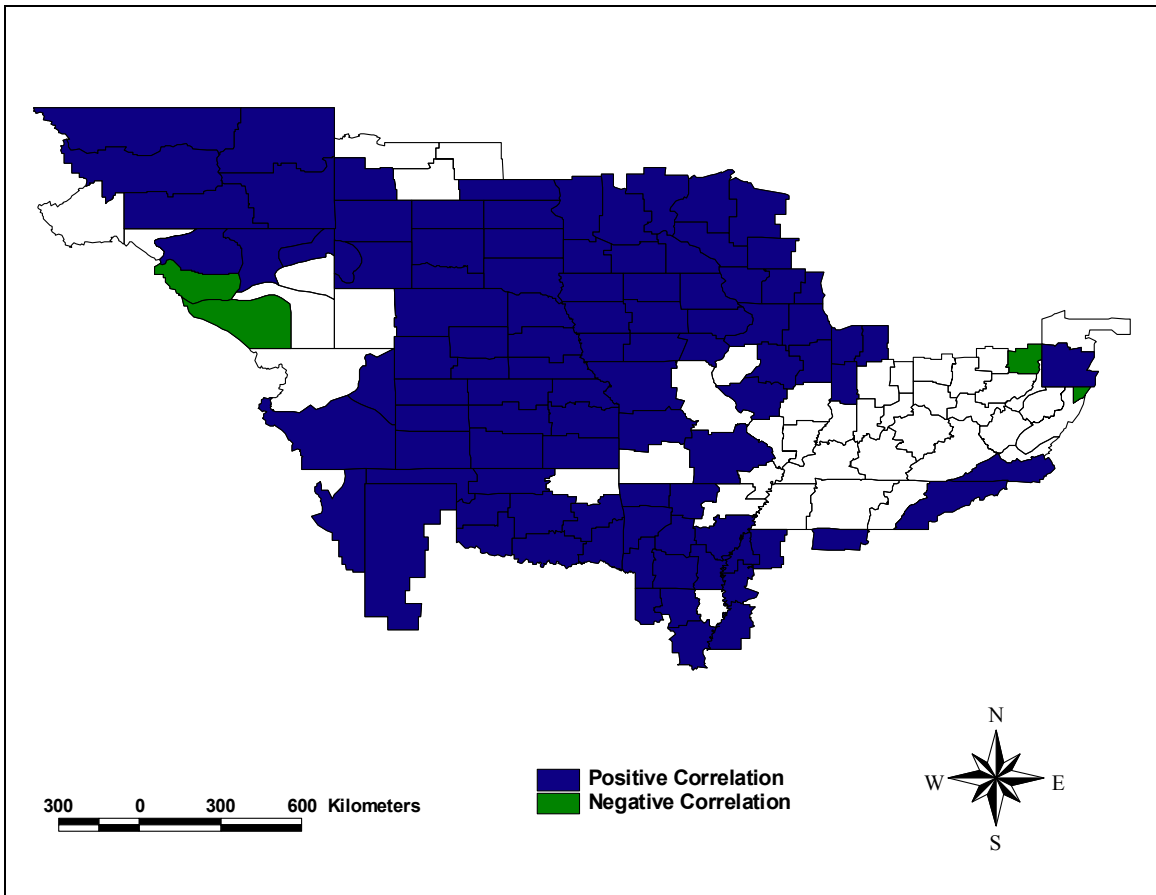


Figure 15: Monthly Niño 3.4 Correlations (January – December) with PHDI ($\alpha \leq 0.05$) in the Annual Cycle

to Figure 9). These divisions are located across the entire MMRB and cover the majority of the Missouri, Upper Mississippi, Arkansas, and Lower Mississippi basins and are also found in the Tennessee and Ohio basins. Figure 15 also shows that the annual Niño 3.4 Index is significantly negatively correlated with four climate divisions in the extreme eastern Ohio basin and the extreme western Missouri basin. These results are very similar to the relationships found between the annual Niño 3.4 Index and the PDSI (Compare Figure 15 to Figure 9).

The annual PDO Index shows a significant positive relationship with the PHDI in 76 climate divisions scattered throughout the basin, but particularly in the middle of the MMRB. These divisions cover large portions of the Arkansas and Missouri basins (Figure 16). The annual PDO Index has a significant negative correlation with the PHDI in seven climate divisions scattered throughout the northwest Missouri, Lower Mississippi, Tennessee, and Ohio River basins (Figure 16). Again, as would be expected, this pattern is very similar to that for the PDSI (compare Figure 16 to Figure 10), and this pattern also closely resembles that shown for the Niño 3.4 Index (compare Figure 16 to Figure 15).

The annual AO Index does not display many significant relationships with the PHDI. A significant ($\alpha \leq 0.05$) positive relationship is found in only ten climate divisions within the Ohio, Tennessee, and Lower Mississippi basins, while a significant negative relationship occurs in 22 divisions, all throughout the Missouri, Upper Mississippi, and Arkansas basins (Figure 17). The PHDI pattern again resembles that for the PDSI (compare Figure 17 to Figure 11). Only one climate division, AL1, shows a

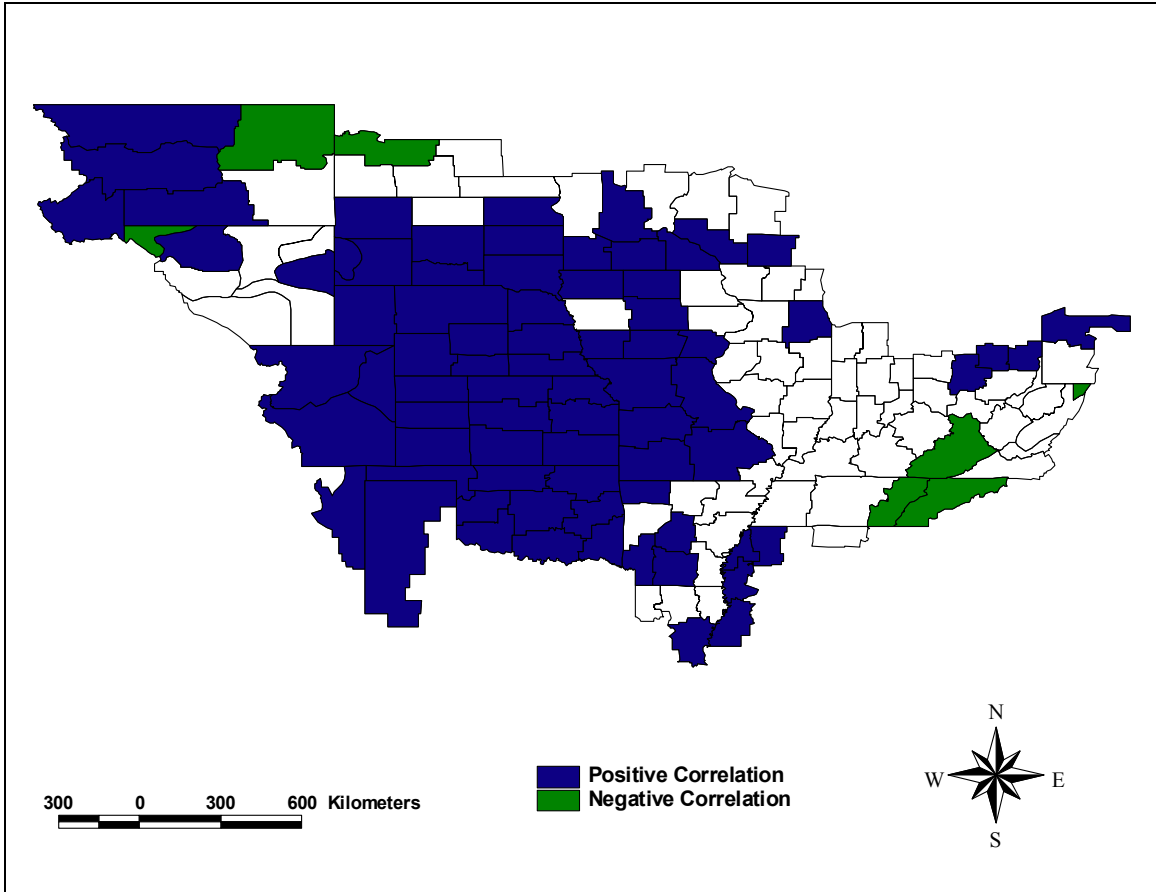


Figure 16: Monthly PDO Correlations (January – December) with PHDI ($\alpha \leq 0.05$) in the Annual Cycle

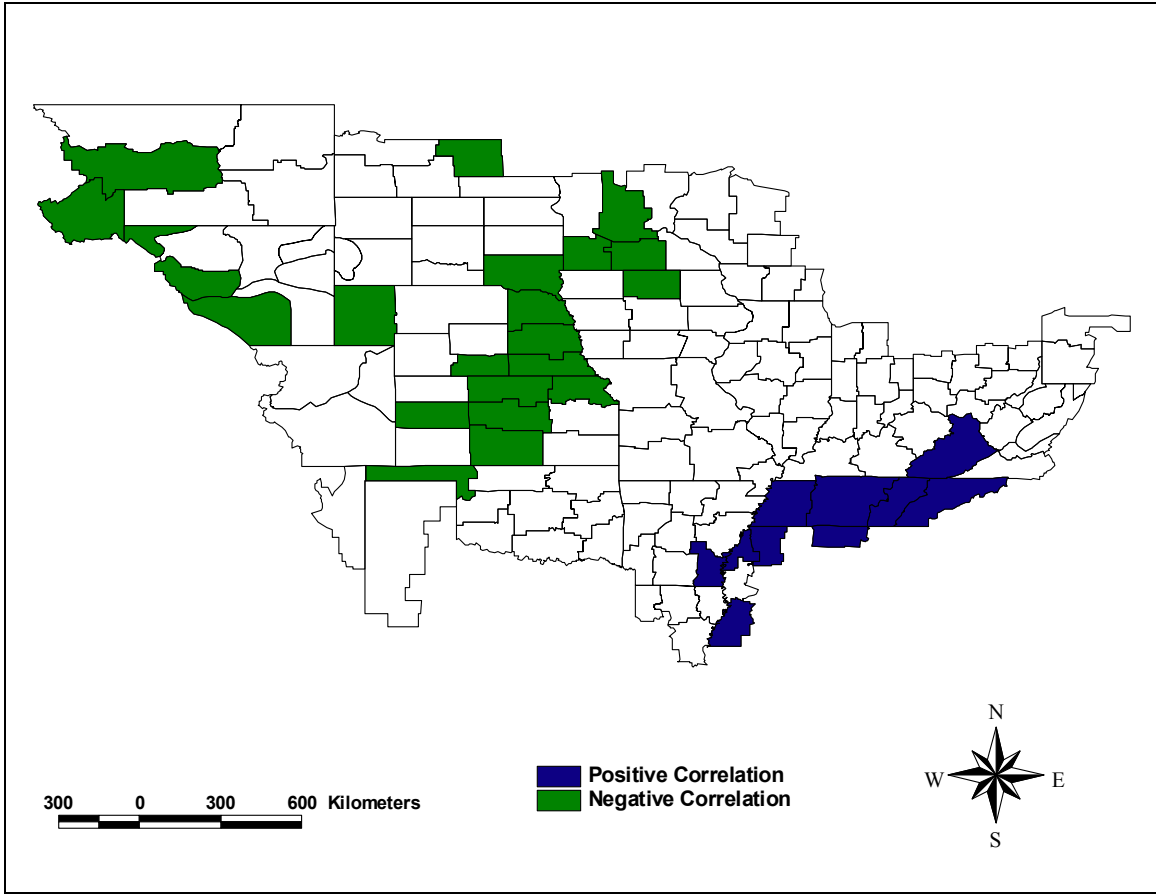


Figure 17: Monthly AO Correlations (January – December) with PHDI ($\alpha \leq 0.05$) in the Annual Cycle

positive correlation between the PHDI and the NAO Index at $\alpha \leq 0.05$ (Figure 18), while a negative correlation occurs in three climate divisions, KS5, KS8, and OK1 (Figure 18). Again, these patterns are similar to those found for AO relationships with the PDSI (compare Figure 18 to Figure 12). Thus, the lack of a relationship between the NAO and surface moisture was verified by use of the PHDI, at least in the annual cycle.

The annual PNA Index shows a positive relationship with the PHDI in only four climate divisions of the western Missouri and Arkansas basins: KS1, KS4, TX1, and WY4 (Figure 19). A negative relationship occurs in the opposite side of the study region. Specifically, negative relationships are found in three climate divisions, KY3, KY4, and WI1 (Figure 19). Although the PHDI has fewer relationships with the annual PNA Index than the PDSI, the areas of the basin showing relationships are similar (compare Figure 19 to Figure 13).

4.5. Spring Correlations between Monthly Teleconnection Indices and the Monthly Palmer Drought Severity Index

The six teleconnection indices were also correlated with the spring (March, April, May, and June) PDSI values for the 146 climate divisions within the MMRB. The rationale is that as the high-flow season, spring runoff totals impact the GMHZ in early summer, the time near which hypoxia is most severe and when GMHZ data are available.

The spring SOI is significantly ($\alpha \leq 0.05$) positively related to the PDSI in only four climate divisions in Wyoming, Montana, and Ohio, within the Missouri and Ohio basins (Figure 20). On the contrary, a negative relationship at the $\alpha \leq 0.05$ level is found in a much larger region, including 42 climate divisions mainly in a swath from the north-central to the south-central parts of the study region (Figure 20). This pattern of

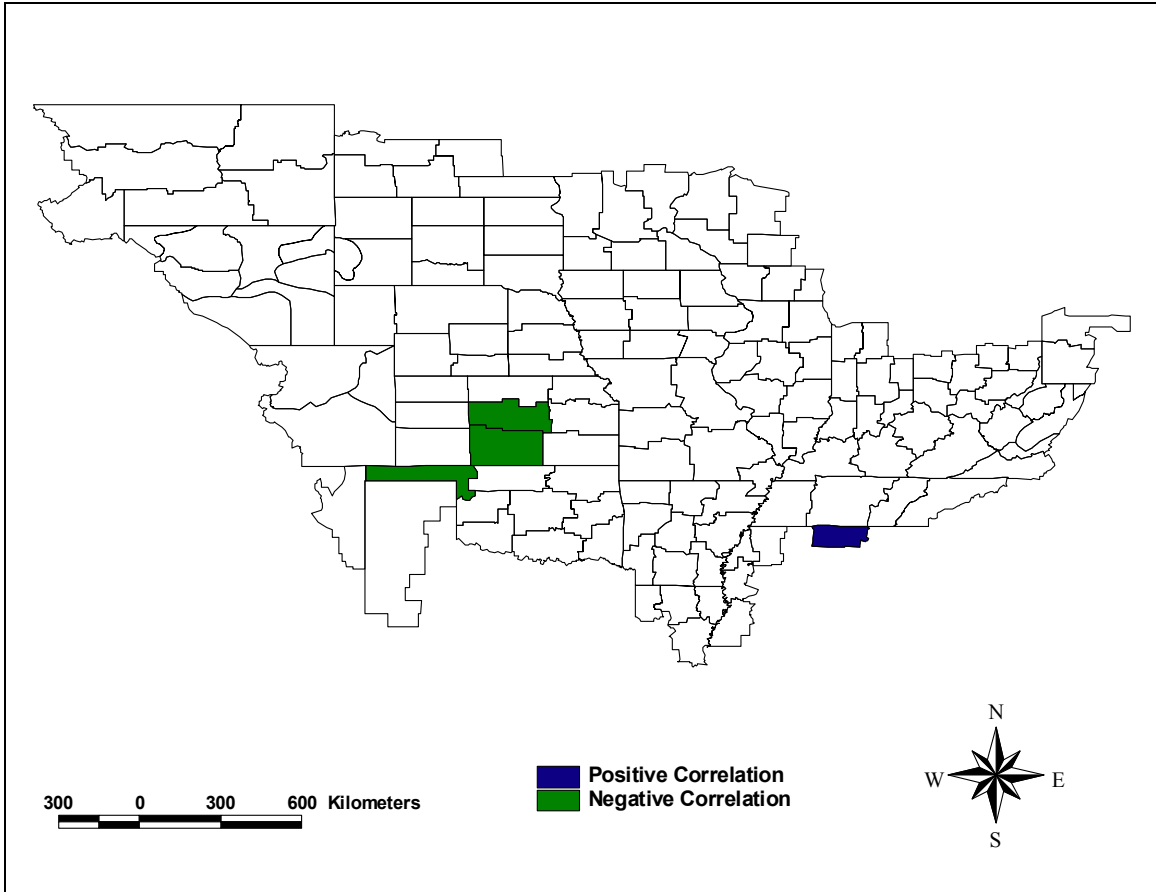


Figure 18: Monthly NAO correlations (January – December) with PHDI ($\alpha \leq 0.05$) in the Annual Cycle

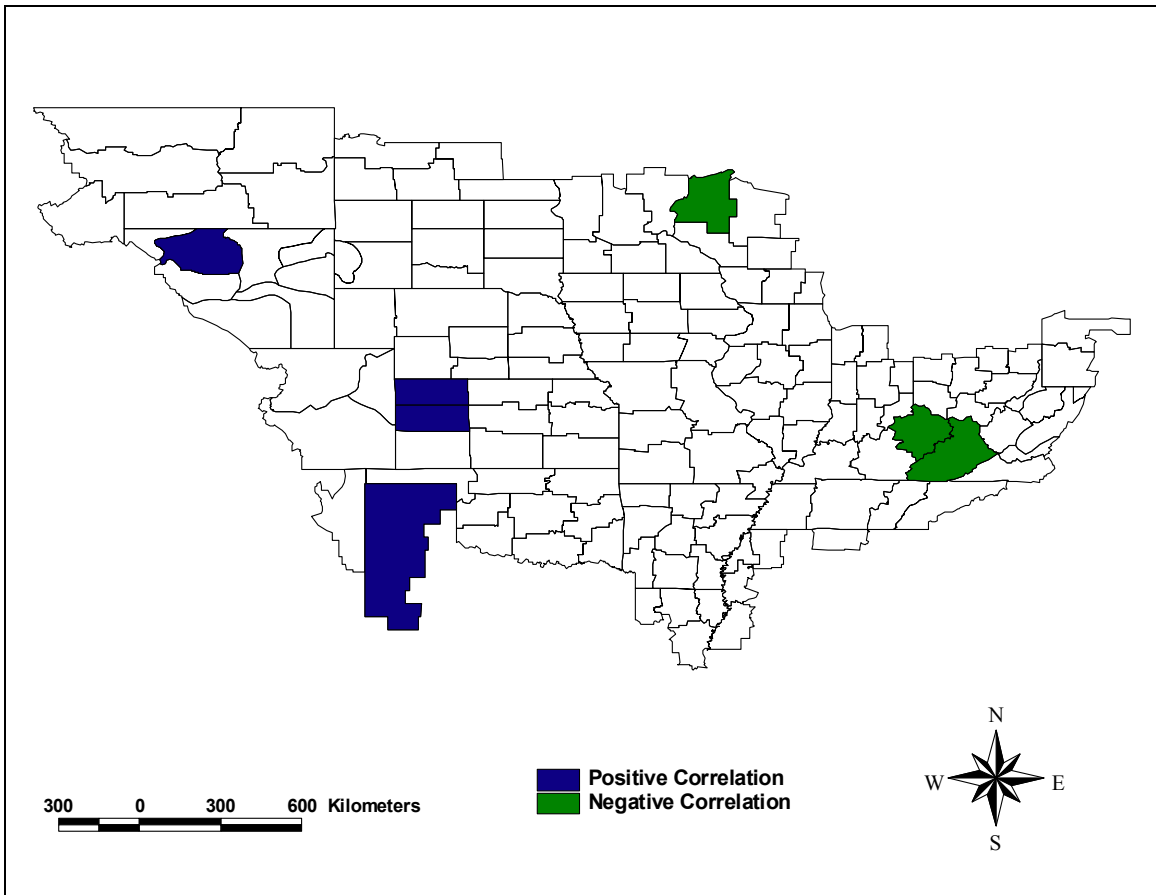


Figure 19: Monthly PNA Correlations (January – December) with PHDI ($\alpha \leq 0.05$) in the Annual Cycle

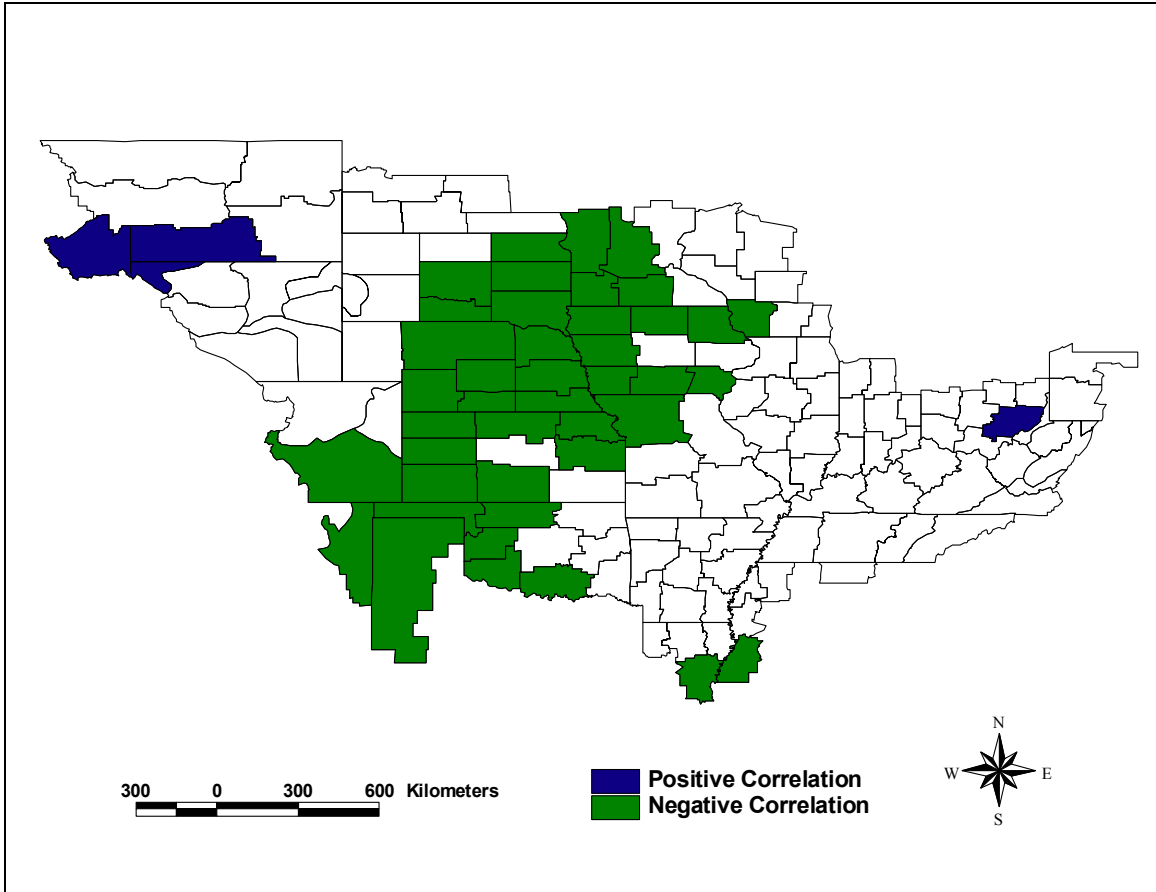


Figure 20: MAMJ SOI Correlations with PDSI ($\alpha \leq 0.05$)

positive and negative relationships corresponds fairly well to the relationships found for the SOI in the annual cycle (compare Figure 20 to Figure 8).

Not surprisingly, the spring Niño 3.4 Index shows a significant ($\alpha \leq 0.05$) positive relationship to PDSI in 64 climate divisions (Figure 21) in geographical areas that are very similar to that of the spring SOI negative relationships (compare Figure 21 to Figure 20). By contrast, a significant ($\alpha \leq 0.05$) negative relationship occurs in six climate divisions within the Ohio and Tennessee River basins (Figure 21).

Another expected result is that the MAMJ PDO Index shows a positive relationship with PDSIs in a similar number of divisions (50) in similar geographical areas as the MAMJ Niño 3.4. These divisions are largely west of the Mississippi River and also within the Arkansas, Missouri, and Upper Mississippi basins, and one climate division within the Lower Mississippi basin (Figure 22). Significant negative correlations are found in eight climate divisions scattered throughout the Missouri, Lower Mississippi, Tennessee, and Ohio River basins within five states: Montana, Wyoming, Tennessee, Maryland, and Kentucky. Again, this is a very similar number of divisions as was identified for the spring Niño 3.4, but the locations shift (compare Figures 21 to 20).

Interestingly, the MAMJ AO Index displays no positive association to PDSI in any climate divisions within the MMRB (Figure 23), despite the fact that a positive relationship was found in 16 climate divisions in the annual cycle (compare Figure 23 to Figure 11). This result requires investigation that is beyond the scope of this thesis, but it seems likely that the AO modulates flow that dictates surface moisture availability in the MMRB in non-spring seasons to a greater extent than during spring. Even more puzzling

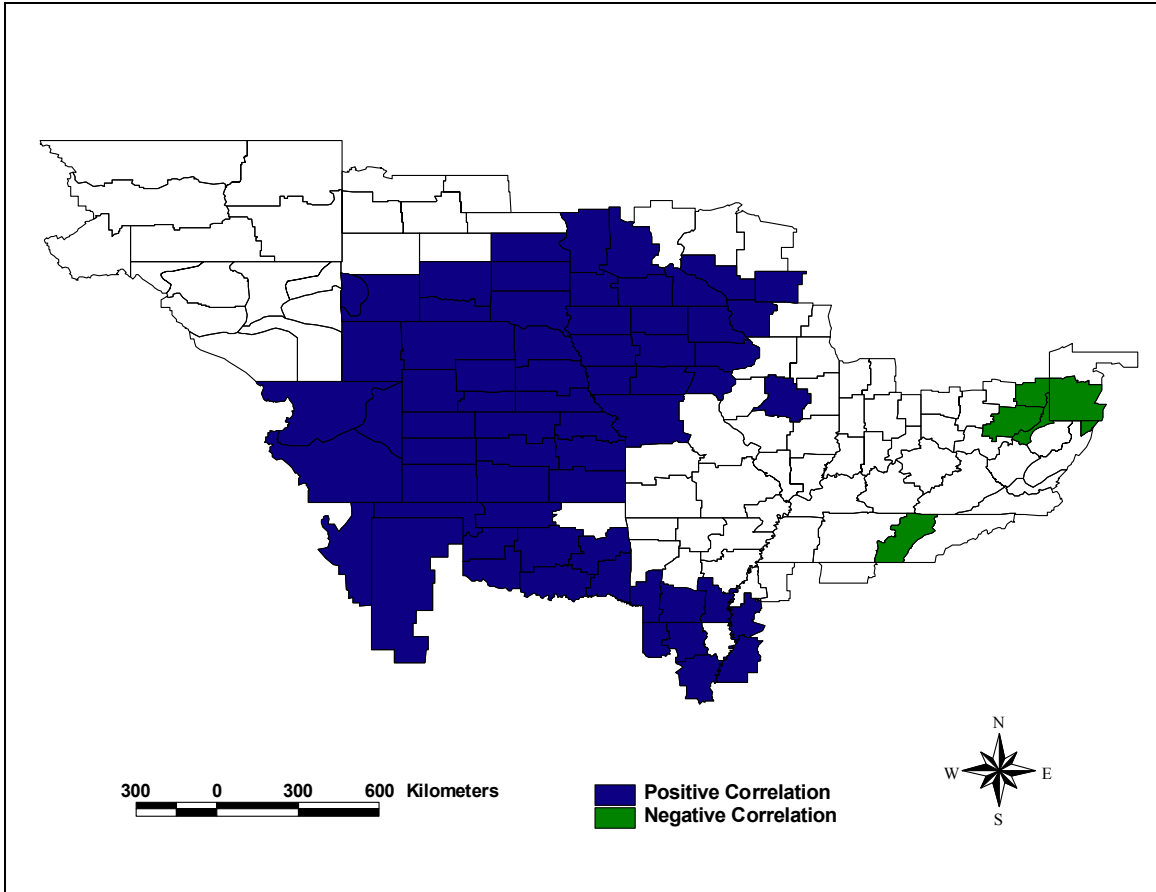


Figure 21: MAMJ Niño 3.4 Correlations with PDSI ($\alpha \leq 0.05$)

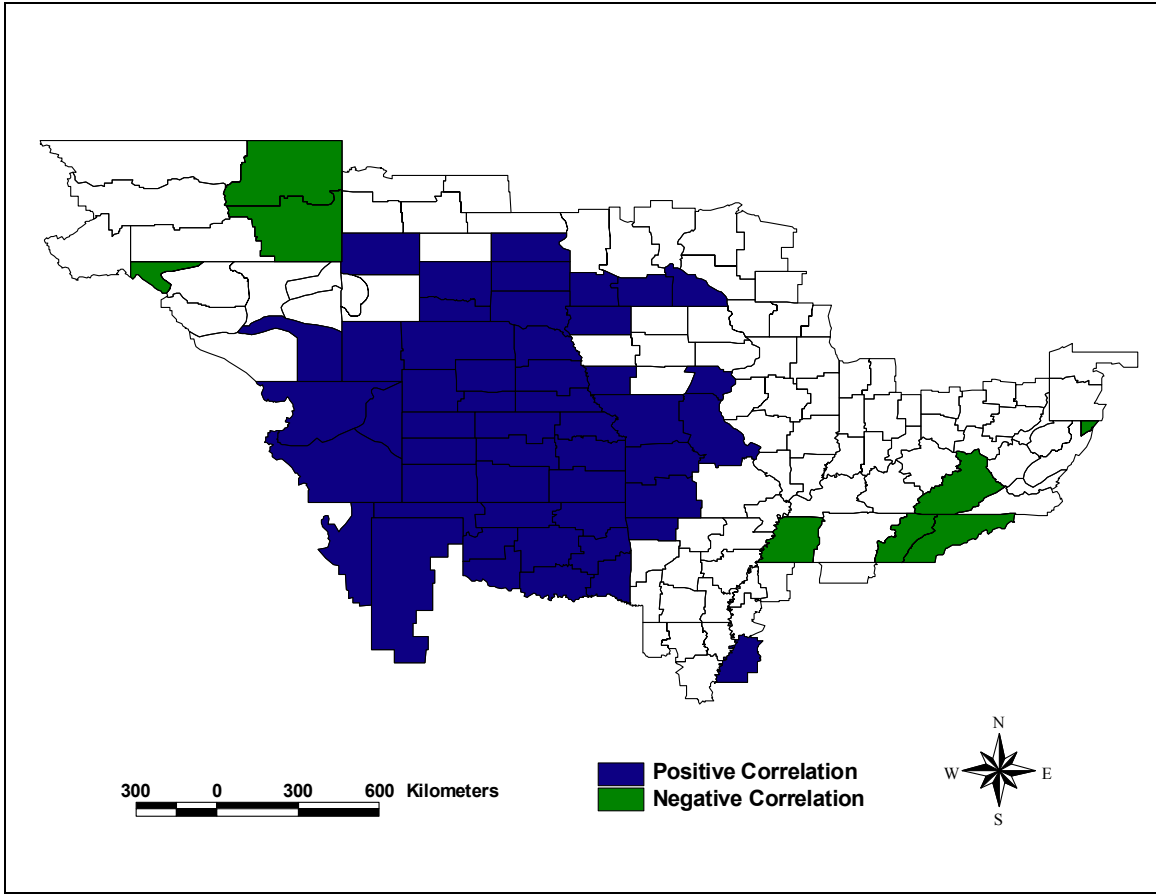


Figure 22: MAMJ PDO Correlations with PDSI ($\alpha \leq 0.05$)

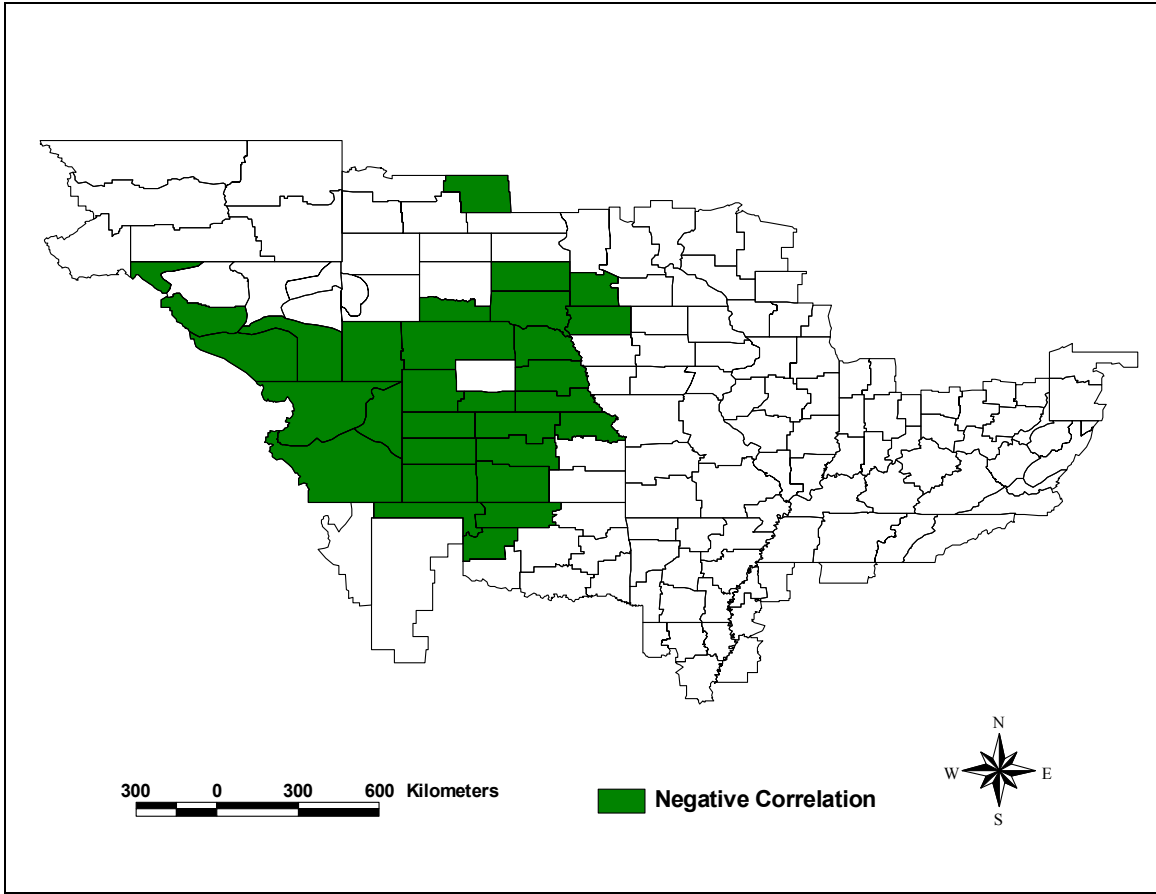


Figure 23: MAMJ AO Correlations with PDSI ($\alpha \leq 0.05$)

is the significant negative relationship in 30 climate divisions within the northwest Arkansas basin, along with the northwest Upper Mississippi and Missouri basins (Figure 23). The negative relationships in the spring are similar to those in the annual pattern, although more divisions show a negative relationship in the spring pattern.

As was the case for the AO Index, no significant positive correlation between the MAMJ NAO Index and PDSI values exist in the MMRB (Figure 24). By contrast, significant negative associations occur in 26 climate divisions scattered across the upper High Plains and Midwest. These divisions lie largely in the Missouri River basin but are also scattered throughout the Upper Mississippi, Arkansas, and Ohio River basins (Figure 24). Consequently, the spring NAO seems to represent a more important control on moisture availability than the NAO in the annual cycle (compare Figure 24 to Figure 12), perhaps because of the demonstrated weakness of the NAO in late spring and summer (Rogers 1990).

Finally, the MAMJ PNA Index is positively linked with the PDSI in 45 climate divisions in the western and central parts of the study region, mostly within the southern Missouri and northern Arkansas basins but also scattered to a lesser degree in the Upper and Lower Mississippi basins (Figure 25). A negative relationship is found in a cohesive region containing eight climate divisions within the Ohio River basin (Figure 25). These results are surprising considering that the positive PNA Index is characteristic of a “ridge-to-trough” subsidence over the very areas that show a positive correlation with the PNA. Furthermore, the region of positive (negative) correlations is much larger (smaller) than that in the annual cycle (compare Figure 25 to Figure 13). This result requires further investigation.

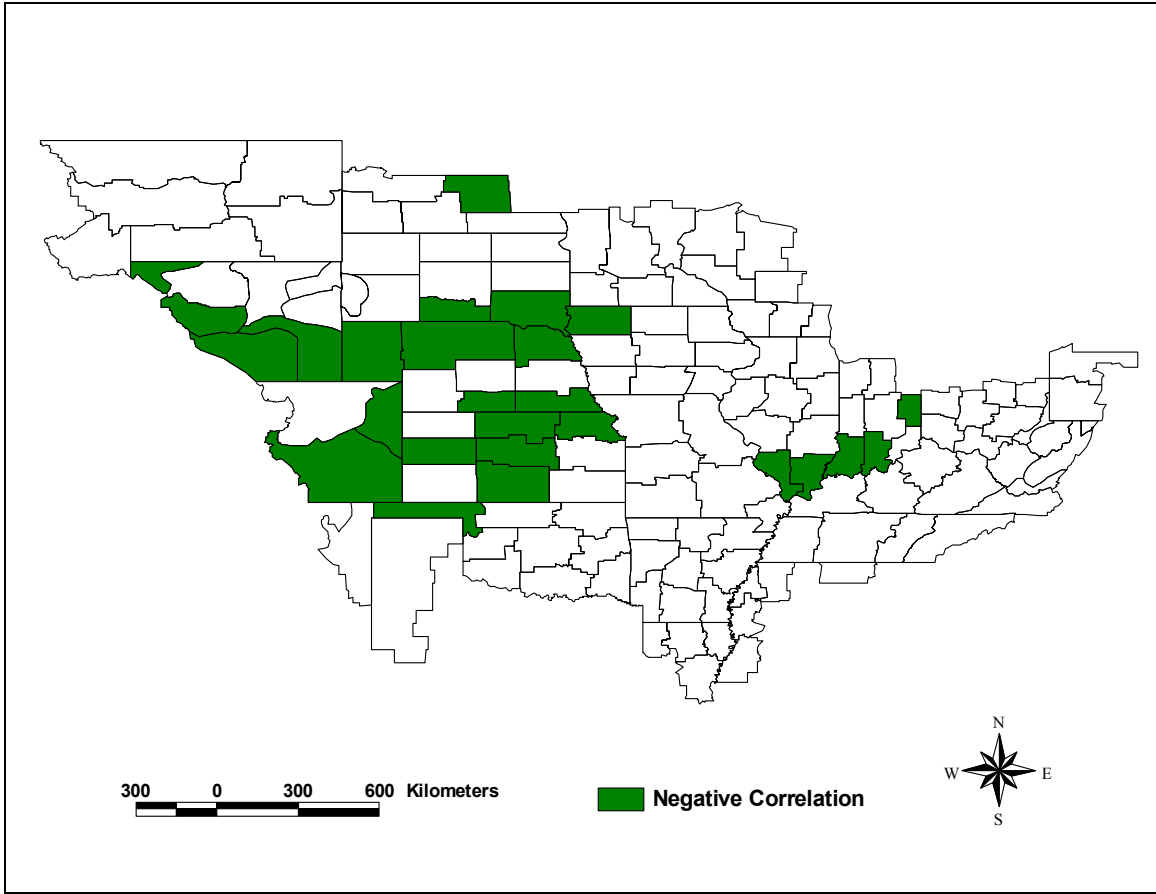


Figure 24: MAMJ NAO Correlations with PDSI ($\alpha \leq 0.05$)

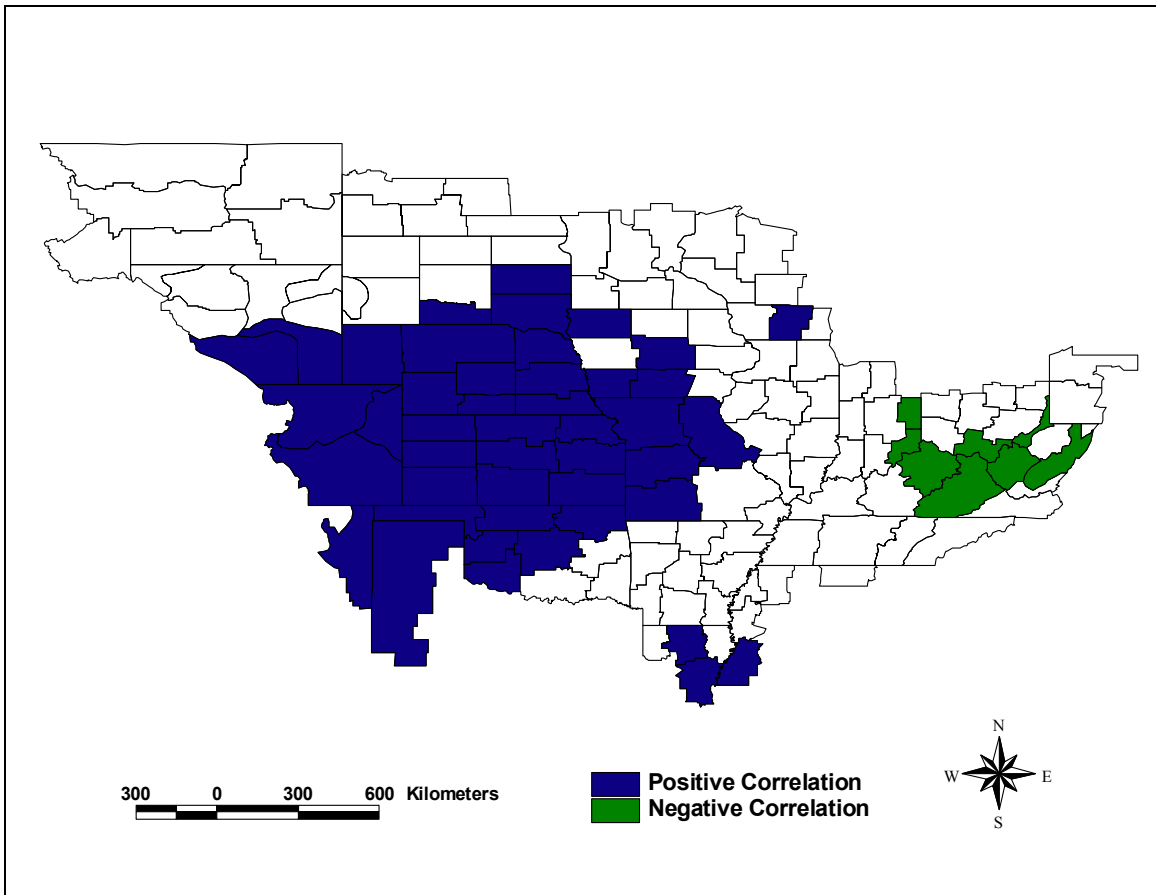


Figure 25: MAMJ PNA Correlations with PDSI ($\alpha \leq 0.05$)

4.6. Spring Correlations between Monthly Teleconnection Indices and the Monthly Palmer Hydrological Drought Index

Again, the six teleconnection indices were also correlated with the spring (March, April, May, and June) PHDI values for the 146 climate divisions within the MMRB.

Overall, the relationships found are very similar to those found for PDSI values.

The spring SOI is positively related to four climate divisions within the MMRB, including three in the extreme northwest Missouri basin and one in the Ohio basin (Figure 26). The spring SOI shows a negative relationship at the $\alpha \leq 0.05$ level with a large region including 32 climate divisions mainly in the north-central and the south-central parts of the study region (Figure 26). Although fewer climate divisions are related, this pattern of negative relationships corresponds very well to the relationships found between the SOI and the PDSI in the spring cycle (compare Figure 26 to Figure 20). In fact, the presence of OH10, LA5, and MS7 in both figures suggests that these isolated pockets of strong correlations are not spurious.

A positive relationship is found between the spring Niño 3.4 Index and the PHDI (Figure 27) in a nearly identical spatial pattern to that between the Niño 3.4 and the PDSI (compare Figure 27 to Figure 21). Furthermore, the 65 climate divisions in which a significant association was found are in similar locations as those for which the SOI was significantly negative (compare Figure 27 to Figure 26). The spring Niño 3.4 index shows a negative relationship with PHDI in only three climate divisions within the Ohio River basin (Figure 27).

The spring PDO Index has a positive relationship with PHDIs in a similar number of divisions (54) as the spring Niño 3.4. These divisions are largely west of the Mississippi River and also within the Arkansas, Missouri, and Upper Mississippi basins,

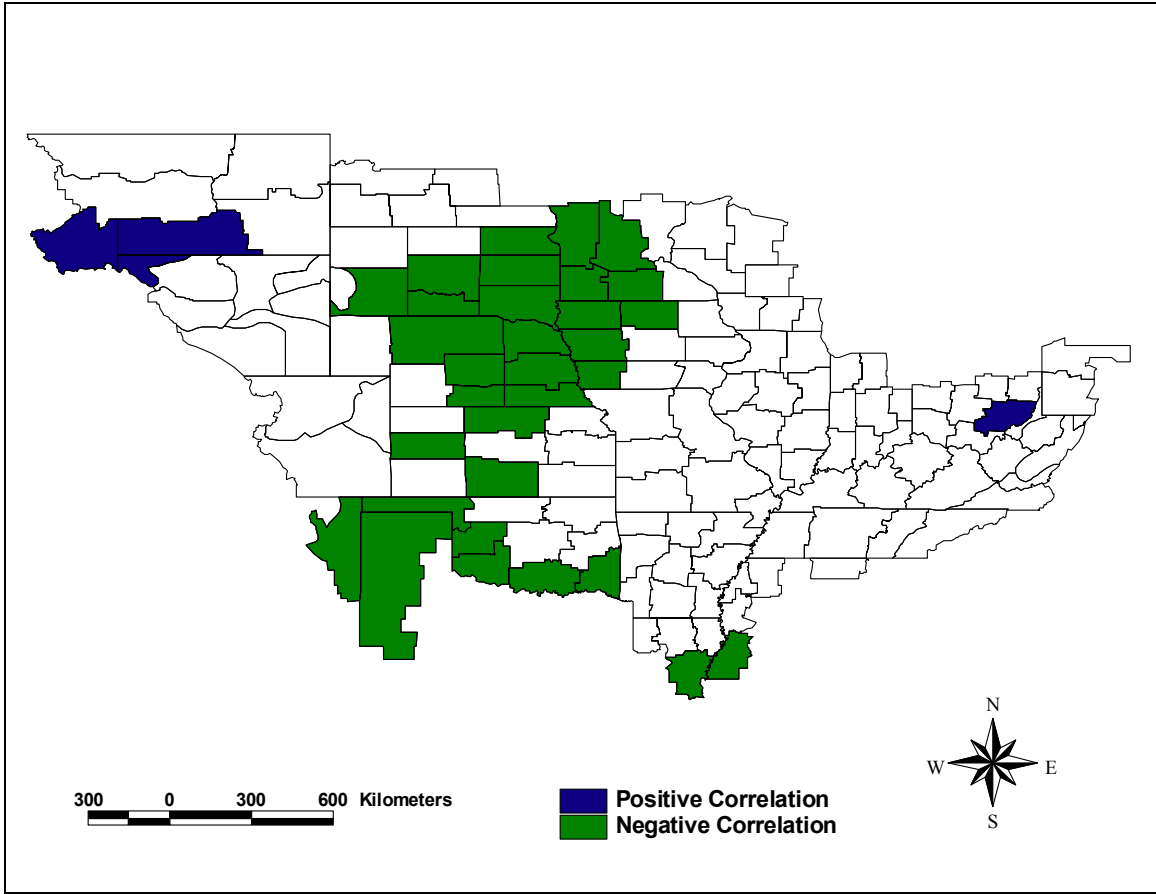


Figure 26: MAMJ SOI Correlations with PHDI ($\alpha \leq 0.05$)

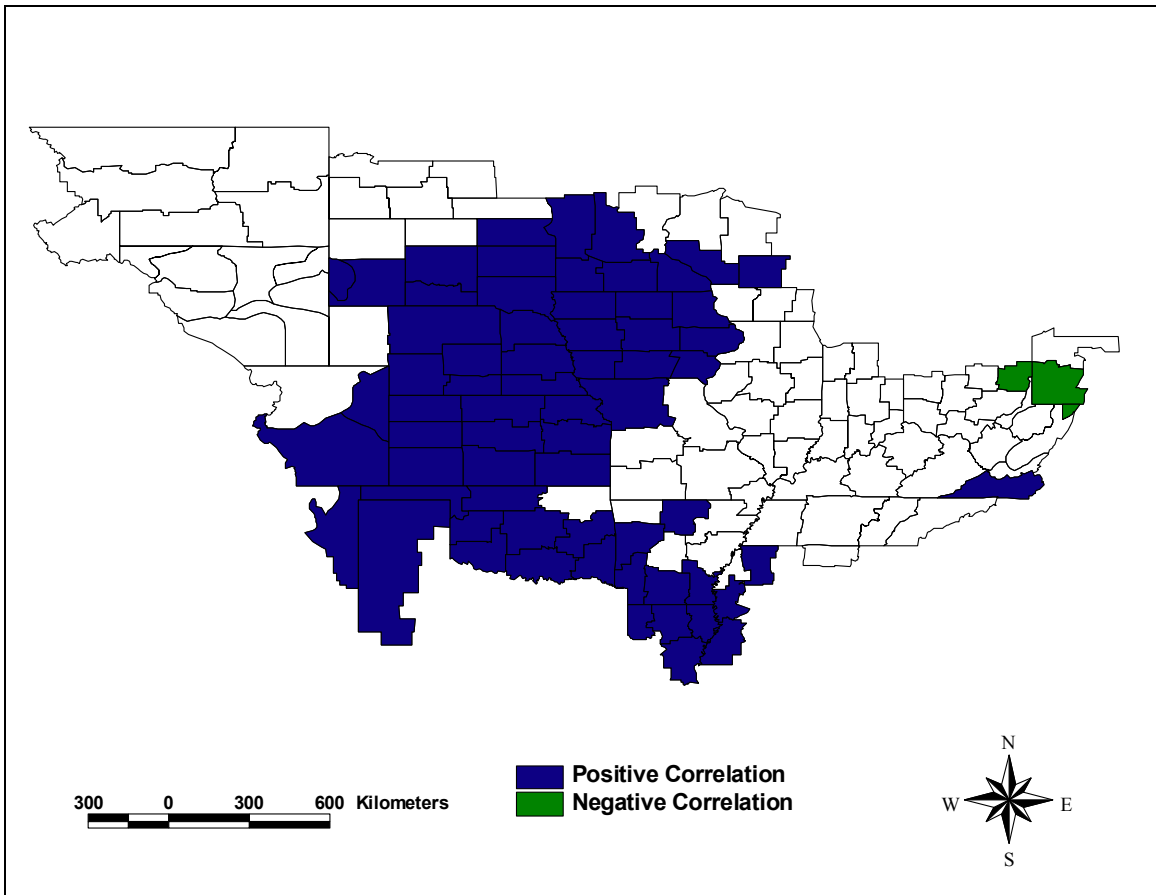


Figure 27: MAMJ Niño 3.4 Correlations with PHDI ($\alpha \leq 0.05$)

with only two climate divisions within the Lower Mississippi basin (Figure 28). A negative correlation is found in five climate divisions in five different states scattered throughout the Missouri, Tennessee, and Ohio River basins. Again, this is a very similar number of divisions as was identified for the spring Niño 3.4, but the locations shift (compare Figure 28 to Figure 27).

As was the case with the PDSI correlations, the spring AO Index does not display a positive relationship to PHDI in any climate divisions within the MMRB, but has a negative correlation to PHDI in 39 climate divisions within the northwest Arkansas basin, along with the northwest Upper Mississippi, and the southern and eastern Missouri basins (Figure 29). Similar to the PDSI correlations, more climate divisions show a negative relationship with the AO during the spring months than in the annual cycle (compare Figure 29 to Figure 17).

No climate divisions have a positive correlation between the MAMJ NAO and the PHDI. These results are the same as those found for the spring PDSI. By contrast, the spring NAO Index shows a negative correlation with the PHDI in 16 climate divisions scattered across the High Plains, lying completely in the Missouri and Arkansas basins (Figure 30). Although few associations were found, the number is larger than those found in the annual cycle (compare Figure 30 to Figure 18).

Finally, the MAMJ PNA Index shows a positive relationship with PHDI in 28 climate divisions in the western and central parts of the study region, within large portions of the Missouri, Arkansas, and Upper Mississippi basins (Figure 31). No negative relationship between these variables exists (Figure 31). The region of positive

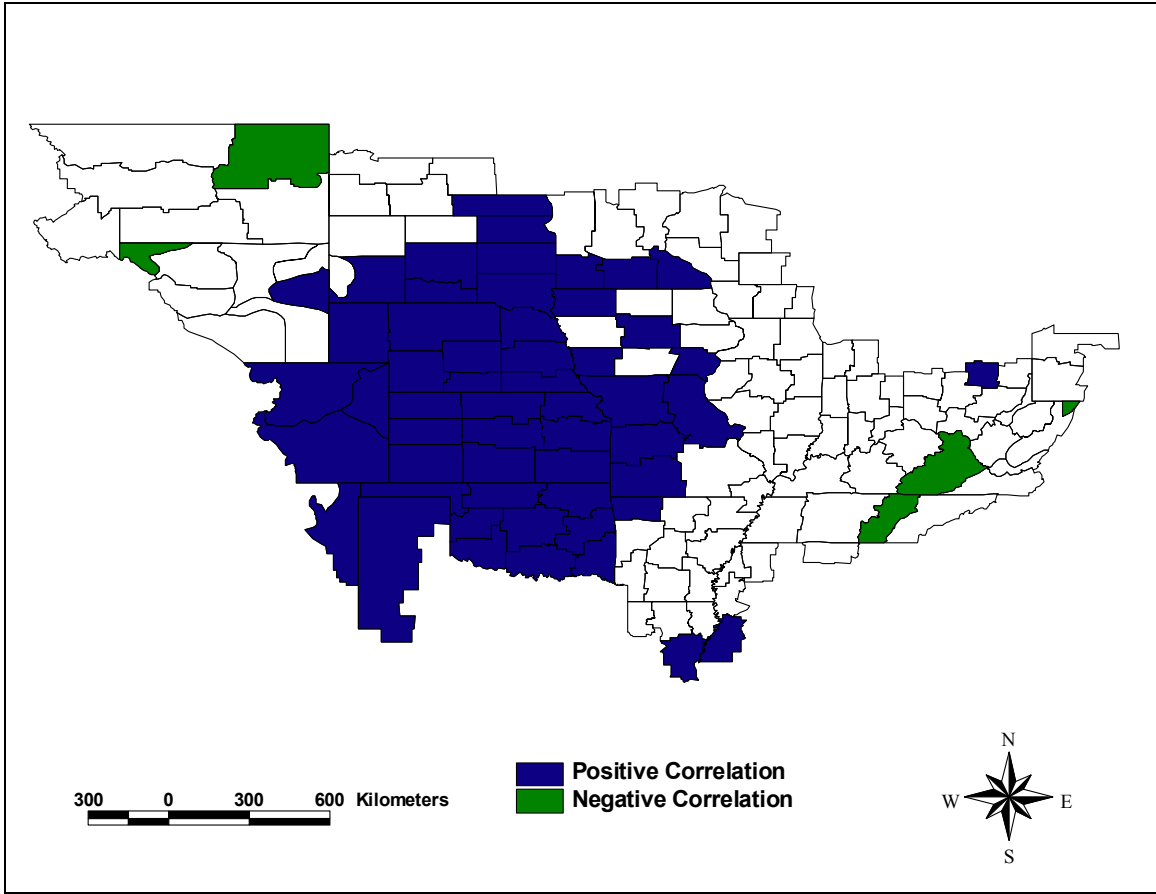


Figure 28: MAMJ PDO Correlations with PHDI ($\alpha \leq 0.05$)

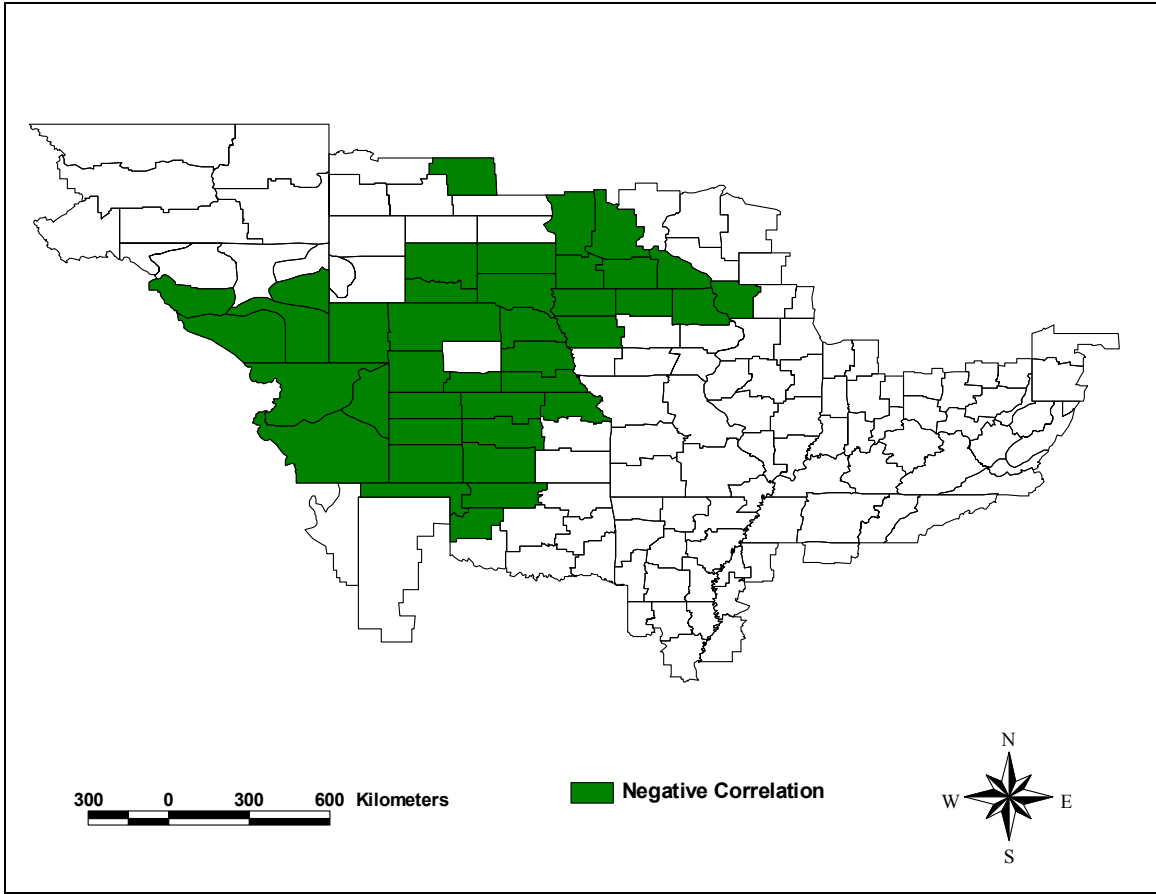


Figure 29: MAMJ AO Correlations with PHDI ($\alpha \leq 0.05$)

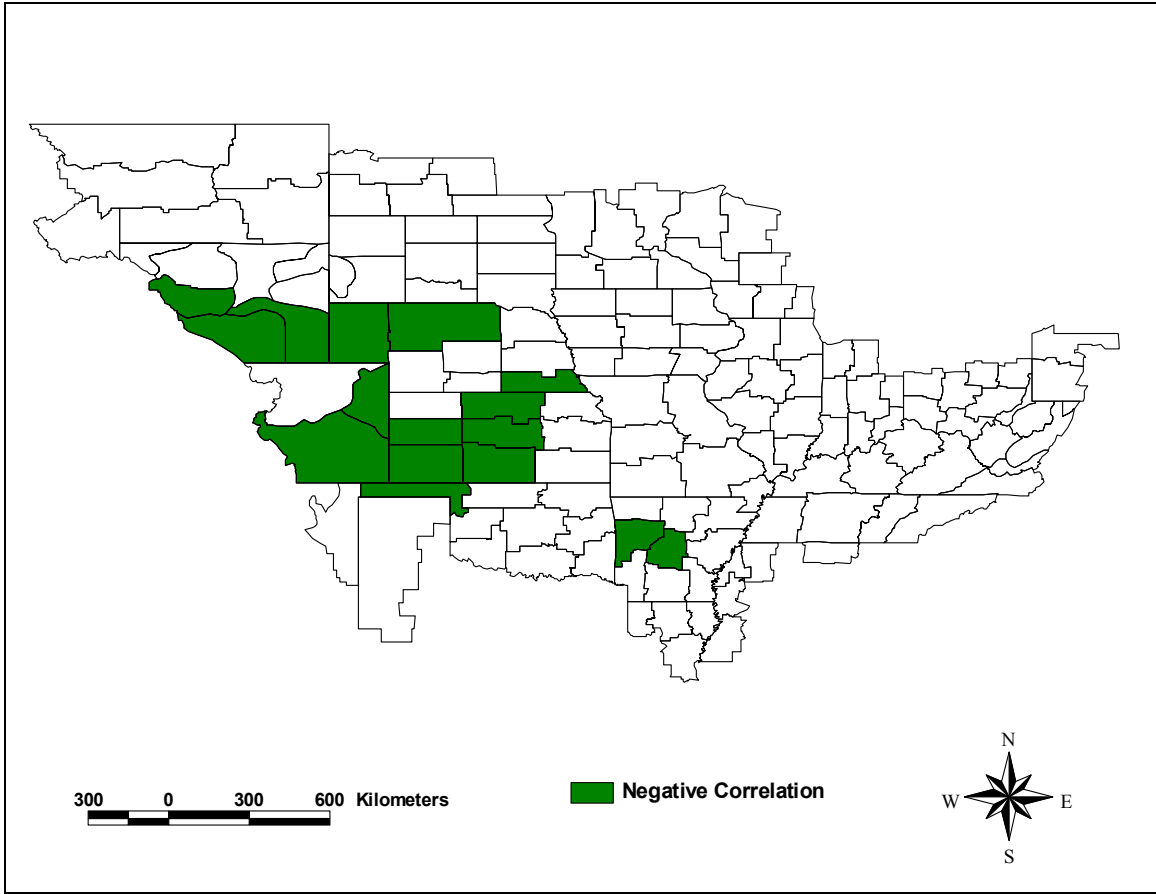


Figure 30: MAMJ NAO Correlations with PHDI ($\alpha \leq 0.05$)

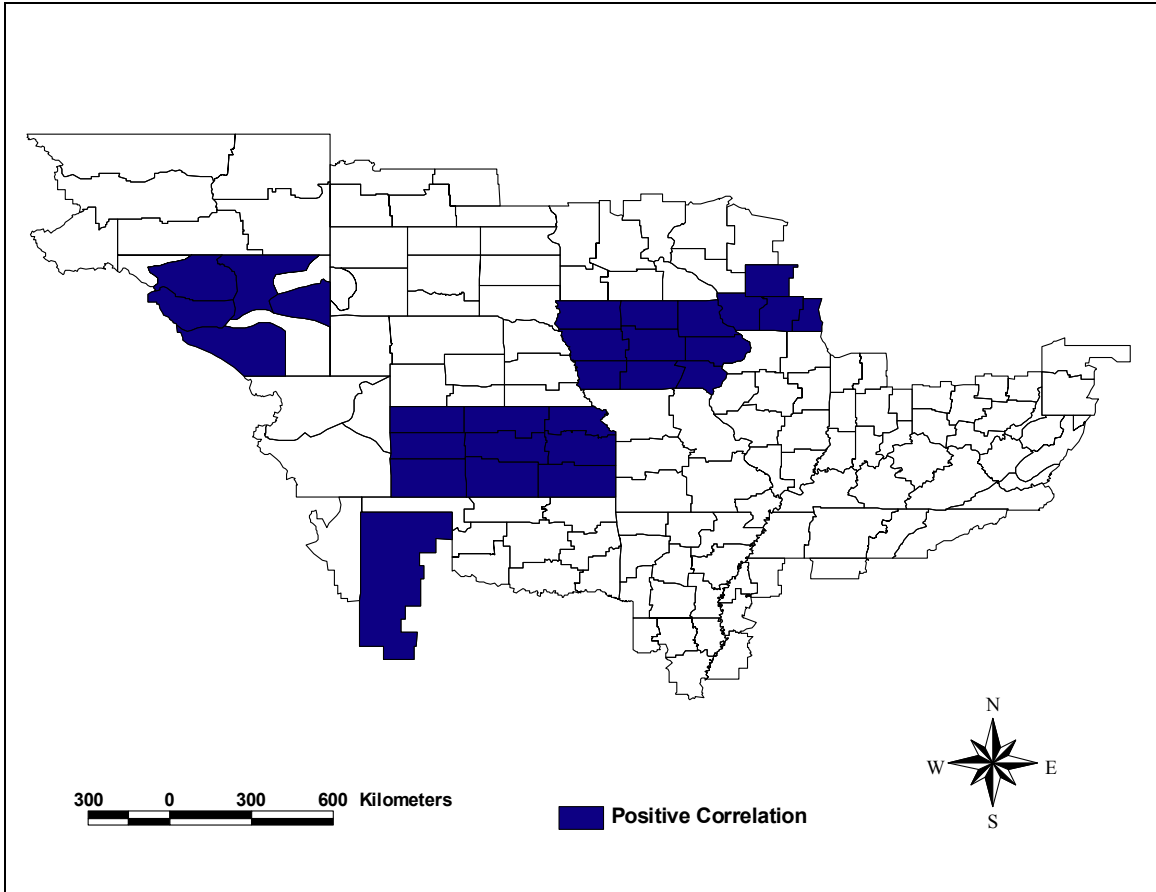


Figure 31: MAMJ PNA Correlations with PHDI ($\alpha \leq 0.05$)

correlations is smaller than for the PDSI analysis (compare Figure 31 to Figure 25) but larger than for the PHDI analysis in the annual cycle (compare Figure 31 to Figure 19).

4.7 Summary

Results presented in this chapter show that there is a strong positive relationship between spring streamflow in the Mississippi River and the area of the GMHZ. Furthermore, relationships between PDSI and PHDI and the area of the GMHZ are shown throughout most of the MMRB. The teleconnections analyzed in this chapter display some relationships with soil moisture and therefore runoff throughout regions within the MMRB that contribute much of the water supply to the Mississippi River. In general, results for the PHDI correspond very closely to those for the PDSI. Chapter 5 will detail the results of principal components analysis, which is used to determine whether surface hydroclimatic variability regions correspond well with sub-basin boundaries in the MMRB.

CHAPTER 5

REGIONALIZATION OF MOISTURE VARIABILITY REGIONS

The previous chapter analyzed relationships between the surface area of the GMHZ and Mississippi River discharge, PDSI, and PHDI. Chapter 4 also analyzed relationships between six teleconnection indices and the PDSI and PHDI in the MMRB. This chapter addresses the fifth research question from Chapter 1. Specifically, do surface hydroclimatic variability regions correspond well with sub-basin boundaries in the MMRB? If there is a high degree of correspondence between homogeneous hydroclimatic variability regions and drainage basins, then hydroclimatic variability in relatively small geographic areas could presumably contribute to great variability in GMHZ surface area. This scenario would be particularly influential in the Ohio and Tennessee basins, which contribute an estimated 50 percent of streamflow through the mouth of the Mississippi (Meade 1995).

To address this research question, rotated PCA is used to regionalize the March-through June surface hydroclimatology of the MMRB (represented by divisional PDSI and PHDI) for the 1895 – 2003 period. These months are selected because they are assumed to represent the high-flow season (Groisman *et al.* 2001) and the period leading up to the measurement of the GMHZ by field cruises conducted by scientists at the Louisiana State University School of the Coast and Environment and Louisiana Universities Marine Consortium. Results of this regionalization provide the focus of this chapter.

5.1 Regionalization Based on the Palmer Drought Severity Index

The unrotated PCA produced eigenvalues of 46.25, 19.12, and 11.85 (of a total of 146), for Components 1 through 3, respectively (Table 3). Three components were

retained for rotation, based on scree plots of eigenvalues (Yarnal 1993). By rotating the three components, less variance is explained for Component 1, but more variance is explained by Components 2 and 3 (Table 4).

Table 3: Eigenvalues of Unrotated PCA Based on PDSI.

Component	Eigenvalue	Explained Variance (Percent)
1	46.25	31.7
2	19.12	13.1
3	11.85	8.1

Table 4: Eigenvalues of Rotated PCA Based on PDSI.

Component	Eigenvalue	Explained Variance (Percent)
1	30.05	20.6
2	29.94	20.5
3	17.23	11.8

Figures 32 through 34 show the spatial pattern of rotated loadings by climate division for the three retained components. The first rotated component has maximum loadings within the eastern Missouri and western Upper Mississippi basins with loadings of opposite sign centered on the Lower Mississippi, Tennessee, and southeastern Ohio basins (Figure 32). Compared to the rest of the U.S., this northern Great Plains region experiences more persistent droughts and wet periods (Soulé 1992). Because of the high explained variance of this component (Table 4), it appears that variability in PDSI in these climate divisions represents an especially important component of hydroclimatic variability, and therefore, the variation between wet years and dry years may have a great impact on the area of the GMHZ.

The second rotated component has a dipole of extreme loadings focused on the Ohio and Tennessee basins, with a secondary center of opposite sign centered on the

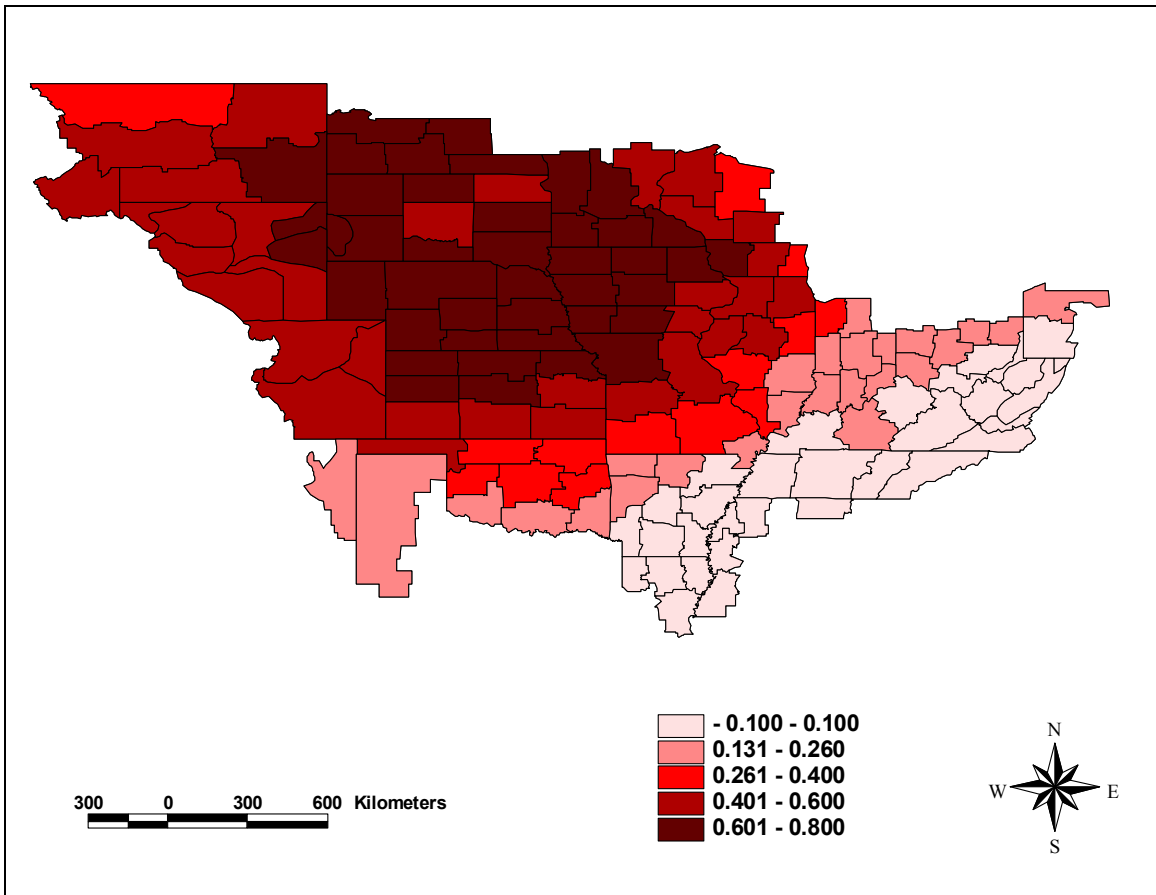


Figure 32: Loadings for MAMJ PDSI Rotated Component 1

northwest Arkansas and southeast Missouri basins (Figure 33). The third rotated component has extreme loadings that are located primarily in the Arkansas and Lower Mississippi basins with a pattern of opposite sign focused on the northwest Missouri basin (Figure 34).

When the climate divisions are mapped to identify the rotated component on which they load most highly in the rotated PCA (Figure 35), it is apparent that the rotated components correspond well to the sub-basins of the MMRB (compare Figure 35 to Figure 5). More specifically, divisions that load highest on Component 1 comprise nearly the entire Missouri basin and the vast majority of the Upper Mississippi basin. Likewise, Component 2 captures the greatest hydroclimatic variability in the entire Ohio and Tennessee basins. Component 3 contains approximately two-thirds of the area of the Arkansas basin and over half of the area of the Lower Mississippi basin. Quantification of the areas within each basin is shown in Table 5. Because only climate divisions with at least half of their area lying within the MMRB are included in this study, some portions of four sub-basins contain areas that are not contained in Components 1, 2, or 3.

Table 5: Percentage of Each Sub-basin Contained in Each Rotated Component Based on PDSI

Sub-basin	Component 1	Component 2	Component 3	Not Contained in MMRB
Arkansas	20.10	9.50	59.29	11.11
Lower Mississippi	0	46.67	53.33	0
Missouri	95.38	2.51	0.30	2.11
Ohio	0	100.00	0	0
Tennessee	0	74.00	0	26.00
Upper Mississippi	71.48	25.38	0	3.14

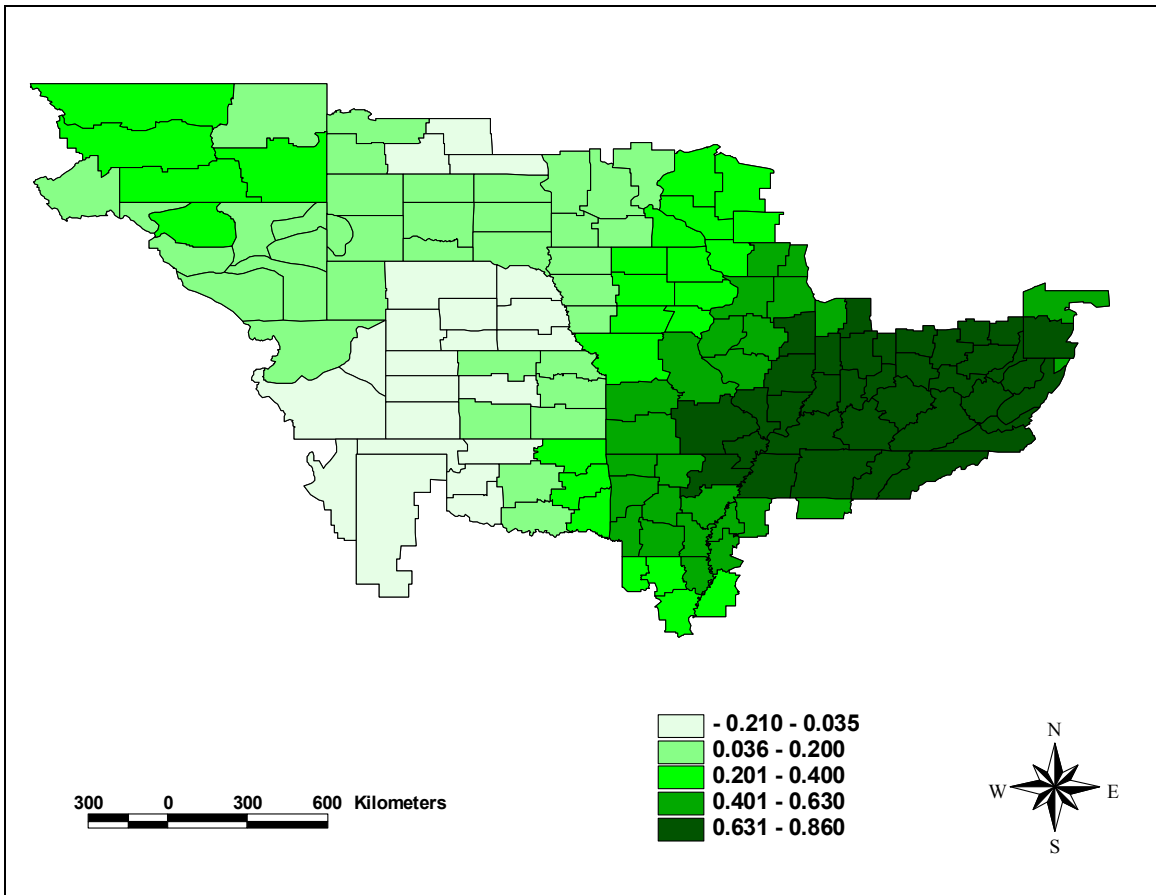


Figure 33: Loadings for MAMJ PDSI Rotated Component 2

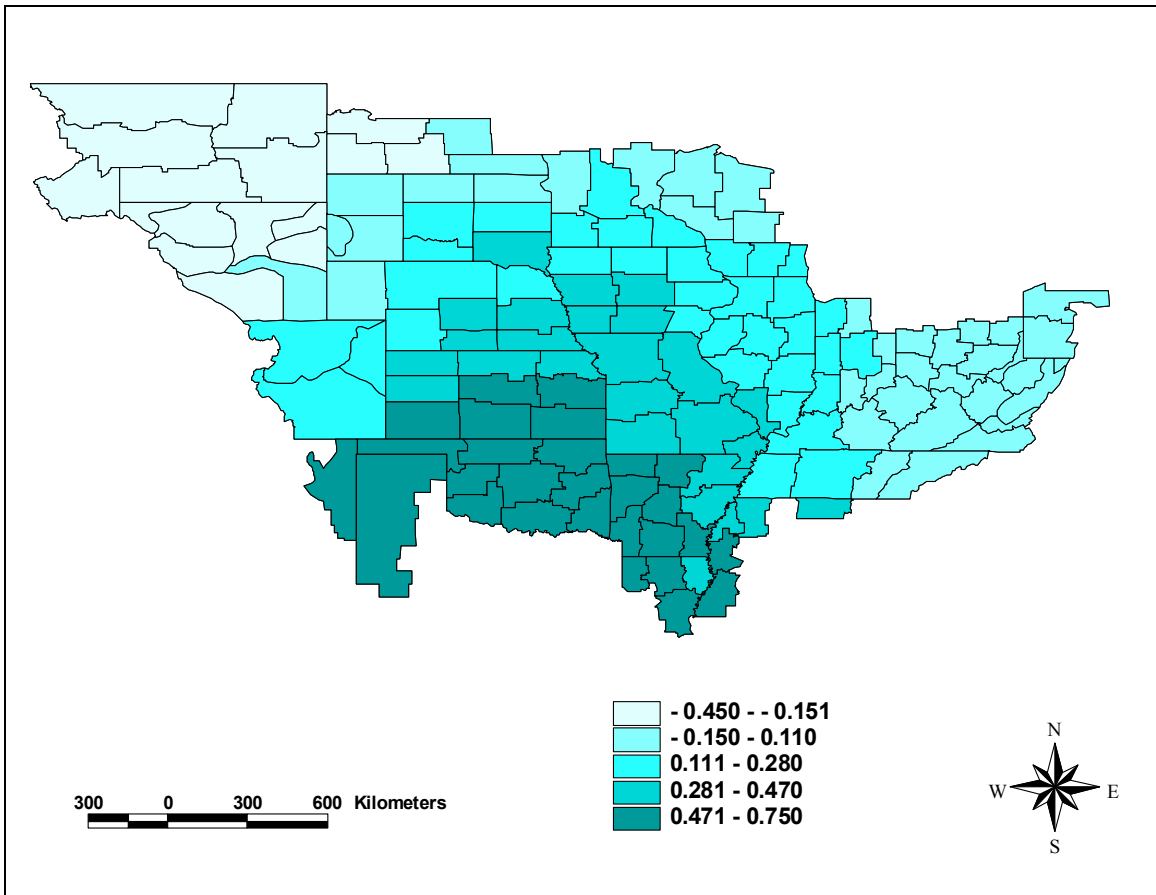


Figure 34: Loadings for MAMJ PDSI Rotated Component 3

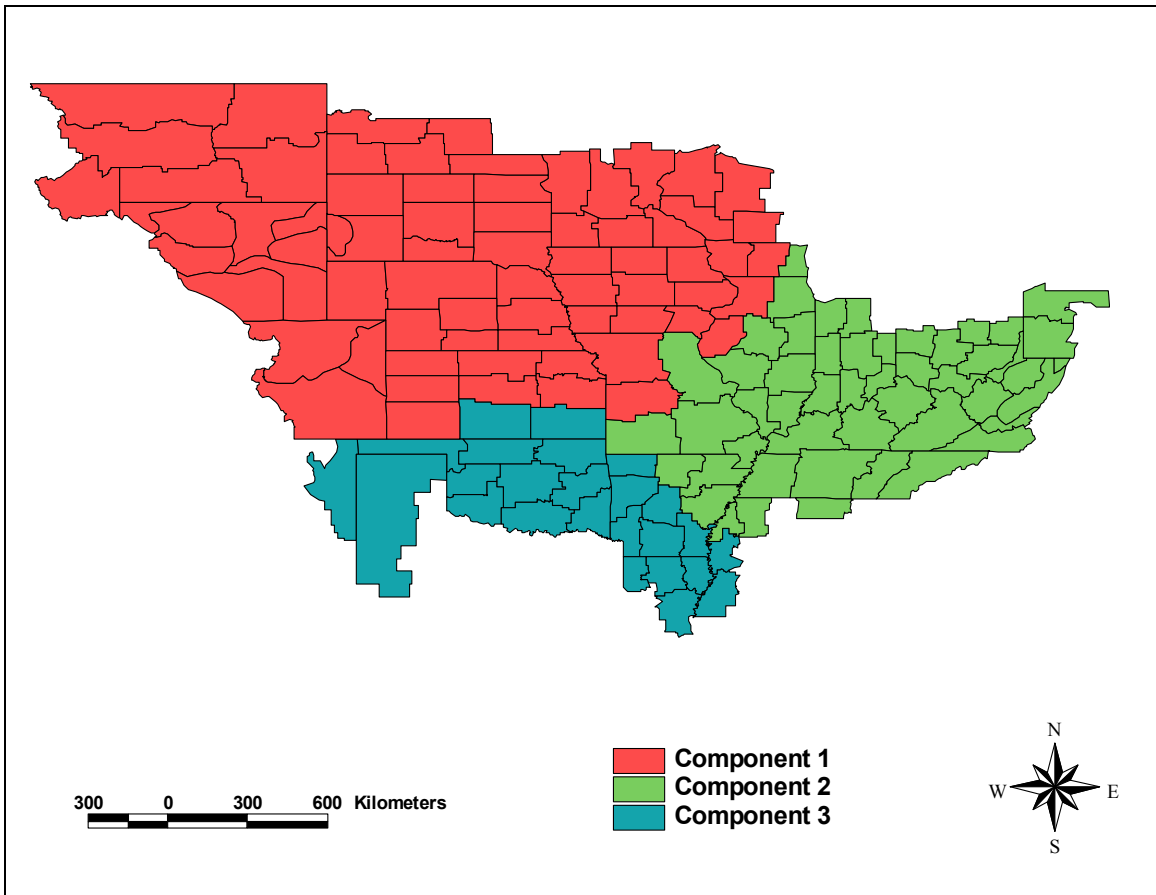


Figure 35: Rotated PCA Component upon Which Climate Divisions Load Most Highly for MAMJ PDSI Analysis

5.2. Regionalization Based on the Palmer Hydrological Drought Index

A rotated PCA was also performed on MAMJ PHDI values for comparison to the patterns generated by PDSI. The resulting patterns are nearly identical to those from the PDSI. The unrotated pattern produces eigenvalues of 49.29, 20.40, and 12.46 for Components 1 through 3, respectively (Table 6). As with the PDSI RPCA, rotating the components results in less explained variance for Component 1, but more explained variance for Components 2 and 3 (Table 7).

Table 6: Eigenvalues of the Unrotated PCA Based on PHDI.

Component	Eigenvalue	Explained Variance (Percent)
1	49.29	33.8
2	20.40	14.0
3	12.46	8.5

Table 7: Eigenvalues of the Rotated PCA Based on PHDI.

Component	Eigenvalue	Explained Variance (Percent)
1	32.19	22.1
2	31.28	21.4
3	18.67	12.8

As with the PDSI rotated PCA, the first component also displays peak loadings centered on the eastern Missouri and western Upper Mississippi basins with loadings of the opposite sign centered on the Lower Mississippi, Tennessee, and Ohio basins (Figure 36).

The second rotated component produces maximum loadings centered in the Ohio and Tennessee basins with loadings of opposite sign centered on the Arkansas and central Missouri basins (Figure 37). The third rotated component is centered on the Arkansas

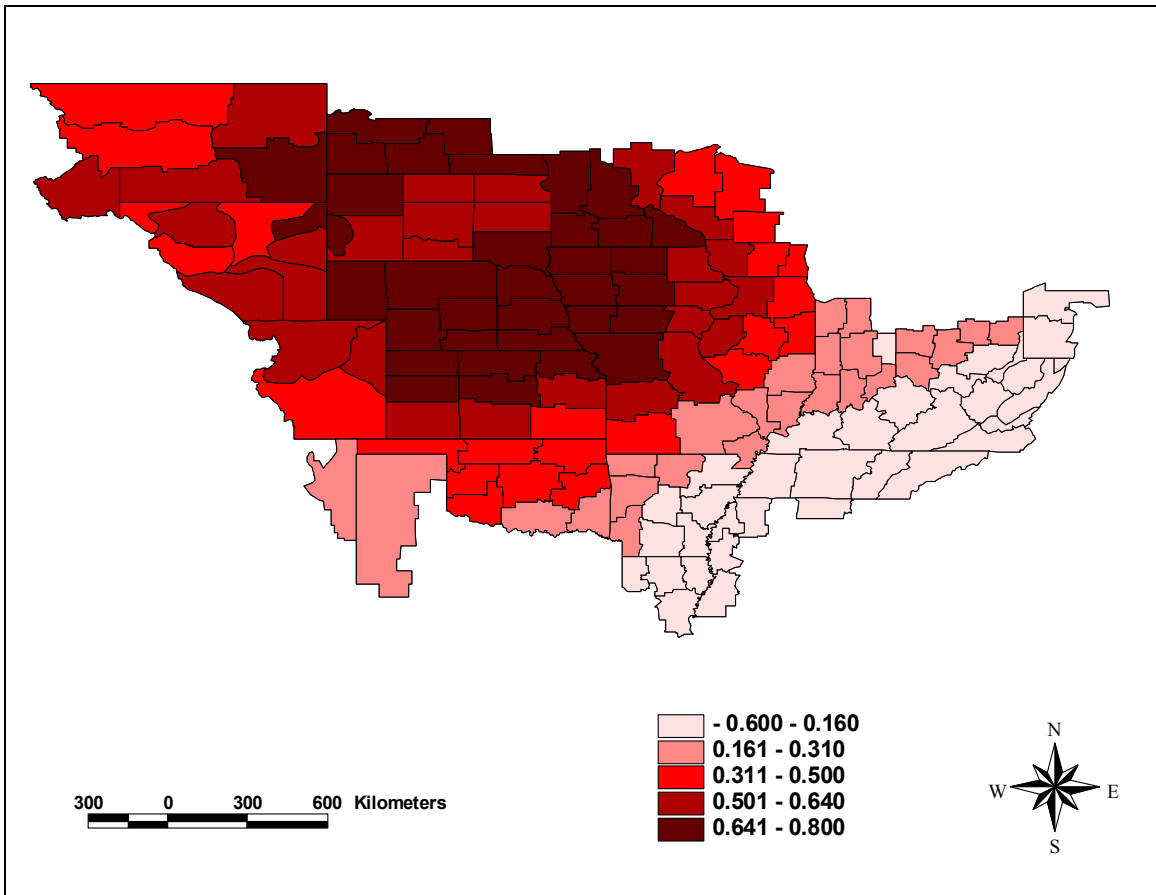


Figure 36: Loadings for MAMJ PHDI Rotated Component 1

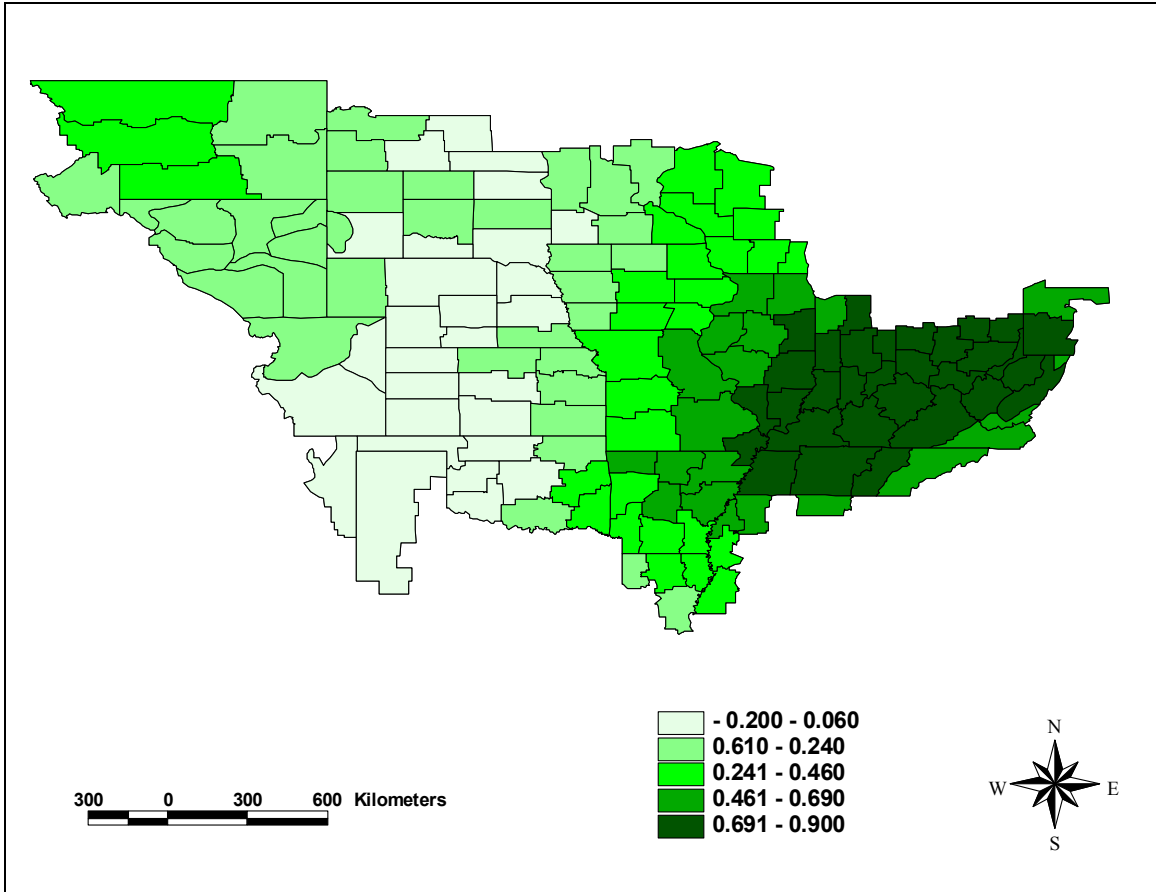


Figure 37: Loadings for MAMJ PHDI Rotated Component 2

basin with loadings of opposite sign centered on the northwest Missouri basin (Figure 38).

Figure 39 shows the rotated component on which each climate division loads most highly. Again, these rotated components correspond well to the sub-basins of the MMRB (compare Figure 5 to Figure 39). Divisions that load highest for rotated components 1, 2, and 3 correspond closely to those results found for the PDSI (compare Figure 39 to Figure 35).

As with the PDSI results, rotated components correspond well to the sub-basins of the MMRB (Table 8). These patterns are nearly identical to those found for the PDSI. Component 1 corresponds very closely to the Missouri basin, Component 2 with the Ohio and Tennessee basins, and Component 3 with the Arkansas basin.

Table 8: Percentage of Each Sub-basin Contained in Each Rotated Component Based on PHDI

Sub-basin	Component 1	Component 2	Component 3	Not Contained in MMRB
Arkansas	20.10	5.63	63.16	11.11
Lower Mississippi	0	45.05	54.95	0
Missouri	95.38	1.55	1.32	1.75
Ohio	0	100	0	0
Tennessee	0	74.00	0	26.00
Upper Mississippi	71.48	25.38	0	3.14

5.3 Summary

This chapter has shown, through the use of both the PDSI and PHDI as indicators of surface moisture availability, that relatively homogeneous hydroclimatic subregions exist in the MMRB for the March through June period. The spatial extent of these regions remains consistent whether the PDSI or PHDI is used to derive them.

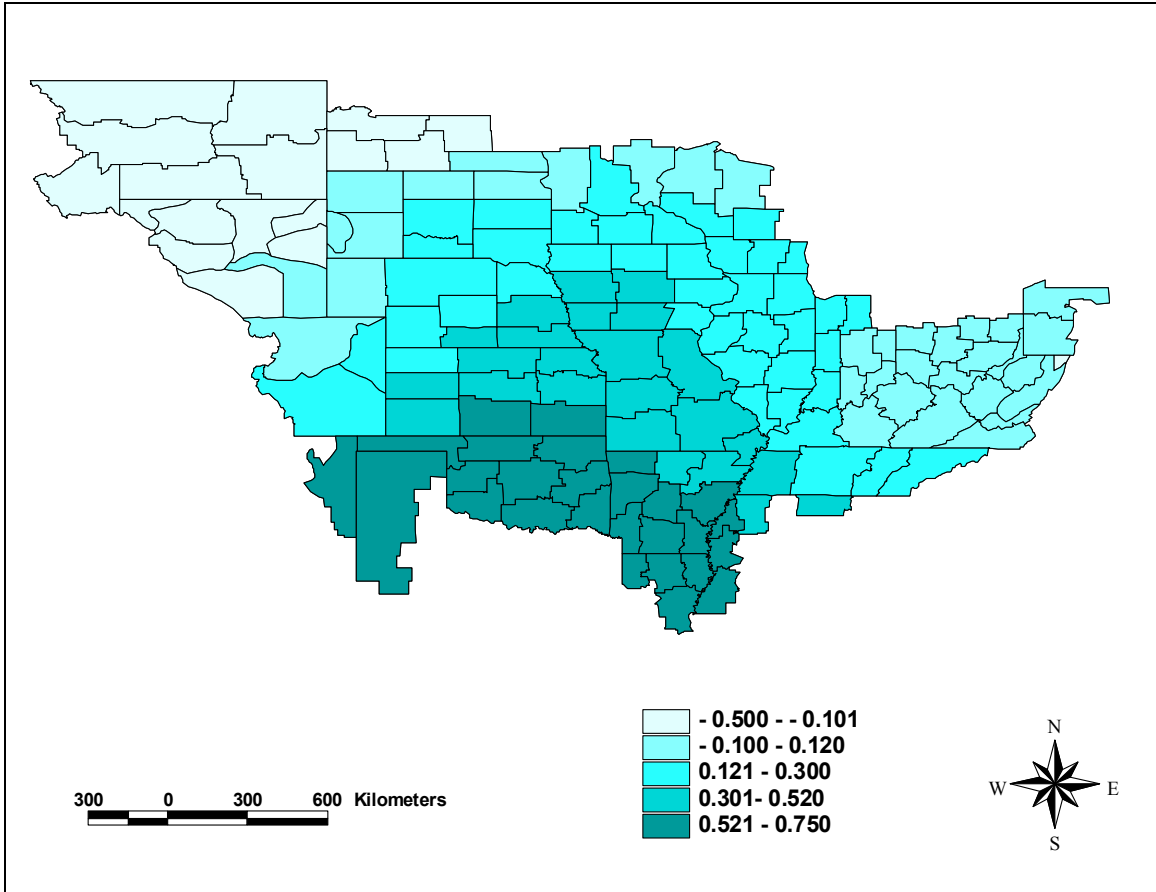


Figure 38: Loadings for MAMJ PHDI Rotated Component 3

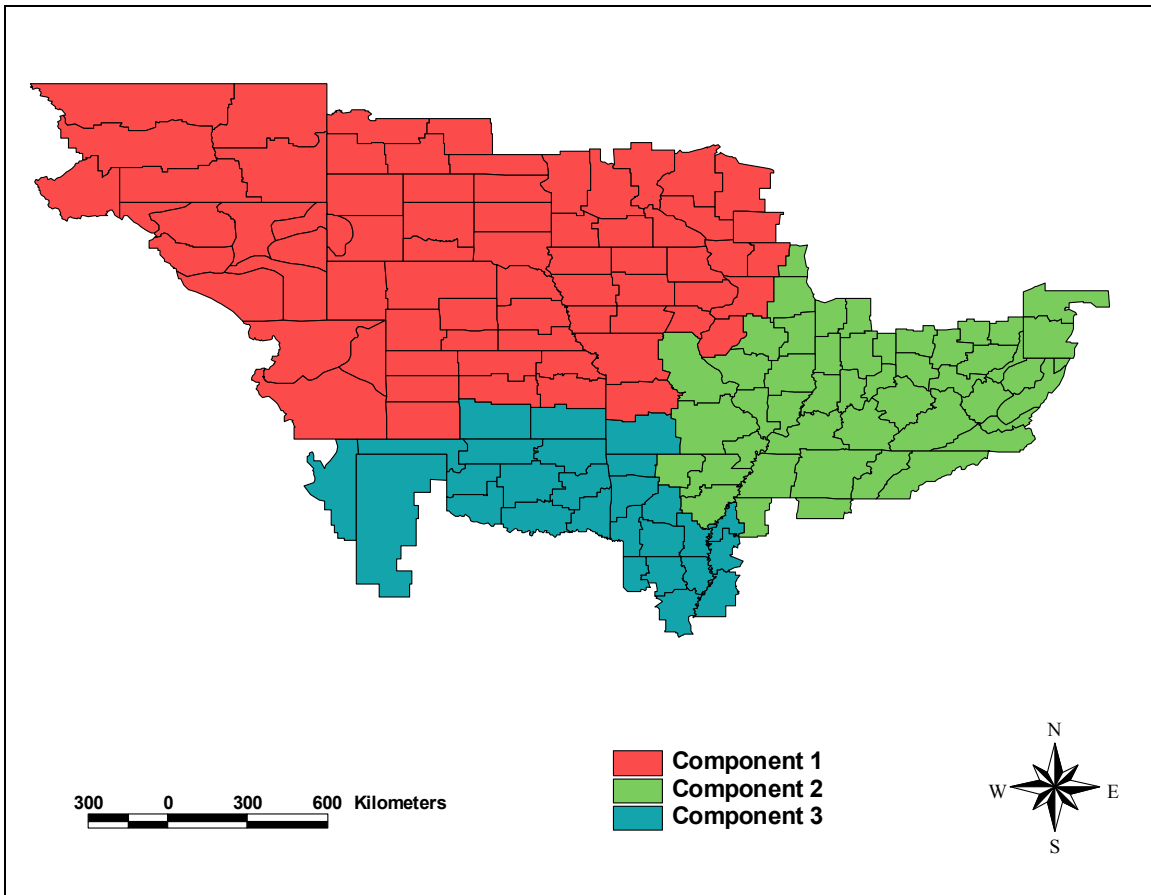


Figure 39: Rotated PCA Component upon Which Climate Divisions Load Most Highly for MAMJ PHDI Analysis

Furthermore, these regions correspond closely to the sub-basins of the MMRB. Specifically, rotated Component 1 (for both the PDSI and PHDI) corresponds well to the Missouri basin, as displayed by the spatial pattern of RPCA loadings. Likewise, Component 2 is reminiscent of the Ohio and Tennessee basins, and Component 3 largely corresponds to the Arkansas basin. Therefore, because it was shown in Chapter 4 that surface moisture is strongly positively correlated to GMHZ area, it seems that anomalously wet conditions within relatively small regions may cause large anomalies of runoff into a particular drainage basin and contribute greatly to anomalously large GMHZ extent, particularly in the basins that contribute large percentages of the Mississippi streamflow, such as the Ohio and Tennessee Rivers. In other words, more runoff would be likely to enter the Mississippi River if heavy precipitation fell in one basin rather than having a chance to affect soil moisture in two sub-basins. Perhaps these findings may explain anomalously large and small measurements of the surface area of the GMHZ. Furthermore, these results may facilitate the use of long-lead climate forecasts for providing environmental planners with information that could assist with forecasting the area of the GMHZ up to several months in advance. Chapter 6 will elaborate on this forecasting theme, by focusing on quantifying the relationship between the PDSI and PHDI in the MMRB and the area of the GMHZ to hindcast and forecast the area of the GMHZ.

CHAPTER 6

A PREDICTIVE MODEL FOR FORECASTING AND HINDCASTING GULF OF MEXICO HYPOXIC ZONE EXTENT

Chapter 4 suggested that moisture seems to be related to GMHZ extent and also to teleconnections. Chapter 5 regionalized the study area to identify the degree of overlap between the sub-basins and homogeneous moisture variability regions. However, the influence of a relationship between the PDSIs and PHDIs in the various climate divisions and the teleconnections on the GMHZ can be quantified to produce a predictive equation. This equation could be used for forecasting future GMHZ area up to several months in advance, and also to hindcast the GMHZ area using historical hydroclimatic and/or teleconnection data. The result may aid the understanding of the range of scenarios to be expected in the GMHZ size.

6.1 Preparation of Data

Because the input data matrix in each monthly analysis contains 146 columns (one for each climate division) and only 19 rows (one for each month from 1985 to 2003, excepting the missing data in 1989), the matrix was computationally unstable to such an extent that the use of a level of significance of 0.05 in the stepwise multiple regression procedure would have included 16 predictor variables in the regression equation for the May PDSI analysis. Analyses for other months and for the PHDI would have also produced large numbers of independent variables, thereby increasing the risk of producing an unacceptable degree of multicollinearity in the regression equation. Therefore, a 0.01 level of significance threshold was implemented in the stepwise multiple regression procedure. After the models were generated, tests for violations of

the heteroscedasticity and serial autocorrelation were conducted using simple tests for trends in the residuals and Durbin-Watson tests, respectively.

The June predictive model was then used to generate hindcasts of the area of the GMHZ for the pre-1985 period. It was decided that the June equation would be most appropriate because GMHZ measurement often occurred in the middle part of July. The use of a July-monthly-averaged PDSI as a predictor would have represented water balance conditions in the post-measurement phase. This hindcast of historical GMHZ area since 1895 due to natural causes may assist in explaining seafood harvests in the past and give an estimate of possible return periods and scenarios for future GMHZ extent.

6.2 Models Based on the Palmer Drought Severity Index

Results suggest that February provides the longest lead forecasts possible, because the R^2 value was insignificant beginning with January data. Furthermore, climate divisions included in the multiple regression equation were as follows: June: Minnesota 8 (Figure 40); May: Missouri 1, Wisconsin 2, and Arkansas 4 (Figure 41); April: Minnesota 8 and Indiana 8 (Figure 42); March: Minnesota 8 (Figure 43); February: Wisconsin 7 and Mississippi 2 (Figure 44). The climate divisions entered their respective stepwise regression equations at a 0.01 level of significance.

The June PDSI of one climate division (MN8) selected by the June data explains 44.6 percent of the variance in the GMHZ area. The equation used to hindcast the area using June PDSI data is:

$$GMHZ (km^2) = 9485.531 + 1685.350 (MN8 PDSI)$$

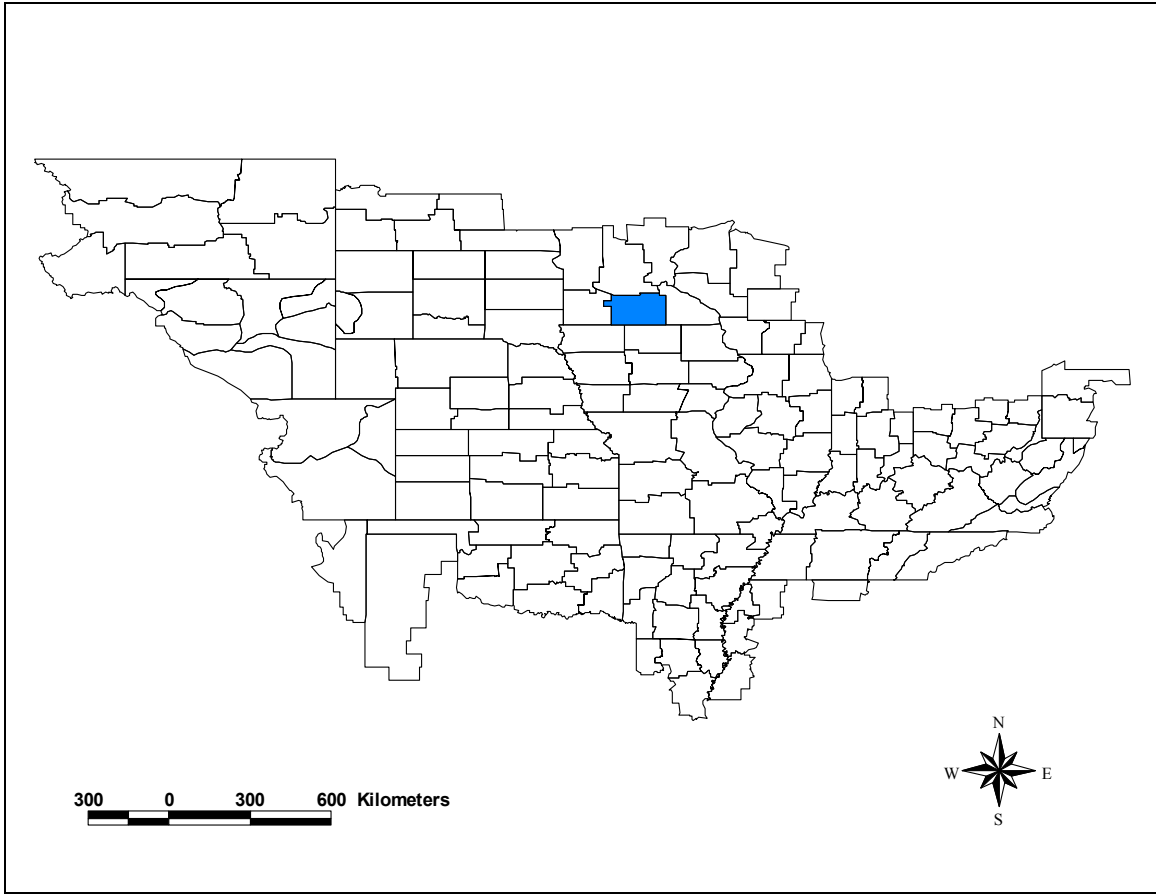


Figure 40: Climate Division for Which the June PDSI is Used to Predict the Area of the July GMHZ

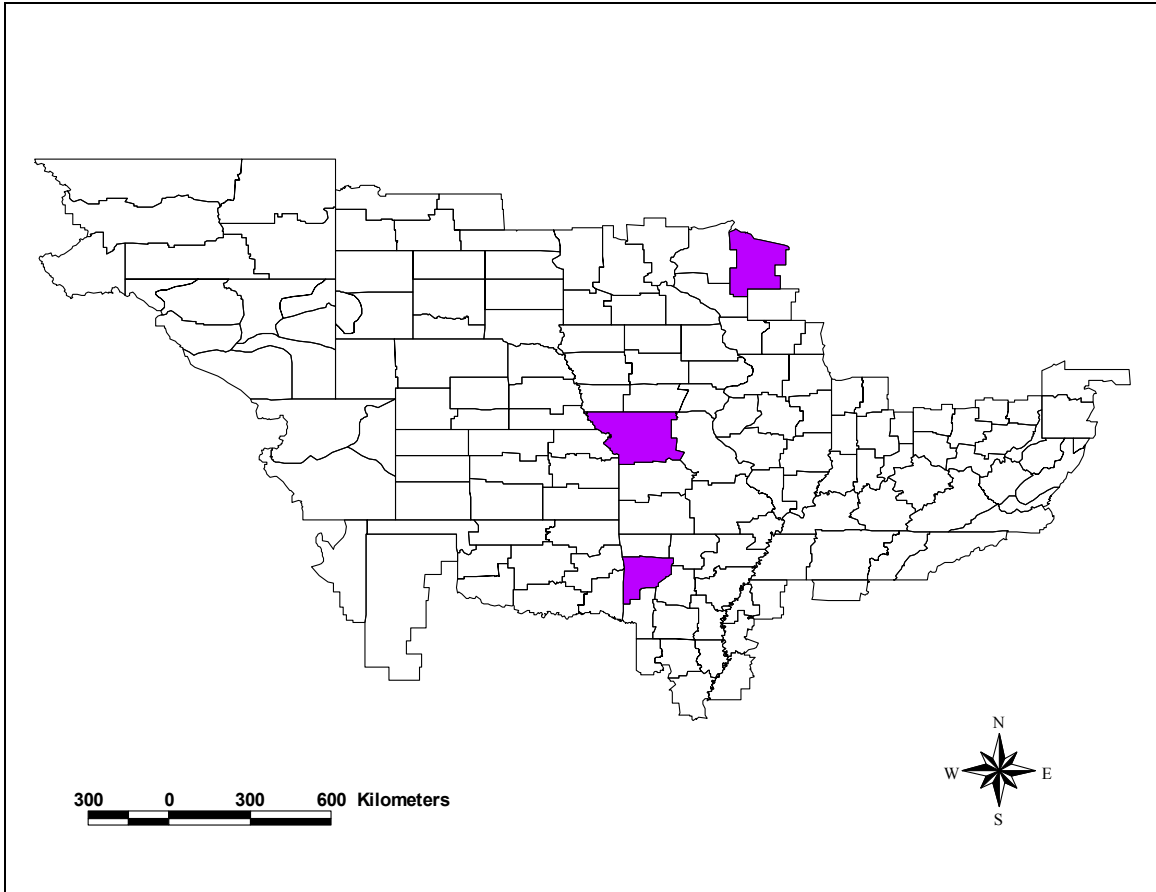


Figure 41: Climate Divisions for Which the May PDSI is Used to Predict the Area of the July GMHZ

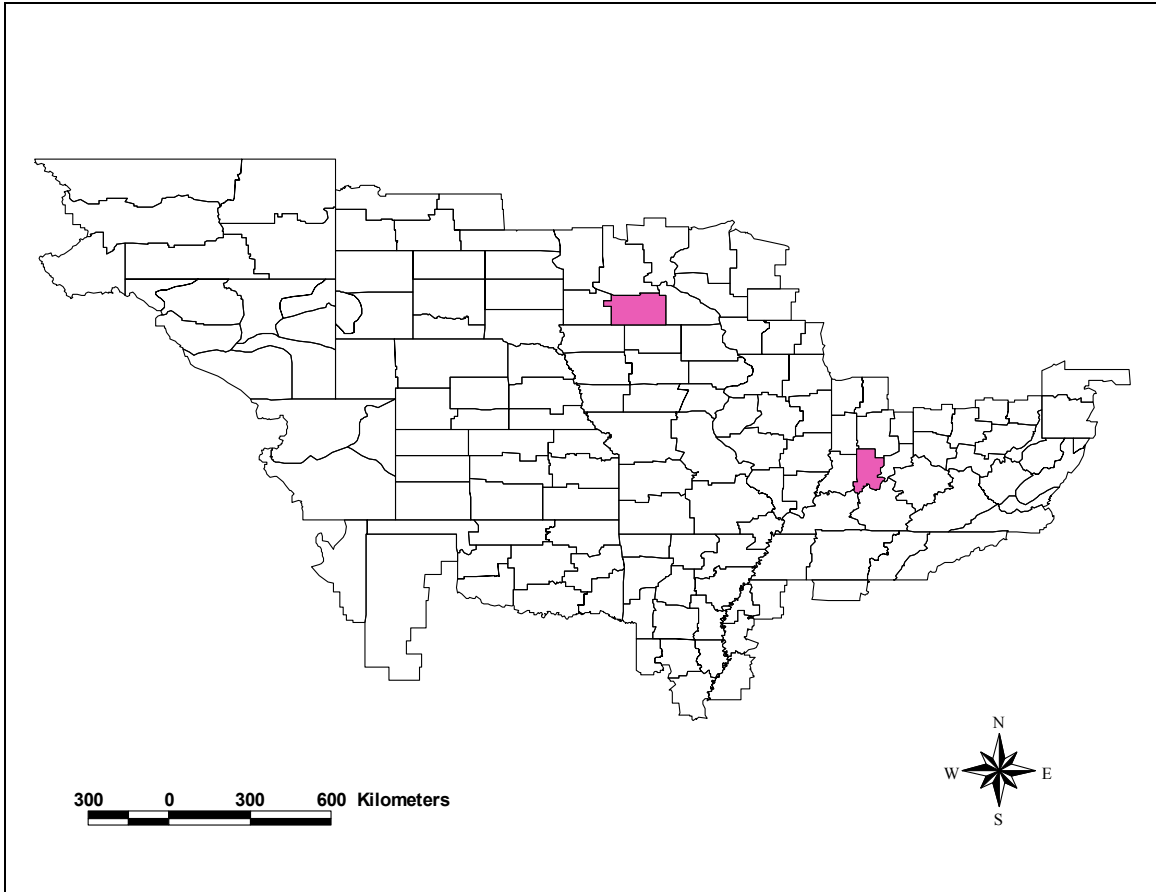


Figure 42: Climate Divisions for Which the April PDSI is Used to Predict the Area of the July GMHZ

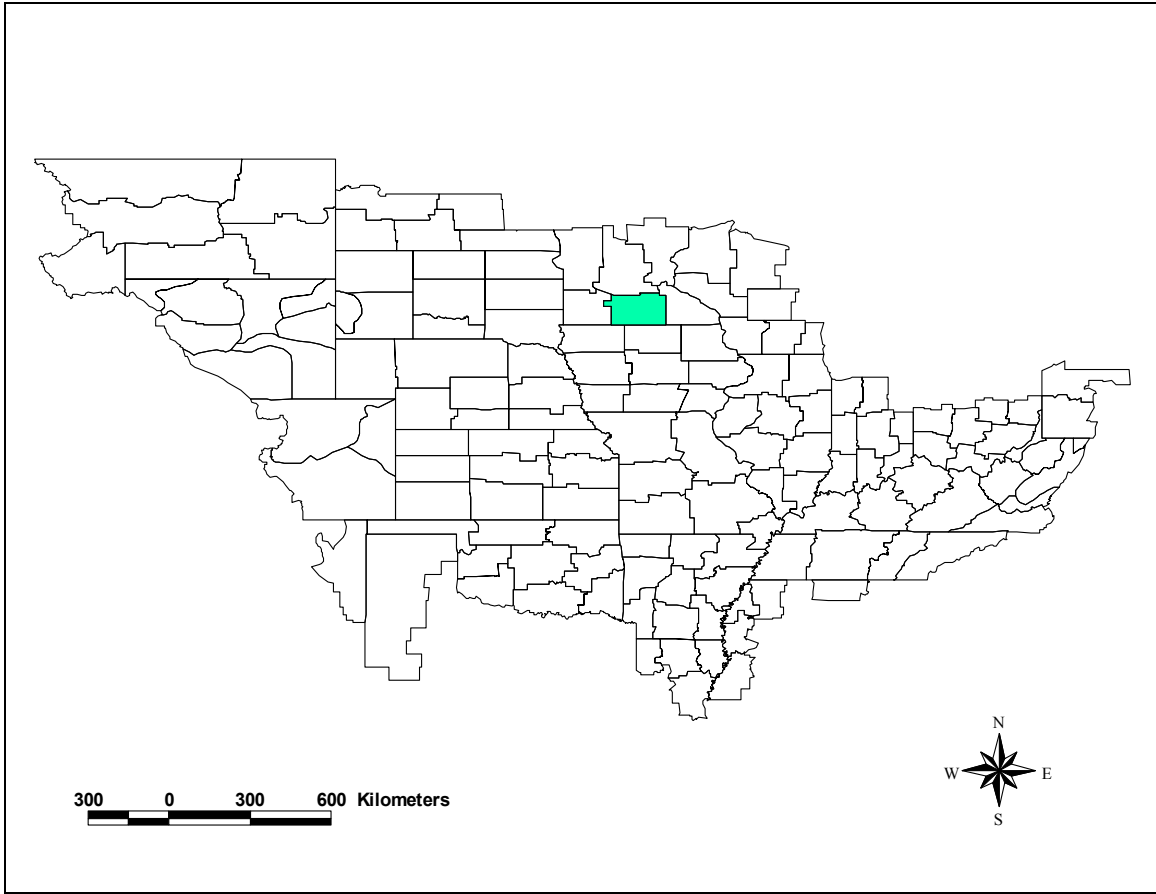


Figure 43: Climate Division for Which the March PDSI is Used to Predict the Area of the July GMHZ

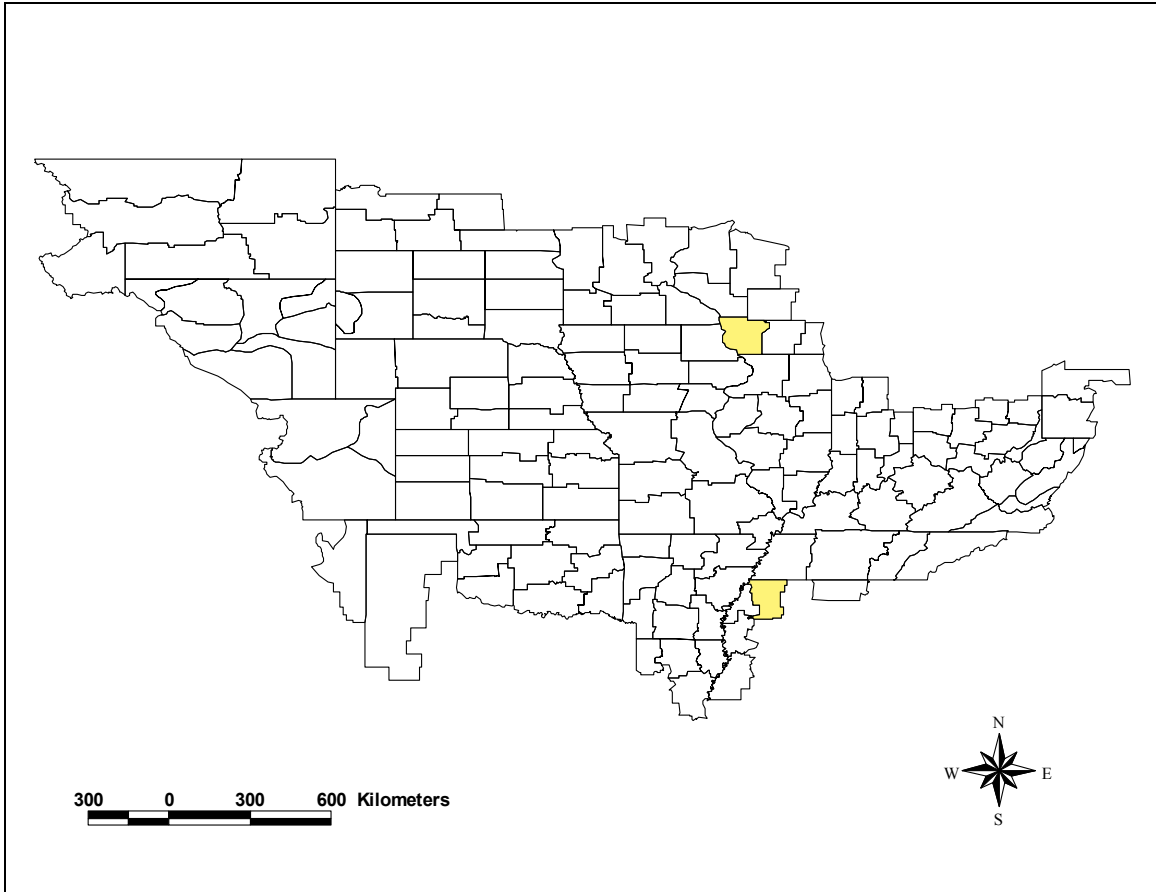


Figure 44: Climate Divisions for Which the February PDSI is Used to Predict the Area of the July GMHZ

Using three climate divisions the May equation explains 92.4 percent of the variance of the GMHZ area. The equation used to hindcast the area using May PDSI data is:

$$GMHZ (km^2) = 8103.18049 + 1491.82443 (WI2 PDSI) + 2645.65745 (MO1 PDSI) - 1627.93722 (AR4 PDSI)$$

In this case, it is noteworthy that wetter (drier) conditions in Arkansas 4 are associated with a smaller (larger) overall GMHZ. This result probably occurs because hydroclimatic anomalies in AR4 tend to be of opposite sign to hydroclimatic anomalies in most of the rest of the MMRB (presumably including the parts of the MMRB that contribute more runoff). Likewise, two climate divisions selected by the April data explain 67.1 percent of the variance of the GMHZ area. The equation used to hindcast the area using April PDSI data is:

$$GMHZ (km^2) = 8797.20187 + 1392.38823 (IN8 PDSI) + 1921.36710 (MN8 PDSI)$$

Similarly, 38 percent of the variance is explained using the one climate division selected in March. The equation used to hindcast the area using March PDSI data is:

$$GMHZ (km^2) = 9151.93563 + 1946.45786 (MN8 PDSI)$$

Finally, 64 percent of the variance of the GMHZ area is explained using the PDSI of two climate divisions in February. The equation used to hindcast the area using February PDSI data is:

$$GMHZ (km^2) = 8934.40487 + 1674.41706 (MS2 PDSI) + 2378.27173 (WI7 PDSI)$$

These results suggest that May PDSI is the best indicator of July GMHZ area.

The climate divisions that have the greatest impact on the GMHZ area tend to be northerly locations near the headwaters of the Mississippi River. All of the climate divisions significant at $\alpha = 0.01$ are either adjacent to or near the Mississippi, Missouri, or

Ohio Rivers. Division 8 in Minnesota is the most significant, being the sole predictor during June and March and the most significant predictor in April. This climate division also shows the highest correlation with the phase of ENSO. Perhaps the location of this division allows it to represent hydroclimatic variability present in the MMRB very effectively, and the northerly location places this division under the influence of the Rossby waves and their associated convergence/divergence for most of the February to June period, unlike more southerly locations which would be farther south than the mean Rossby wave position in late spring.

Signs of heteroscedasticity in the model fit are identifiable, as the residuals increased significantly over the 18-year study period for May ($\alpha = 0.0010$), April ($\alpha = 0.0295$), and March ($\alpha = 0.0418$). Therefore, caution should be exercised in the interpretation of results because the heteroscedasticity assumption of regression analysis appears to have been violated in some cases. However, no serial autocorrelation is identified by the Durbin-Watson Test at $\alpha = .05$.

When the May predictive equation is used to generate estimates of the GMHZ in the pre-measurement period, some interesting results are apparent. Specifically, the GMHZ is estimated to have been non-existent in a few years, such as 1934, 1946, 1948, 1949, 1956, 1957, and 1977. Even though the equation produced negative hindcasted areas for these years, these surface areas will be represented with a zero (Table 9). Many of these years were characterized by drier-than-normal periods in the MMRB, as the dry years of the “Dust Bowl” and the 1950s had no GMHZ according to the equation. Interestingly, a hint of the 22-year sunspot cycle (Tsiropoula 2003) is present, with years

in the 1930s, 1950s, and 1970s represented among these years with no hindcasted GMHZ. These results should be investigated more thoroughly.

Table 9: Smallest Hindcasted GMHZ Surface Areas based on the May PDSI

Year	Hindcasted GMHZ Surface Area(km ²)
1957	0
1934	0
1989*	0
1977	0
1949	0
1956	0
1946	0
1931	0
1948	0
1940	1094
1941	1988
1958	2373
1980	2698
1937	3376
1930	3429
1975	3453
1939	3630
1954	3920
1966	4027
1955	4695

(* Although 1989 is contained in the study period of mapping cruised, no data are available for that year. Therefore, the hindcasted value of zero is presented among the smallest hindcasted GMHZ years.)

On the other hand, an intense GMHZ is suggested for some years in the pre-1985 period. Specifically, four pre-measurement years have a hindcasted value exceeding 20,000 km²: 1983 (23,172 km²), 1916 (22,911 km²), the well-known Mississippi flood year of 1973 (22,603 km²), and 1904 (20,636 km²) (Table 10). It is well-known that intense El Niño years occurred in 1972-73 and 1982-83. However, the spring of 1904 and summer of 1916 were two of the most intense La Niña events on record (CDC 2005). Therefore, ENSO signals appear contradictory for these probable large-GMHZ years.

Once again, further research should be conducted to identify a “common thread” that may unite these years. For example, other teleconnection indices may provide evidence of such a link, but the Niño 3.4, NAO, AO, and PNA Indices cannot be used to find a commonality among these years because they only exist in direct form since 1950. The PDO Index does exist for the early 1900s, but it does not show any pattern among these years.

Table 10: Largest Hindcasted GMHZ Surface Areas based on the May PDSI

Year	Hindcasted GMHZ Surface Area (km ²)
1983	23172
1916	22911
1973	22603
1904	20636
1942	19619
1978	19464
1929	18482
1982	18326
1974	17074
1951	16775
1947	16674
1960	15084
1899	14921
1927	14773
1903	14625
1943	14391
1915	14334
1908	14310
1984	13704
1945	13637

In addition to the Great Mississippi Flood of 1973, the Great Flood of 1927 was even more notable in terms of human and environmental impacts (Barry 2002). However, the hindcast suggests that the 1927 GMHZ extent ranked only 15th of the 91 pre-measurement years. Perhaps poor model performance and/or other factors may account for the relatively benign GMHZ in that year. This result supports the work of

Rabalais *et al.* (2002a), which found that the surface area of the GMHZ has increased since the 1950s. One reason for this result may be the time frame in which the rainfall came that contributed to the Great Flood of 1927. The Mississippi River began to rise in August of 1926, reached flood stage in Illinois Climate Division 8 on the first day of 1927, and remained flooded through May 1927 at some locations (Barry 1997). Although the Mississippi River levels decreased by May, the PDSI in some areas continued to rise throughout 1927, and remained elevated well into 1928. This discrepancy between maximum streamflow and soil moisture levels may account for the unexpected results. The model failed to produce hindcasted GMHZ as large as would be expected because the PDSI was high in both Arkansas 4 and Missouri 1 during May of 1927 but relatively low in Wisconsin 2. Perhaps peak rainfall at this time occurred over the southern portion of the basin.

6.3 Models Based on the Palmer Hydrological Drought Index

Results suggest that April provides the longest lead forecasts possible, since no climate divisions remained in the model at $\alpha = 0.01$ beginning with March data. Furthermore, climate divisions included in the multiple regression equation were as follows: June: Missouri 1 and Wisconsin 2 (Figure 45); May: Iowa 9 (Figure 46); April: Iowa 9, Nebraska 6, and South Dakota 7 (Figure 47). These climate divisions are all significant at the 0.01 level.

A total of 80.0 percent of the variance of the GMHZ area is explained by the June PHDI in two climate divisions. The equation used to hindcast the area using June PHDI data is:

$$GMHZ (km^2) = 10373 + 2025.351 (MO1 PHDI) + 1235.364 (WI2 PHDI)$$

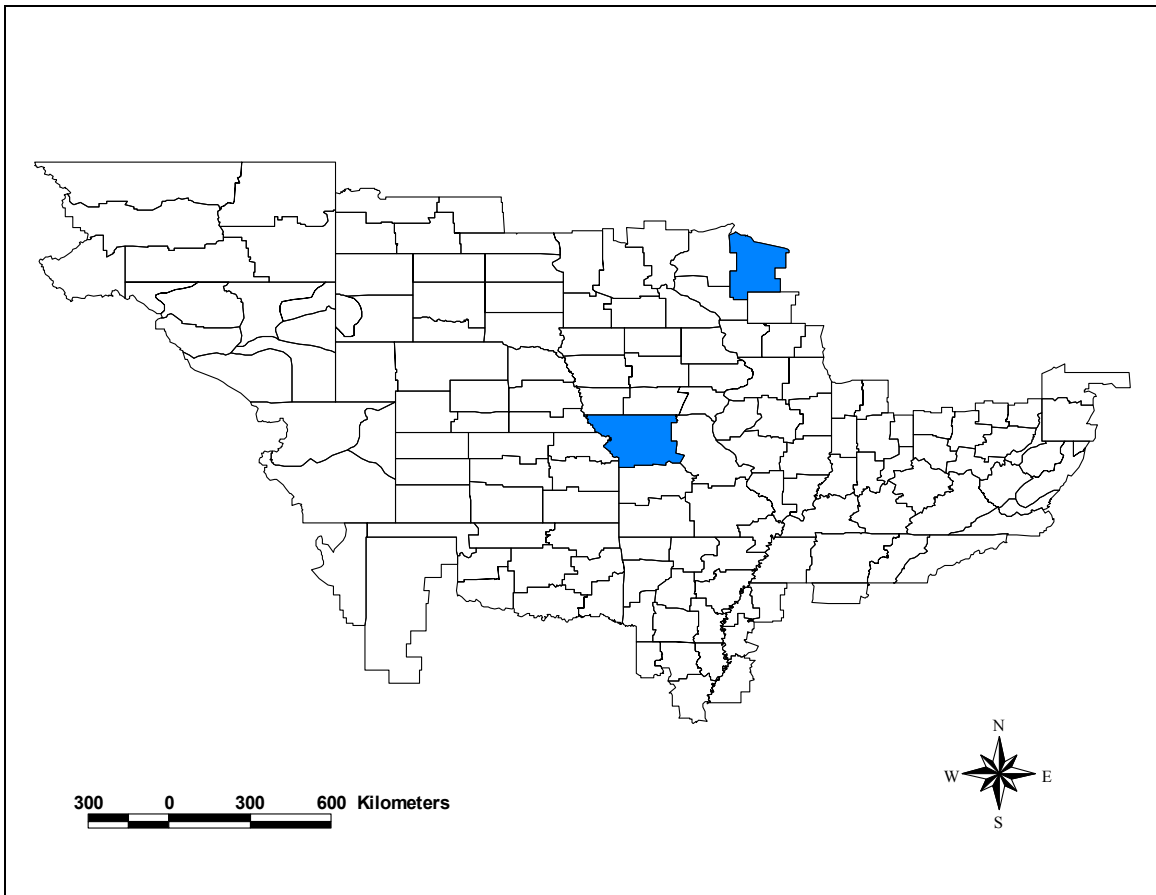


Figure 45: Climate Divisions for Which the June PHDI is Used to Predict the Area of the July GMHZ

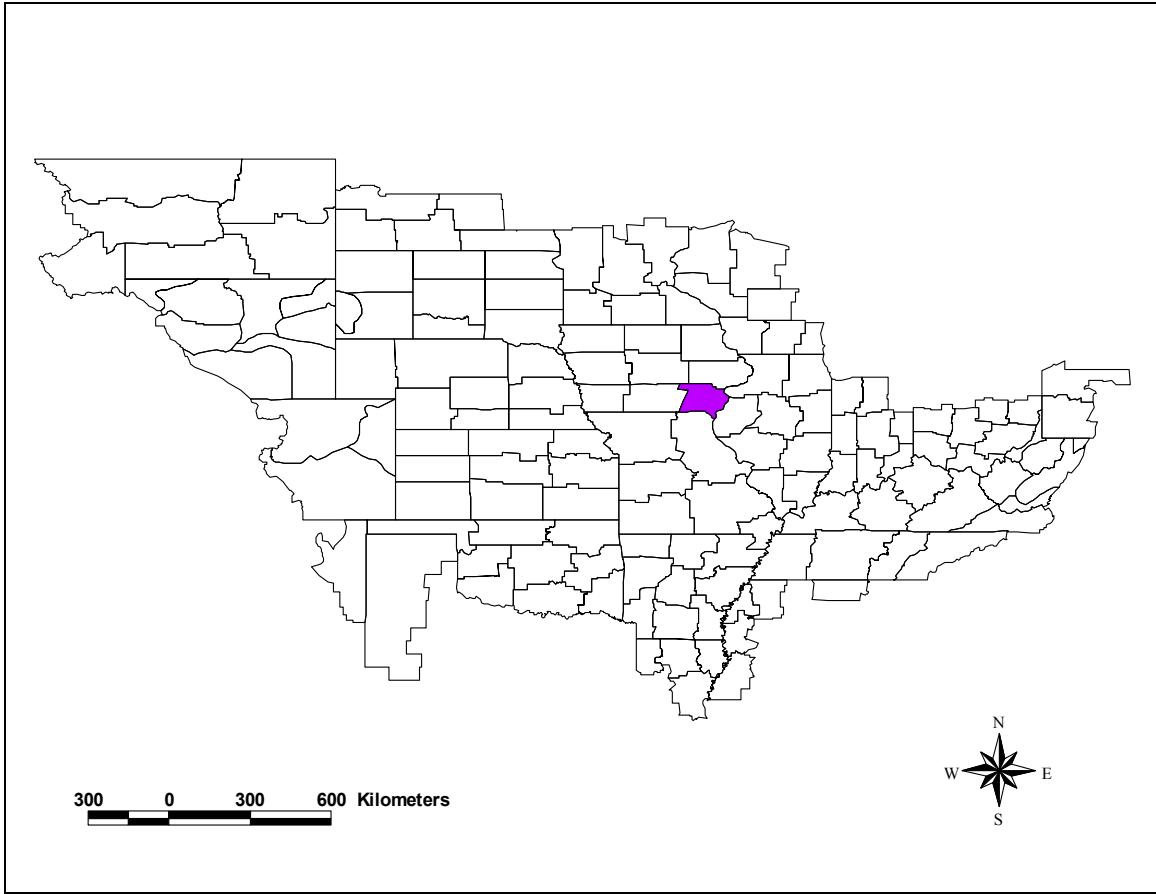


Figure 46: Climate Division for Which the May PHDI is Used to Predict the Area of the July GMHZ

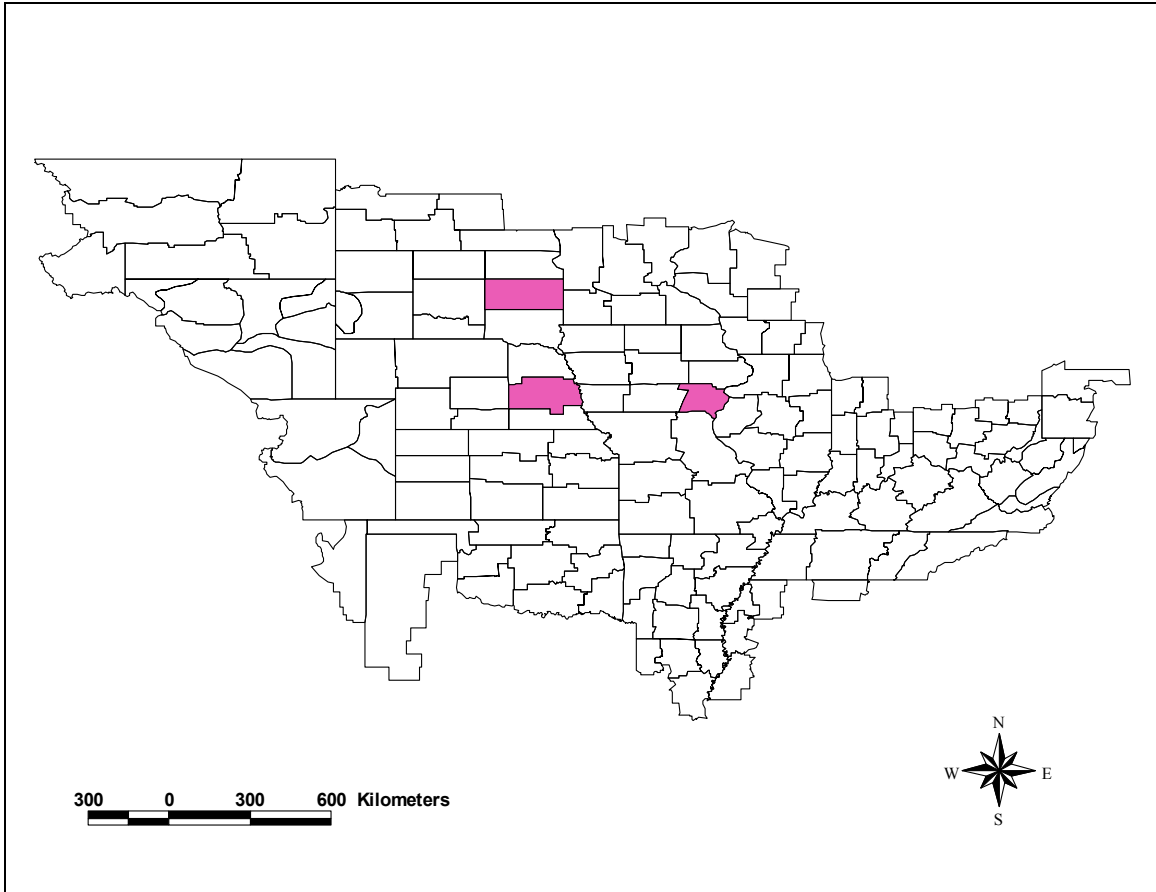


Figure 47: Climate Divisions for Which the April PHDI is Used to Predict the Area of the July GMHZ

Likewise, 70.1 percent of the variance in the GMHZ area is explained by May PHDI in Iowa's Division 9. The equation used to hindcast the area using May PHDI data is:

$$GMHZ (km^2) = 10005 + 2328.970 (IA9 PHDI)$$

Finally, 86.5 percent of the variance of the GMHZ area is explained by April PHDI in three divisions. The equation used to hindcast the area using April PHDI data is:

$$GMHZ (km^2) = 9622.278 + 2662.190 (IA9 PHDI) - 2326.845 (NE6 PHDI) + 1205.839 (SD7 PHDI)$$

It is interesting to note that wetter (drier) conditions in Nebraska 6 are associated with smaller (larger) GMHZ extent.

Unlike the PDSI predictive equations, April PHDI values provide the highest level of explained variance. When the April predictive equation was used to generate estimates of the GMHZ in the pre-measurement period, the GMHZ is estimated to have been virtually non-existent in a few years, such as 1931, 1934, and 1958 (Table 11). As was found with the PDSI results, many of these years were characterized by drier-than-normal periods in the MMRB.

In contrast, an intense GMHZ is suggested for some years in the pre-1985 period. Specifically, eight pre-measurement years have a hindcasted value exceeding 16,000 km²: 1939 (19573 km²), 1946 (17880 km²), 1981 (17406 km²), 1943 (17399 km²), 1967 (19362 km²), 1975 (16793 km²), 1937 (16776 km²), and 1947 (16118 km²) (Table 12).

6.4 Teleconnection Indices as Predictors

Six indicators of atmospheric longwave flow (teleconnection indices – the SOI, Niño 3.4, PDO, NAO, AO, and PNA patterns) are entered into another stepwise multiple regression equation to predict GMHZ size based only on the teleconnections. Only the May NAO

Table 11: Smallest Hindcasted GMHZ Surface Areas Based on the April PHDI

Year	Hindcasted GMHZ Surface Area (km ²)
1914	0
1902	0
1905	0
1915	0
1934	0
1900	0
1901	0
1931	0
1906	0
1958	0
1925	73
1989	89
1951	1058
1980	1861
1924	1939
1954	2053
1903	2614
1927	2874
1956	2944
1913	3129

appeared as a predictor of the July-measured GMHZ:

$$GMHZ \text{ area (km}^2\text{)} = 14017 - 4426.35 (\text{May NAO})$$

Thus, when the NAO Index is positive (negative), indicating zonal (meridional) westerlies over the north Atlantic, the GMHZ tends to be anomalously small (large). However, r^2 was only 23 percent, suggesting that teleconnection indices do not offer any additional predictive value over moisture indices, particularly since the moisture indices are available on a near-real-time basis. This result is not surprising, because the teleconnection indices represent the longwave flow, which influences surface moisture availability, which in turn influences the GMHZ. Thus, the moisture indices provide the

most direct relationship to GMHZ area. Furthermore, the existence of the NAO Index only back to 1950 precludes its use for hindcasting into the early 20th century.

Table 12: Largest Hindcasted GMHZ Surface Areas Based on the April PHDI

Year	Hindcasted GMHZ Surface Area (km ²)
1939	19573
1946	17880
1981	17406
1943	17399
1967	17362
1975	16793
1937	16776
1947	16118
1938	15098
1944	15023
1979	14316
1970	14294
1962	14187
1928	13963
1983	13869
1972	13817
1942	13393
1973	13318
1922	13112
1968	13054

An additional analysis identifies a predictive equation that includes both divisional moisture indices and teleconnection indices as potential predictors. The NAO seems to be more strongly related to the July GMHZ area than other teleconnections, but even the NAO does not provide much predictive value. This supports the hypothesis that teleconnections are not as effective as the climate divisional moisture indices for predicting GMHZ area.

6.5 Summary

This research has estimated the surface area of the GMHZ since 1895 in a stepwise multiple regression approach using PDSI and PHDI data to represent surface moisture availability. The resulting equations can be used to predict the July area of the GMHZ as soon as the end of February, providing a 120-day forecast. However, accuracy seems to improve when the lead time is reduced through the use of May PDSI or the April PHDI data.

Results of the hindcasting procedure seem to be consistent with what should be expected given known atmospheric and hydrologic anomalies that occurred during historical years. Further research must be conducted to provide additional explanations for the estimated area of the GMHZ, such as land-use changes and trends in agricultural fertilizer use. In addition, the results can be used to assist in explanations of variability in seafood harvests, thereby benefiting not only the seafood industry but also ecotourism in Louisiana by providing environmental planners and wildlife and fisheries officials with long-lead information in setting upcoming seasonal boundaries for commercial fisheries harvests. These and future results may prove useful in our understanding of this complex issue that involves natural and social causes and impacts.

CHAPTER 7 SUMMARY AND CONCLUSIONS

This chapter summarizes the major results from Chapters 4-6 in the context of the hypotheses presented in Chapter 1. The chapter concludes with suggestions for future research that will expand upon the results shown here.

7.1 Summary

This research has shown that there is a strong positive relationship between spring streamflow in the Mississippi River and the surface area of the GMHZ. Results also suggest a relationship between PDSI/PHDI and the surface area of the GMHZ throughout most of the MMRB. The teleconnections analyzed in Chapter 4 display some relationships with soil moisture and therefore runoff throughout regions within the MMRB that contribute much of the water supply to the Mississippi River. Therefore, the first four hypotheses presented in Chapter 1 were confirmed or partially confirmed.

Chapter 5 has shown, through the use of both the PDSI and PHDI as indicators of surface moisture availability, that relatively homogeneous hydroclimatic subregions exist in the MMRB for the March through June period. The spatial extent of these regions remains consistent whether the PDSI or PHDI is used to derive them. These regions correspond closely to the sub-basins of the MMRB. Thus, Hypothesis 5 in Chapter 1 was also verified. It seems that anomalously wet conditions within relatively small regions may cause large anomalies of runoff into a particular drainage basin and contribute greatly to anomalously large GHMZ extent, particularly in the basins that contribute large percentages of the Mississippi streamflow, such as the Ohio and Tennessee Rivers. Perhaps these findings may explain anomalously large and small measurements of the surface area of the GMHZ. In addition, land use and water policy changes within one

sub-basin of the MMRB could have a dramatic influence on the area of the GMHZ. Furthermore, these results may facilitate the use of long-lead climate forecasts for providing environmental planners with information that could assist with forecasting the area of the GMHZ up to several months in advance.

In Chapter 6, the area of the GMHZ since 1895 was estimated using a stepwise multiple regression approach based on PDSI and PHDI data to represent surface moisture availability. Teleconnection indices are less useful than moisture indices as predictor variables, as was suggested by Hypothesis 6 in Chapter 1. The resulting equations can be used to predict the July area of the GMHZ as soon as the end of February. However, accuracy seems to improve when the lead time is reduced through the use of May PDSI or April PHDI data. Several well-known flood (drought) years are well associated with a large (small) predicted GMHZ area, thus partially confirming Hypothesis 7 in Chapter 1. The hindcasted values of the GMHZ provide a range of scenarios to be expected in the area of the GMHZ. Caution should be used, however, in the interpretation of these results due to the limited amount of GMHZ data.

7.2 Suggestions for Future Research

Further research must be conducted to provide additional explanations for the estimated surface area of the GMHZ, such as land-use changes and trends in agricultural fertilizer use. Because uniform fertilizer use data for the MMRB are not available for the study period. GMHZ area could not be analyzed according to changing fertilizer use. Fertilizer statistics for the U.S. from the late nineteenth century through the early twentieth century list fertilizer use by state. Current available records list fertilizer use by crop and then only for rotating years. These and future results may prove useful in our

understanding of this complex issue that involves natural and anthropogenic causes and impacts.

LITERATURE CITED

- Alley W.M. 1984. The Palmer Drought Severity Index- limitations and assumptions. *Journal of Climate and Applied Meteorology* 23(7): 1100-1109.
- Ambaum M.H.P., Hoskins B.J., and Stephenson D.B. 2001. Arctic Oscillation or North Atlantic Oscillation. *Journal of Climate* 14(16): 3495-3507.
- Barlow M., Nigam S., and Berbery E.H. 2001. ENSO, Pacific decadal variability, and U.S. summertime precipitation, drought, and streamflow. *Journal of Climate* 14(9): 2105-2128.
- Barry J.M. 2002. The 1927 Mississippi River flood and its impact on U.S. society and flood management strategy. Paper No. 225-2. *The Geological Society of America 2002 Denver Annual Meeting*.
- Barry J.M. 1997. *Rising Tide: The Great Mississippi Flood of 1927 and How it Changed America*. Simon and Schuster, New York. p. 67.
- Bradbury J.A., Keim B.D., and Wake C.P. 2003. The influence of regional storm tracking and teleconnections on winter precipitation in the northeastern United States. *Annals of the Association of American Geographers* 93(3): 544-556.
- Barnston A.G. and Livezey R.E. 1987. Classification, seasonality and persistence of low-frequency atmospheric circulation patterns. *Monthly Weather Review* 115(6): 1083-1126.
- Bratkovich A., Dinnel S.P., and Goolsby D.A. 1994. Variability and prediction of freshwater and nitrate fluxes for the Louisiana-Texas shelf: Mississippi and Atchafalaya River source functions. *Estuaries* 17(4): 766-78.
- Briffa K.R., Jones P.D., and Hulme M. 1994. Summer moisture variability across Europe, 1892-1991: An analysis based on the Palmer Drought Severity Index. *International Journal of Climatology* 14(5): 475-506.
- Buermann W., Anderson B., Tucker C.J., Dickinson R.E., Lucht W., Potter C.S., and Myneni R.B. 2003. Interannual covariability in Northern Hemisphere air temperatures and greenness associated with El Niño-Southern Oscillation. *Journal of Geophysical Research- Atmospheres* 108(D13) Art. No. 4396.
- Bunkers M.J., Miller J.R., and DeGaetano A.T. 1996. An examination of El Niño-La Niña related precipitation and temperature anomalies across the Northern Plains. *Journal of Climate* 9(1): 147-160.

- Carpenter S.R., Caraco N.F., Correll D.L., Howarth R.W., Sharpley A.N., and Smith V.H. 1998. Nonpoint pollution of surface waters with phosphorus and nitrogen. *Ecological Applications* 8(3): 559–568.
- Climate Diagnostics Center. 2005. United States Department of Commerce, National Oceanic and Atmospheric Administration. SOI Ranked by Year 1896-1995 Accessed 3/1/05 <<http://www.cdc.noaa.gov/Climaterisks/years.risk.html>>
- Climate Prediction Center. (a) 2003. United States Department of Commerce, National Oceanic and Atmospheric Administration. Southern Oscillation Index. Accessed 11/16/03 <<ftp://ftpprd.ncep.noaa.gov/pub/cpc/wd52dg/data/indices/soi>>
- _____ (b) 2003. Monthly Niño 3.4 Index. Accessed 11/16/03 <<ftp://ftpprd.ncep.noaa.gov/pub/cpc/wd52dg/data/indices/sstoi.indices>>
- _____ (c) 2003. Weekly Niño 3.4 Index. Accessed 11/16/03 <<ftp://ftpprd.ncep.noaa.gov/pub/cpc/wd52dg/data/indices/wksst.for>>
- _____ (d). 2003. Average December-February (3 month) precipitation rankings during ENSO events. Accessed 11/14/03 <http://www.cpc.ncep.noaa.gov/products/predictions/threats2/enso/el_nino/USprank/djf.gif>
- _____ (e) 2003. Standardized Northern Hemisphere teleconnection indices. Accessed 11/16/03 <ftp://ftpprd.ncep.noaa.gov/pub/cpc/wd52dg/data/indices/tele_index.nh>
- _____ (f) 2003. Monitoring weather and climate. Accessed 11/16/03 <http://www.cpc.ncep.noaa.gov/products/precip/CWlink/daily_ao_index/ao_index.html>
- Coleman J.S.M. and Rogers J.C. 2003. Ohio River Valley winter moisture conditions associated with the Pacific-North American teleconnection pattern. *Journal of Climate* 16(6): 969-981.
- Cook E.R., Meko D.M., Stahle D.W., and Cleaveland M.K. 1999. Drought reconstruction for the continental United States. *Journal of Climate* 12(4): 1145-1162.
- Douglas A.V. and Englehart P.J. 1981. On a statistical relationship between autumn rainfall in the central equatorial Pacific and subsequent winter precipitation in Florida. *Monthly Weather Review* 109(11): 2377-2382.
- Dracup J.A. and Kahya E. 1994. The relationships between United States streamflow and La Niña events. *Water Resources Research* 30(7): 2133-2141.

- Englehart P.J. and Douglas A.V. 2003. Assessing warm season drought episodes in the central United States. *Journal of Climate* 16(11): 1831-1842.
- Gershunov A. and Cayan D.R. 2003. Heavy precipitation frequency over the contiguous United States: Sources of climatic variability and seasonal predictability. *Journal of Climate* 16(16): 2752-2765.
- Grigg B.C., Southwick L.M., Fouss J.L., and Kornecki T.S. 2004. Climate impacts on nitrate loss in drainage waters from a southern alluvial soil. *Transactions of the ASAE* 47(2): 445-451.
- Groisman P.Y., Knight R.W., and Karl T.R. 2001. Heavy precipitation and high streamflow in the contiguous United States: Trends in the twentieth century. *Bulletin of the American Meteorological Society* 82(2): 219-246.
- Guttman N.B. 1991. A sensitivity analysis of the Palmer Hydrologic Drought Index. *Water Resources Bulletin* 27(5): 797-807.
- _____ and Quayle R.G. 1996. A historical perspective of U.S. climate divisions. *Bulletin of the American Meteorological Society* 77(2): 293-303.
- Halpert M.S. and Ropelewski C.F. 1992. Surface temperature patterns associated with the Southern Oscillation. *Journal of Climate* 5(6): 577-593.
- Hanley D.E., Bourassa M.A., O'Brien J.J., Smith S.R., and Spade E.R. 2003. A quantitative evaluation of ENSO indices. *Journal of Climate* 16(8): 1249-1258.
- Hoff J.L. 1994. *A water balance evaluation of the effects of climate variability and human modification on the flow regime of the Mississippi River: 1932-1988*. Doctoral Dissertation. Louisiana State University, Baton Rouge, Louisiana.
- Jickells T.D. 1997. Nutrient biogeochemistry of the coastal zone. *Science* 281(5374): 217-221.
- Justić D., Rabalais N.N., and Turner R.E. 1997. Impacts of climate change on net productivity of coastal waters: implications for carbon budgets and hypoxia. *Climate Research* 8(3): 225-237.
- _____, _____, _____. 1996. Effects of climate change on hypoxia in coastal waters: A doubled CO₂ scenario for the northern Gulf of Mexico. *Limnology and Oceanography* 41(5): 992-1003.
- _____, _____, _____, and Wiseman W.J. 1993. Seasonal coupling between riverborne nutrients, net productivity and hypoxia. *Marine Pollution Bulletin* 26(4): 184-189.

- Kahya E. and Dracup J.A. 1994. The influence of Type-1 El-Niño and La-Niña events on streamflows in the Pacific southwest of the United States. *Journal of Climate* 7(6): 965-976.
- _____ and _____. 1993. United States streamflow patterns in relation to the El Niño-Southern Oscillation. *Water Resources Research* 29(8): 2491-2503.
- Karl T.R. 1986. The sensitivity of the Palmer Drought Severity Index and Palmer's Z-Index to their calibration coefficients including potential evapotranspiration. *Journal of Climate and Applied Meteorology* 25(1): 77-86.
- Karl T.R. and Koscielny A.J. 1982. Drought in the United States, 1895-1981. *Journal of Climatology* 2(2): 313-329.
- Keables M.J. 1988. Spatial associations of midtropospheric circulation and Upper Mississippi River Basin hydrology. *Annals of the Association of American Geographers* 78(1): 74-92.
- Keim B.D., Fischer M.R., and Wilson A.M. 2005. Are there spurious precipitation trends in the United States Climate Division database? *Geophysical Research Letters* 32(4): Art. No. L04702.
- Knapp P.A. 2004. Window of opportunity - The climatic conditions of the Lewis and Clark expedition of 1804-1806. *Bulletin of the American Meteorological Society* 85(9): 1289-1304.
- Kousky V. El Niño/La Niña Discussion. 11 Nov. 2003.
<<http://lwf.ncdc.noaa.gov/oa/climate/research/teleconnect/discussion.html#ELN>>
- LaCoast. 2005. Mississippi River Delta Basin.
<<http://www.lacoast.gov/geography/mr/index.asp>> Accessed 1/20/05.
- Lamb P.J. and Pepler R.A. 1987. North Atlantic Oscillation: Concept and application. *Bulletin of the American Meteorological Society* 68(10): 1218-1225.
- Leathers D.J., Yarnal B., and Palecki M.A. 1991. The Pacific/North American teleconnection pattern and United States climate. Part I: Regional temperature and precipitation associations. *Journal of Climate* 4(5): 517-528.
- Leung L.R., Hamlet A.F., Lettenmaiter D.P., and Kumar A. 1999. Simulations of the ENSO hydroclimate signals in the Pacific Northwest Columbia River Basin. *Bulletin of the American Meteorological Society* 80(11): 2313-2329.
- Linsley R.K. Jr., Kohler M.A., and Paulhus J. 1975. *Hydrology for Engineers (second edition)*. McGraw-Hill, New York, USA.

- Lohani V.K., Longanathan G.V., and Mostaghimi S. 1998. Long term analysis and short-term forecasting of dry spells by Palmer Drought Severity Index. *Nordic Hydrology* 29(1): 21-40.
- Mantua N. 2003. The Pacific Decadal Oscillation. *Encyclopedia of Global Environmental Change*.
<http://www.atmos.washington.edu/~mantua/REPORTS/PDO/PDO_egec.htm>
- Marshall J., Johnson H., and Goodman J. 2001. A study of the interaction of the North Atlantic oscillation with ocean circulation. *Journal of Climate* 14(7): 1399-1421.
- Mauget S.A. 2003. Intra-to multidecadal climate variability over the continental United States: 1932-99. *Journal of Climate* 16(13): 2215-2231.
- _____ and Upchurch D.R. 1999. El Niño and La Niña related climate and agricultural impacts over the Great Plains and Midwest. *Journal of Production Agriculture* 12(2): 203-215.
- Maurer E.P. and Lettenmaier D.P. 2003. Predictability of seasonal runoff in the Mississippi River basin. *Journal of Geophysical Research – Atmospheres* 108 (D16): Art. No. 8607.
- McCabe G.J. and Dettinger M.D. 2002. Primary modes and predictability of year-to-year snowpack variations in the western United States from teleconnections with Pacific Ocean climate. *Journal of Hydroclimatology* 3(1): 13-25.
- _____ and Muller R.A. 2002. Effects of ENSO on weather-type frequencies and properties at New Orleans, Louisiana, USA. *Climate Research* 20(2): 95-105.
- _____ and Wolock D.M. 1997. Climate change and the detection of trends in annual runoff. *Climate Research* 8(2):129-134.
- McGregor G.R. and Nieuwolt S. 1977. *Tropical Climatology: Second Edition*. John Wiley and Sons Ltd., West Sussex.
- Meade R.H. 1995. Setting: Geology, Hydrology, Sediments, and Engineering of the Mississippi River. Contaminants in the Mississippi River. U.S. Geological Survey Circular 1133. <http://water.usgs.gov/pubs/circ/circ1133/geosetting.html>
- Miles E.L., Snover A.K., Hamlet A.F., Callahan B., and Fluharty D. 2000. Pacific northwest regional assessment: The impacts of climate variability and climate change on the water resources of the Columbia River Basin. *Journal of the American Water Resources Association* 36(2): 399-420.
- Montroy D.L. 1997. Linear relation of central and eastern North American precipitation to tropical Pacific sea surface temperature anomalies. *Journal of Climate* 10(4): 541-558.

- National Climatic Data Center(a) 2004. Record maximum annual precipitation by state (thru 1998).
< <http://www.ncdc.noaa.gov/oa/pub/data/special/maxann.pdf>> Accessed 2/01/05.
- _____ (b) 2004. Record minimum annual precipitation by state (thru 1998).
<<http://www.ncdc.noaa.gov/oa/pub/data/special/minann.pdf>> Accessed 2/01/05.
- _____ (a) 2003. ERSST PDO Index.
<<ftp://ftp.ncdc.noaa.gov/pub/data/ersst/pdo.1854.latest.ts>> Accessed 11/16/03.
- _____ (b) 2003. U.S. Palmer drought indices
<<http://www1.ncdc.noaa.gov/pub/data/cirs/>>
- _____ (c) 2003. U.S. Palmer drought indices
<<http://www.ncdc.noaa.gov/oa/climate/research/prelim/drought/palmer.html>>
- _____ 2002. Climatology of the United States No. 8. Divisional normals and standard deviations of temperature, precipitation, and heating and cooling degree days 1971-2000 (and previous normals periods). Section 2: precipitation.
<http://www5.ncdc.noaa.gov/climatenormals/clim85/CLIM85_PRCP02.pdf>
- _____ 1994. Time Bias Corrected Divisional Temperature-Precipitation-Drought Index.
<<http://www1.ncdc.noaa.gov/pub/data/cirs/drought.README>> Accessed 1/10/05.
- National Oceanic and Atmospheric Administration. 2005. NOAA's drought information center. The Palmer drought severity index.
<<http://www.drought.noaa.gov/palmer.html>> Accessed 1/31/05/
- National Research Council. 1993. *Managing Wastewater in Coastal Urban Areas*, National Academy Press, Washington DC.
- Neff R., Chang H.J., Knight C.G., Najjar R.G., Yarnal B., and Walker H.A. 2000. Impact of climate variation and change on Mid-Atlantic Region hydrology and water resources. *Climate Research* 14(3): 207-218.
- New M., Todd M., Hulme M., and Jones P. 2001. Precipitation measurements and the trends in the twentieth century. *International Journal of Climatology* 21(15): 1899-1922.
- Nigam S., Barlow M., and Berberg E.H. 1999. Analysis links Pacific decadal variability to drought and streamflow in United States. *EOS* 80(61): 621-625.
- Nkemdirim L. and Weber L. 1999. Comparison between the droughts of the 1930s and the 1980s in the southern prairies of Canada. *Journal of Climate* 12(8): 2434-2450.

- Ntale H.K. and Gan T.Y. 2003. Drought indices and their application to East Africa. *International Journal of Climatology* 23(11): 1335-1357.
- One Gulf.org. 2002. The Gulf of Mexico: A Valuable Natural Resource. Accessed 11/09/03. <http://www.onegulf.org/gomfacts.html>
- Palmer W.C. 1965. Meteorological Drought. Research Paper No. 45, U.S. Department of Commerce Weather Bureau, Washington, D.C.
- Pandzic K. and Trinic D. 1991. Principal component analysis of hydrological and meteorological fields in a river basin. *International Journal of Climatology* 11(8): 909-922.
- Panu U.S. and Sharma T.C. 2002. Challenges in drought research: some perspectives and future directions. *Hydrological Sciences Journal* 47(SI): S19-S30.
- Piechota T.C. and Dracup J.A. 1996. Drought and regional hydrologic variation in the United States: Associations with the El Niño Southern Oscillation. *Water Resources Research* 32(5): 1359-1373.
- Piechota T.C., Dracup J.A., and Fovell R.G. 1997. Western US streamflow and atmospheric circulation patterns during El Niño Southern Oscillation. *Journal of Hydrology* 201(1-4): 249-271.
- Rabalais N.N., Turner R.E., and Wiseman W.J. 2004. Personal communication, 11/22/04.
- _____, _____, and Wiseman W.J. (a). 2002. Gulf of Mexico Hypoxia, aka “The Dead Zone.” *Annual Review of Ecology and Systematics* 33(1): 235-263.
- _____, _____, and Scavia D. (b). 2002. Beyond science into policy: Gulf of Mexico hypoxia and the Mississippi River. *BioScience* 52(2): 129-142.
- _____, _____, Justić D., Dortch Q., Wiseman W.J., and Sen Gupta B.K. 1996. Nutrient changes in the Mississippi River and system responses on the adjacent continental shelf. *Estuaries* 19(2B): 386-407.
- Rodionov S.N. 1994. Association between winter precipitation and water level fluctuations in the Great Lakes and atmospheric circulation patterns. *Journal of Climate* 7(11): 1693-1706.
- Rogers J.C. 1993. Climatological aspects of drought in Ohio. *Ohio Journal of Science* 93(3): 51-59.

- _____. 1990. Patterns of low-frequency monthly sea level pressure variability (1899-1986) and associated wave cycle frequencies. *Journal of Climate* 3(12): 1364-1379.
- _____. 1984. The association between the North-Atlantic oscillation and the Southern Oscillation in the Northern Hemisphere. *Monthly Weather Review* 112(10): 1999-2015
- _____, Winkler J.A., Legates D.R., and Mearns L.O. 2004. *Geography in America: Chapter 3-Climate* p. 32-46.
- _____ and Coleman J.S.M. 2003. Interactions between the Atlantic Multidecadal Oscillation, El Niño/ La Niña, and the PNA in winter Mississippi Valley stream flow. *Geophysical Research Letters* 30(10): Art. No. 1518.
- _____ and McHugh M.J. 2002. On the separability of the North Atlantic oscillation and the Arctic oscillation. *Climate Dynamics* 19(7): 599-608.
- Rohli, R.V., 2001: Moisture variability regions and atmospheric circulation anomalies in the Mississippi-Missouri River Basin. In Tobin, G.A., B.E. Montz, and F.A. Schoolmaster (eds.), *Proceedings and Papers of the Applied Geography Conferences* 24: 82-90.
- Ropelewski C.F. and Halpert M.S. 1986. North American precipitation and temperature patterns associated with the El Niño/Southern Oscillation (ENSO). *Monthly Weather Review* 114(12): 2352-2362.
- _____ and _____. 1996. Quantifying Southern Oscillation-precipitation relationships. *Journal of Climate* 9(5):1043-1059.
- Schleifstein, M. 2003. EPA task force to tackle hypoxia in Gulf this fall. *The Times-Picayune* July 31: A-1, A-12.
- Scian B. and Donnari M. 1997. Retrospective analysis of the Palmer drought severity index in the semi-arid Pampas region, Argentina. *International Journal of Climatology* 17(3): 313-322.
- Smith K. and Richman M.B. 1993. Recent hydroclimatic fluctuations and their effects on water- resources in Illinois. *Climatic Change* 24(3): 249-269.
- Soulé P.T. 1992. Spatial patterns of drought frequency and duration in the contiguous USA based on multiple drought event definitions. *International Journal of Climatology* 12(1): 11-24.

- Tadesse T., Wilhite D.A., Harms S.K., Hayes M.J., and Goddard S. 2004. Drought monitoring using data mining techniques: A case study for Nebraska, USA. *Natural Hazards* 33(1): 137-159.
- Thompson D.W.J. and Wallace J.M. 1998. The Arctic Oscillation signature in the wintertime geopotential height and temperature fields. *Geophysical Research Letters* 25(9): 1297-1300.
- _____ and _____. 2001. Regional climate impacts of the Northern Hemisphere annular mode. *Science* 293(5527): 85-89.
- Thornthwaite C.W. 1948. An approach toward a rational classification of climate. *Geographical Review* 38(1): 55-94.
- Tsiropoula G. 2003. Signatures of solar activity variability in meteorological parameters. *Journal of Atmospheric and Solar-Terrestrial Physics* 65(4): 469-482.
- Turner R.E., Rabalais N.N., Swenson E.M., Karprzak M., and Romaine T. 2005. Summer hypoxia in the northern Gulf of Mexico and its prediction from 1978 to 1995. *Marine Environmental Research* 59(1): 65-77.
- _____, Milan C.S., Rabalais N.N. 2004. A retrospective analysis of trace metals, C, N and diatom remnants in sediments from the Mississippi River delta shelf. *Marine Pollution Bulletin* 49(7-8): 548-556.
- _____ and Rabalais N.N. 2003. Linking landscape and water quality in the Mississippi river basin for 200 years. *Bioscience* 53(6): 563-572.
- United States Environmental Protection Agency. 1999. Integrated Assessment of Hypoxia in the northern Gulf of Mexico.
<<http://www.epa.gov/msbasin/ia/index.html>> Accessed 3/9/05.
- Velasco I., Aparicio J, Valdes J.B., Velazquez J., and Kim T.W. 2004. Drought index assessment in the watersheds of affluents from the Rio Bravo/ Rio Grande River. *Ingenieria Hidraulica en Mexico* 19(3): 37-53.
- Vitousek P.M., Aber J.D., Howarth R.W., Likens G.E., Matson P.A., Schindler D.W., Schlesinger W.H., and Tilman D.G. 1997. Human alteration of the global nitrogen cycle: sources and consequences. *Ecological Applications* 7(3): 737-750.
- Wallace J.M. and Gutzler D.S. 1981. Teleconnections in the geopotential height field during the Northern Hemisphere winter. *Monthly Weather Review* 109(4): 784-812.

_____, Thompson D.W.J., and Fang Z. 2000. Comments on “Northern Hemisphere teleconnection patterns during extreme phases of the zonal-mean circulation.” *Journal of Climate* 13(5): 1037-1039.

Yarnal B. 1993. *Synoptic Climatology in Environmental Analysis: A Primer*. Belhaven Press, London and Florida.

Yin Z.Y. 1994. Moisture condition in the south-eastern USA and teleconnection patterns. *International Journal of Climatology* 14(9): 947-967.

VITA

Natalie Amanda Vines was born in Baton Rouge, Louisiana, in 1977. She moved to Florida in 1988 where she attended Winter Park High School and began college at the University of Florida. She returned to Baton Rouge in 1997 when she transferred to Louisiana State University. She earned her Bachelor of Science Degree in Geography in 2003. She went on to attend graduate school at Louisiana State University where she received her Master of Science Degree in Geography in 2005.